Summer 2011

Dynamics of Bottom Boundary Layer Thickness in Monterey Bay Canyon

Katherine Jane Morrice
San Jose State University

DYNAMICS OF BOTTOM BOUNDARY LAYER THICKNESS IN MONTEREY BAY CANYON

A Thesis
Presented to
The Faculty of Moss Landing Marine Laboratories
San Jose State University

In Partial Fulfillment
of the Requirements for the Degree
Master of Science

by
Katherine Morrice
August 2011

The Designated Thesis Committee Approves the Thesis Titled

DYNAMICS OF BOTTOM BOUNDARY LAYER THICKNESS IN MONTEREY BAY CANYON

by

Katherine Morrice

APPROVED FOR THE DEPARTMENT OF MOSS LANDING MARINE LABORATORIES

SAN JOSÉ STATE UNIVERSITY

August 2011

Dr. Erika McPhee-Shaw	Moss Landing Marine Laboratories
Dr. Michael Graham	Moss Landing Marine Laboratories
Dr. James Girton	University of Washington, Applied Physics Laboratory

ABSTRACT

DYNAMICS OF BOTTOM BOUNDARY LAYER THICKNESS IN MONTEREY BAY CANYON

by Katherine Morrice

Submarine canyons serve an important role as conduits for exchange, funneling sediment and nutrients between shallow shelf waters and the open ocean. The steep and sloping topography intensifies internal waves that dissipate energy directly by friction at the boundary and indirectly when they are reflected and break distant from the boundary. Although bottom boundary layers (BBL) on continental slopes and abyssal regions have been described, deep continental boundary layers are poorly understood. This study examined along-canyon variability in BBL thicknesses and whether BBL heights were related to previously identified regions of high energy dissipation. Temporal variations in BBL thickness were also studied to see if significant variability was associated with an internal tide phase. In August and September 2008, we collected profiles at multiple stations along the Monterey Bay Canyon axis. Measurements included conductivity, temperature and depth (CTD), expendable current profiler (XCP), lowered acoustic Doppler current profiler (LADCP), and vertical microstructure profiler (VMP) profiles of turbulent mixing. BBL heights varied spatially and temporally. BBLs were typically thicker in deeper waters near the Monterey Bend and the canyon mouth; however, heights were not closely in phase with the internal tide. Although turbulence extended 200-300 m above the seafloor, bottom mixed layers were thin or absent. This suggests that stratification and internal tidal oscillations limit the growth of BBLs in the canyon.

ACKNOWLEDGEMENTS

I would like to thank my advisor, Erika McPhee-Shaw, for her guidance and support throughout my time at Moss Landing Marine Laboratories. I am grateful for the advice and expertise that I received from others working on this project, particularly James Girton and Eric Kunze. I would like to thank the crews of the *R/V* Point Sur and the *R/V* John Martin and all of the people who contributed to the August 2008 cruise. This includes Kevin Bartlett, Chris MacKay, Reyna Jenkyns, and Jeannette Bedard from the University of Victoria as well as Paul Aguilar, Jim Johnson, and Richard Dewey from the University of Washington, Applied Physics Laboratory. In particular, I would like to thank Samantha Terker for all of her work with the data processing following the cruise.

This research was made possible by funds from the National Science Foundation, project OCE-0728341. I am grateful for the additional opportunities that I had as a student at Moss Landing Marine Laboratories, including work with the U.S. CLIVAR program and the Monterey Bay Aquarium Research Institute.

TABLE OF CONTENTS

LIST OF TABLES

LIST OF FIGURES

LIST OF SYMBOLS

Table 1. List of symbols used throughout thesis

δ_E	Ekman layer depth
H_{BML}	Bottom mixed layer height
H_{FBBL}	Frictional bottom boundary layer height
H_{WS}	Weakly stratified bottom boundary layer height
H_S	Observed shear layer height
H_{Oa}	Oscillatory boundary layer height (Prandle 1982)
H_{Ob}	Oscillatory boundary layer height (Maas and van Haren (1987))
BLS	Buoyancy length scale
H_P	Stratified boundary layer height (Pollard et al. 1973)
K_Z	Eddy viscosity
ε	Turbulent kinetic energy dissipation rate
f	Coriolis parameter
N	Buoyancy frequency
g	Gravitational acceleration
ρ	Density
ρ_0	Mean Density
z	Depth
u	Velocity
u_*	Shear velocity
κ	Von Karman's constant
ω	Tidal frequency

1. Introduction

This study is part of a larger project in which the role of canyons in boundary mixing is investigated by examining internal wave energetics, turbulence, and intermediate nepheloid layers. Near-boundary mixing and exchange between boundaries and the ocean interior may account for the discrepancy between diapycnal diffusivities of O (10^{-4} m^2/s) (Munk 1966; Munk and Wunsch 1998) and observed diffusivities that are an order of magnitude smaller. To account for this mixing paradox, researchers have looked at the effects of rough topography and canyons as sites of elevated mixing. In addition to the surface mixed layer, the bottom boundary layer is a region of enhanced diapycnal mixing and may contribute to abyssal mixing through along-isopycnal advection and boundary layer detachment (Munk 1966; Armi 1978).

Submarine canyons are common features of continental margins and incise up to 20% of the western North American continental shelf and 50% of the shelf at latitudes north of 45° (Hickey 1995). Near-critical topography, sloping bottoms and steep and variable topography intensify internal waves, resulting in increased turbulence and enhanced mixing (Carter and Gregg 2002; Kunze et al. 2006). In many canyons, the internal tide dominates the internal wave field (Shepard et al. 1979; Hotchkiss and Wunsch 1982; Kunze et al. 2002), and energy is dissipated from breaking internal waves through turbulence (Carter and Gregg 2002). Increased levels of turbulence are seen near the bottom along the canyon axis (Lueck and Osborn 1985; Carter and Gregg 2002), and semidiurnal internal tides are amplified near the canyon floor (Xu et al. 2002). The

elevated turbulence levels and increased mixing in canyons suggest that focusing of internal waves and topographic interactions largely contribute to the energy budget.

a. Bottom Boundary Layer Dynamics

Frictional stress at the seabed produces shear resulting in turbulence proximal to the boundary (Thorpe 2005). Turbulence varies within the boundary layer; closer to the seafloor it is most intense, and it diminishes towards the outer edge of the boundary layer. Energy from low-mode internal waves supports boundary mixing and shifts to smaller scales of turbulence production through interactions with topography (Garrett and Gilbert 1988; Toole et al. 1997). The bottom boundary causes internal wave separation and reflection resulting in dissipation and mixing distant from the boundary.

Frequent interactions with rough topography and local bathymetry result in greater mixing, but whether this energy dissipation is direct or indirect is not well understood. Direct energy dissipation occurs when internal waves break at the boundary and produce turbulence. Indirect energy dissipation occurs when internal waves are refracted off the boundary and break away from the boundary, as observed by Polzin et al. (1997). Investigations measuring the direct frictional energy loss to the boundary are more common; however, few studies have investigated the effect of sloping bottoms. Most research on bottom boundary layers has focused on continental shelves. Few studies have explored bottom boundary layers in the deep-ocean, whether on slopes or abyssal plains.

The thickness of the bottom boundary layer (H_{BBL}), where the majority of frictional dissipation occurs in classical direct boundary layer dynamics, depends on buoyancy, changes in flow velocities and Earth's rotation (Richards 1990). Ekman described frictional boundaries on a rotating planet in 1905 and explained how surface Ekman layers result from wind stress at the boundary between the ocean and the atmosphere and how bottom Ekman layers result from frictional stress between currents and the boundary (the air-sea interface and/or the seafloor). Ekman assumed steady state conditions and a homogenous horizontal flow. Over flat and immobile surfaces, viscosity reduces the flow to zero at the seabed. Shear stress on the seabed, τ, is determined from U_∞, the speed of currents distant from the boundary, by $\tau = \rho_0 C_D U_\infty^2$, where C_D is the drag coefficient (Batchelor 1967). We also describe the intensity of shear-driven turbulence by the parameter u_*, shear velocity given by $u_* = \sqrt{\tau/\rho_0}$. The frictional bottom boundary layer, when modeled as a turbulent Ekman layer is directly related to the shear velocity and Coriolis force, f and is approximately $h_E = 0.4\,u_*/f$. Shear stress in the Ekman layer causes turbulence, and over time produces a bottom mixed layer (BML) where temperature or density is well mixed (Lentz and Trowbridge 1991). Over a flat seabed, the thickness of this well-mixed layer may be six times the turbulent Ekman layer thickness (Armi and Millard 1976).

Armi and Millard (1976) investigated bottom boundary layers in the Hatteras abyssal plain over flat and sloping bottoms. They found bottom mixed layer heights between 10 and 100 m over an area spanning 20 km that were present for extended periods of time, even over sloping bottoms. However, in areas of rough topography, the

bottom mixed layers were irregular and consisted of several stratified layers; their thickness was between the Ekman layer height, h_E, and the bottom mixed layer height observed on the abyssal plain (Armi and Millard 1976). Lentz and Trowbridge (1991) observed bottom mixed layers, on the northern California Shelf that were present 90% of the time measuring between 5 and 15 m that varied due to upslope and downslope advection.

The dynamics of bottom boundary layers on continental slopes are of interest because restratification associated with boundary layer detachment means exchange with the ocean interior (McPhee-Shaw and Kunze 2002). Outcropping of isopycnals, ventilation of mid-depth abyssal isopycnals and exchange between the bottom boundary and ocean interior have important implications for sediment transport and ocean biochemistry. Greater mixing associated with continental slopes, and submarine canyons in particular, may result in increased exchange between the continental shelf and the open ocean. Locations of offshore versus onshore transport can be identified by nepheloid layers and clear water.

b. Significance of Semidiurnal Tide and Internal Waves in Canyons

One of the main mechanisms responsible for generating velocities in canyons is the surface tide (Hotchkiss and Wunsch 1982). Hotchkiss and Wunsch suggested that tidal velocities near the canyon head are reduced because of the steep slope. The other important mechanism that affects velocities is stratification. Stratification in Monterey Bay shows major temporal variations due to coastal upwelling, changes in the California

Current system, and other mesoscale processes (e.g. Hickey 1979; Rosenfeld et al. 1994). In the Monterey Bay Canyon, Carter (2010) points out that variations in stratification alter the internal tide's propagation.

Shepard et al. (1979) observed tidal frequencies from velocity data in canyons. Xu and Noble (2009) observed intense tidal currents, particularly the semidiurnal, in the Monterey Canyon that accounted for 90% of the total energy. Petruncio et al. (1998) observed semidiurnal currents of 0.2 m s^{-1} and displaced isopycnals up to 50 m in the upper canyon. Other studies have shown that semidiurnal internal tides make up the bulk of the internal wave field in the canyon, particularly near the bottom (Rosenfeld et al. 1994; Petruncio et al. 1998; Kunze et al. 2002; Carter and Gregg 2002). Petruncio (1998) observed more energetic semidiurnal tides during spring tides than during neap tides.

When the barotropic tide interacts with variable topography, internal waves are generated that typically have tidal periods (Wunsch 1975; Hotchkiss and Wunsch 1982). Near the Mid-Atlantic Ridge, interactions between the barotropic tide and rough topography generate internal waves which in turn causes mixing (Polzin et al. 1997). In the Monterey Canyon, internal tides are generated offshore to the south on the California continental margin (Jachec et al. 2006), and the steep canyon walls generate and focus baroclinic tides (Carter 2010). Carter and Gregg (2002) and Kunze et al. (2002) suggested that the semidiurnal internal tide is generated along the canyon axis. The canyon slope is typically super-critical and the thalweg is near-critical, causing internal tides to be most intense following along the bottom axis (Kunze et al., *submitted*).

In the Monterey Submarine Canyon (MSC), currents and internal wave energy fluxes are steered by the canyon's topography (Kunze et al. 2002). The topography's influence is greatest along the canyon floor (Xu and Noble 2009). Internal tide energy fluxes are upcanyon at deeper sites, and downcanyon at shallower sites (Kunze et al. 2002; Xu and Noble 2009). Kunze et al. (2002) investigated internal waves in the MSC and observed a loss of energy going shoreward along the canyon axis. The greatest energy loss occurred at the second bend along the canyon axis at 900 to 1000-m depth. This concentrated energy flux convergence, or hotspot of energy dissipation, suggests that this region may be a focal point of increased turbulence and greater bottom boundary layer mixing.

c. Purpose of Overall Investigation

Physical processes in canyons and bottom boundary layer dynamics are investigated to understand how energy is dissipated directly and indirectly. Following Kunze et al.'s (2002) study of internal tides in the MSC, our current study returned to that study site to examine dissipation of internal wave energy along the canyon axis, effects on boundary mixing, and to measure evidence of boundary-interior exchange. This thesis explores the boundary layer piece of this puzzle.

The goal of my research was to describe bottom mixed layer heights (H_{BML}) and frictional bottom boundary layer heights (H_{FBBL}) from density and velocity observations. Neglecting stratification and tidal forcings, the frictional bottom boundary layer height was initially modeled as an Ekman layer affected by friction and Coriolis acceleration.

My objective was to test the hypotheses that thicker bottom boundary layers occur in regions of intense internal wave dissipation in the canyon and that significant variability in boundary layer thickness is associated with tide phase. Further details were considered, including a bottom boundary layer affected by buoyancy forces and oscillatory layers affected by eddy diffusivity, and tidal frequencies.

2. Background and Theory

Boundary layers are regions where friction is a dominant force in the fluid adjacent to the boundary. They are characterized by vertical shear and elevated turbulence. Ekman layers are found along the bottom of the ocean and at the interface between the atmosphere and the ocean. Ekman layers found in the surface mixed layer of the ocean have received more attention compared to bottom boundary layers because of their accessibility and importance in understanding wind-driven circulation of the ocean. Ekman theory is a balance of the Coriolis, the horizontal pressure gradient, and vertical shear stress terms in the equations of motion

$$\begin{aligned} fu &= -\frac{1}{\rho}\frac{\partial P}{\partial y} + K_z \frac{\partial^2 v}{\partial z^2} \\ -fv &= -\frac{1}{\rho}\frac{\partial P}{\partial x} + K_z \frac{\partial^2 u}{\partial z^2} \end{aligned} \quad (1)$$

The Ekman-layer thickness, throughout which the shear stress acts is

$$\delta_E = \left(\frac{2K_z}{f}\right)^{\frac{1}{2}} \quad (2)$$

where K_z is the eddy viscosity and f is the Coriolis parameter (Souza and Friedrichs 2005).

Bottom mixed layers and frictional bottom boundary layers are often erroneously assumed to be the same and used interchangeably. They are in fact different and should be considered independently. Bottom mixed layers are regions of homogenous density, while frictional bottom boundary layers are regions of intense vertical shear and increased turbulence (Figure 1). The bottom boundary layer is a consequence of flow

over a fixed boundary or the "no-slip" condition: at the stationary seabed the fluid's velocity is zero relative to the boundary.

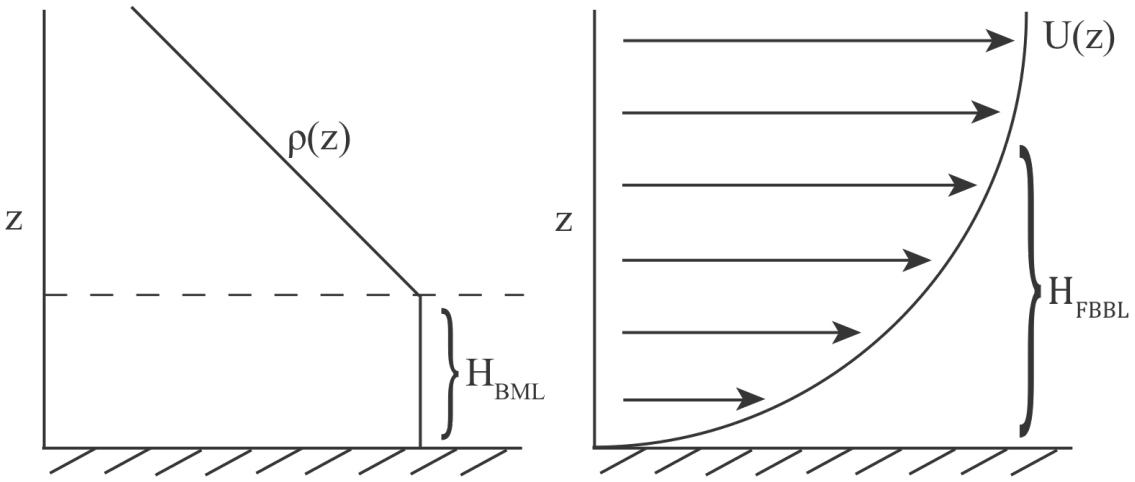

Figure 1. (*left*) Bottom mixed layer height (H_{BML}) and (*right*) frictional bottom boundary layer height (H_{FBBL}).

The law-of-the-wall describes a layer close to the seafloor, where the velocity profile is logarithmic (Figure 1) and can be described by the law-of-the-wall

$$u(z) = \frac{u_*}{\kappa} \cdot \ln\left(\frac{z}{z_0}\right) \tag{3}$$

where u_* is the shear velocity, κ is the von Kármán's constant, 0.41, and z_0 is the bottom roughness scale. To predict the frictional bottom boundary layer height (H_{FBBL}), one can assume the law-of-the-wall to estimate a bulk u_*. Alternatively, u_* can be calculated using the following equation

$$u_*^2 = C_d \cdot u^2 \tag{4}$$

where C_d is an empirical drag coefficient, (an example for flow above a seafloor is $C_d = 3.1 \times 10^{-3}$ (Sternberg 1968)), and u is the free-stream velocity or the maximum "nose"

velocity, where the velocity profile reaches a maximum above the bottom. The shear velocity and the Coriolis parameter are used to calculate H_{FBBL}, which is initially modeled as an Ekman layer

$$h_{FBBL} = 0.4 \cdot \frac{u_*}{f}. \quad (5)$$

H_{FBBL} is proportional to u_*: as turbulence intensity (shear) increases, so does H_{FBBL}. Likewise, greater shear stress translates into increased turbulence in the bottom boundary layer, which contributes to greater diffusivities (K_z). This is the same as the definition of a turbulent Ekman layer ($h_E = 0.4\,u_*/f$) used in Armi and Millard (1976). The shear layer thickness, H_S, is an observed quantity from the velocity magnitude and may be defined as the height at which the velocity is 90% of the free-stream velocity. Its thickness is comparable to H_{FBBL}; however, unlike H_{FBBL}, H_S is an observed quantity, whereas H_{FBBL} is a modeled height.

The bottom mixed layer is a region where turbulence and mixing have created a homogenous fluid over a particular height off the seabed. It is characterized by zero or minimal stratification. The height of the bottom mixed layer (H_{BML}) is determined from temperature and density profiles, specifically the region where density is homogenous i.e. $N^2 = \frac{-g}{\rho_0} \cdot \frac{\partial \rho}{\partial z}$ approaches zero or where stratification is very weak. Armi and Millard (1976) identified H_{BML} as the region near the bottom where the temperature was within 1 mK of the near-bed temperature. Lentz and Trowbridge (1991) identified bottom mixed layers for the northern California shelf from temperature profiles, where the temperature was within 0.02° C of the near-bed temperature. Perlin et al. (2007) defined a region that

incorporated a bottom mixed layer and a weakly stratified layer, and they described this region as a remnant layer, where the thickness was the height over which the potential density was within 0.003 kg m^{-3} of the bottom. The height of this layer is a weakly stratified layer (H_{WS}).

The above equations allow for predictions of H_{FBBL} and H_{BML} under the assumption that they behave as Ekman boundary layers with unidirectional steady flow. Oceanic boundary layers, however, can experience additional oscillations that cause reversals in current velocities, producing shear stress in the opposite direction and constraining boundary layer development. Two such examples include 1) a wave-driven boundary layer associated with orbital velocities under surface waves on the shelf and nearshore, and 2) Ekman layers where the inertial frequency, $f = 2\Omega\sin(\theta)$ characterizes oscillation associated with Earth's rotation. Oscillating currents in our study have tidal frequencies. Van Haren et al. (1994) observed boundary layer thicknesses of 3-30 m on the Scotian Shelf and found thicknesses to be modulated at M2 tidal frequency.

When considering bottom boundary layers under oscillatory flow, the boundary of interest often lies somewhere between the logarithmic layer and the Ekman layer (Souza and Friedrichs 2005). The equation of momentum for an oscillatory flow is

$$\frac{\partial u}{\partial t} = -g\frac{\partial \zeta}{\partial x} + \frac{\partial}{\partial z}\left(K_z \frac{\partial}{\partial z}\right) \tag{6}$$

where ζ is the surface elevation and K_z is the eddy viscosity. Assuming a single harmonic with frequency ω and following Prandle (1982), there are the following solutions: $u(z,t) = \mathrm{Re}\{U(z)e^{i\omega t}\}$ and $\zeta(t) = \mathrm{Re}\{We^{i\omega t}\}$. Substituting these back into the

momentum equation, we get $i\omega U = -g\frac{\partial W}{\partial x} + K_z\frac{\partial^2 U}{\partial z^2}$ with the solution

$U = A_1 e^{\frac{iz}{\delta}} + A_2 e^{-\frac{iz}{\delta}} + C$, where

$$C = -\frac{g}{i\omega}\frac{\partial W}{\partial x}$$

and $H_{Oa} = \left(\frac{K_z}{i\omega}\right)^{\frac{1}{2}}$ (7)

(Prandle 1982, Souza and Friedrichs 2005). We ignore C because of the hydrostatic assumption in which we assume $\frac{\partial W}{\partial x} = 0$. Since we are addressing deep ocean boundary layers, the ζ solution is also ignored. This definition of oscillatory boundary layer thickness H_{Oa} bears resemblance to the Ekman-layer thickness, δ_E (eq. 5), because it is an exponential decay with height above bottom; however, a tidal frequency appears in place of the Coriolis frequency.

Alternatively, an oscillatory boundary layer height is predicted from

$$\delta_O = \sqrt{2K/(|f \pm \sigma|)} \quad (8)$$

(Maas and van Haren 1987). This oscillatory boundary layer height is similar to the oscillatory boundary layer height described in Equation 7; however, it also incorporates the Coriolis frequency. This oscillatory boundary layer will hereafter be described as $H_{Ob.}$.

In oceanic bottom boundary layers, stratification limits the development of turbulent length scales and inhibits velocity fluctuations, thereby affecting velocity

veering (Perlin et al. 2007). Stratification also limits Ekman bottom boundary layer development. Pollard et al. (1973) found stratification to play an important role in the height of the Ekman layer such that the thickness of the layer is

$$H_P = \frac{u_*}{\sqrt{Nf}} \tag{9}$$

where $N \geq f$, and N is the stratification of the layer just above the mixed layer, representing the background stratification. Stratification limits or damps out turbulence; as N increases, H_P decreases. The effects of stratification on bottom boundary layer structure can also be examined using the buoyancy length scale (BLS) $l = \frac{u_*}{N}$ (Taylor and Sarkar 2008). Off the northern California shelf, Lentz and Trowbridge (1991) identified mixed layers whose heights varied from a few meters to a few tens of meters due to variations in interior stratification and velocity.

Determining observed BBL heights (H_{BML}, H_{WS}) from CTD data and observed H_S from velocity data is relatively straightforward; however, quantifying H_{FBBL} becomes increasingly complicated when there are factors such as tidal oscillations and stratification that may constrain bottom boundary layer development. Sampling must be rapid to observe these oscillations. In the presence of strong turbulence, we expect mixing to homogenize stratification near the frictional boundary and for H_{BML} to approximate H_{FBBL} as observed in the surface mixed layer, where after periods of strong winds and storms, a thick mixed layer develops. However, studies have shown thin or nonexistent mixed layers despite the presence of thick bottom frictional boundary layers over continental slopes (McPhee-Shaw et al. 2004; Nash et al. 2004). The presence of

strong shear yet lack of a mixed layer suggests that restratification is intense and rapid. Carter and Gregg (2002) observed bottom mixed layers that were usually thinner than 15 m in the Monterey Submarine Canyon, although we know that both turbulence and tidal velocities are strong in the canyon (Kunze et al. 2002; Petruncio et al. 1998). In contrast, H_{FBBL} varied from 70-100 m during the neap tide and up to 200 m during the spring tide (Kunze et al. 2002). This discrepancy indicates that stratification may have a strong influence on bottom boundary layer structures over sloping topography. It has been suggested that the discrepancy may be explained by rapid restratification after mixing (McPhee-Shaw and Kunze 2002).

3. Research Objectives and Specific Questions

a. Objectives

This project used CTD, LADCP, XCP, and VMP data to document spatial and high-frequency temporal variability in the thickness of frictional bottom boundary layers and bottom mixed layers. A minimum N^2 was used to identify H_{BML}, and shear velocities were used to estimate H_{FBBL}. Surface tide and moored temperature data were used to relate the phase of the tide to temporal variations in boundary layer thicknesses. Sediment samples and transmissometer data were used to identify sites along the canyon axis where there was greater suspended sediment and increased boundary mixing. I tested the hypothesis that bottom boundary layers were thicker at sites where there was more elevated suspended particulate matter, possibly indicating greater energy loss from internal waves. For VMP profiles that landed near the bottom, the turbulent kinetic energy dissipation rate, ε, and N^2 from the smoothed VMP profiles were used to determine the thickness of an oscillatory boundary layer. I examined whether different stations along the canyon axis had thicker boundary layers. This helped to address whether or not there was a gradual loss of energy proceeding upcanyon or alternatively a hotspot of energy loss focused near the Monterey bend. These data were also compared to turbulence profiles from data collected by Eric Kunze and other descriptions of the dynamics described by this research group in Kunze et al. (*submitted*). Comparing observations to predictions that incorporated shear velocities, eddy diffusivities, tidal oscillations, stratification, and Coriolis frequency gives us a better understanding of the primary dynamics affecting boundary layers in canyons.

b. Specific Questions

This thesis examined the following questions:

1. How do bottom boundary layers vary spatially along the canyon-axis? Do the shallower stations (<700 m) have thicker bottom boundary layers or do thicker bottom boundary layers correspond to regions of enhanced energy dissipation as observed by Kunze et al. (*submitted*)?
2. How does bottom boundary layer thickness vary over internal tide time scales? As deep cold waters come up and then sink back, replaced by shallower, warmer waters, how does boundary layer height change over these regular phases of the internal tide?
3. Do theoretical scaling predictions of bottom boundary layer heights match observed bottom boundary layer heights?
4. Are there spatial variations in bottom nepheloid layers, as seen from the transmissometer and sediment sample data? If so, do bottom nepheloid layers match spatial patterns in energy or in H_{BBL} along the canyon-axis?

4. Methods

This project used data collected from the R/V *Point Sur* and the R/V *John Martin* during a 15-day spring to neap tidal cycle in August 2008 and a two-day cruise in October 2008 (Figure 2). For the purpose of this study, data collected from August 17-31, 2008 were considered. Microstructure surveys were conducted from 7 am to 7 pm PST and CTD/LADCP surveys were conducted from 7 pm to 7 am PST so that each survey spanned a period representing the semidiurnal tide.

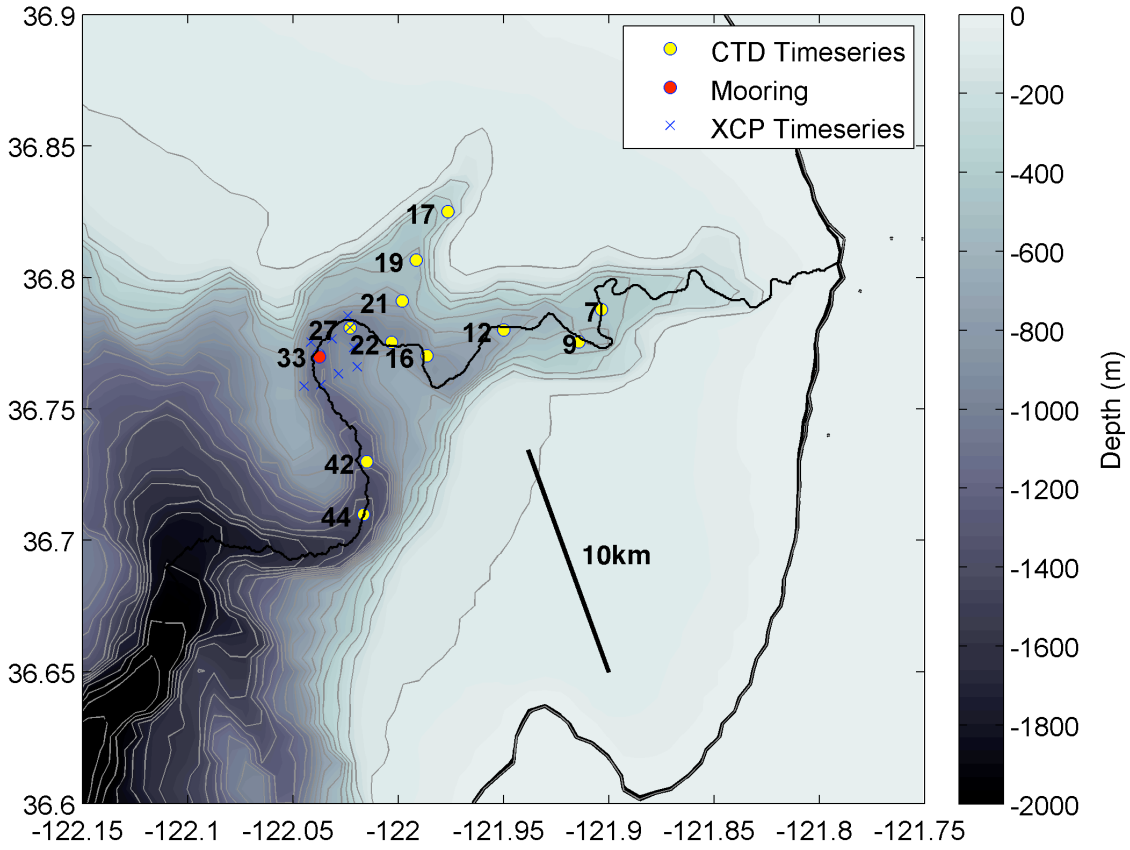

Figure 2. Stations occupied during cruise, including CTD/LADCP time series, a near-bottom mooring and XCP time series. CTD station numbers are indicated.

Measurements included conductivity, temperature, depth (CTD) and lowered acoustic doppler current profiler (LADCP) profiles from the Point Sur cruise, velocity data from Sippican Expendable Current Profilers (XCP), and microstructure (VMP) data from locations along the canyon-axis. From August to October 2008, we deployed a short mooring with three ADCPs, a transmissometer, and a chain of thermistors that recorded water temperatures.

a. CTD/LADCP Time Series

Twelve CTD/LADCP stations were occupied along the canyon-axis, including three stations from Soquel Canyon (Table 2). Repeat profiles were taken at each station over the 12-hour period to get a time series spanning the tide cycle. A Sea Bird 911+CTD/Rosette was used that included twelve 10-L Niskin bottles. The CTD package included dual SBE 3Plus Temperature sensors, SBE 4C Conductivity sensors, Wet Labs CST 25 cm path length Transmissometer, and a Tri-Tech Altimeter. These sensors were rated to 6000 m and provided high-resolution (1 m) density and suspended sediment data, throughout the water column. Readings from the altimeter indicated the proximity of the bottom. Casts typically reached 10-40 m within the bottom. An RDI 300 kHz Workhorse Sentinel LADCP (rated to 6000 m) was mounted to the bottom of the CTD frame with the transducers facing downward. It collected velocity data from the water column, and its vertical resolution was 8 m. The LADCP ran on internal batteries and data was downloaded at the end of each cast.

Table 2. CTD time series stations and nominal locations from August 2008 cruise.

CTD Station	Latitude	Longitude
7	36° 47.27' N	121° 54.22' W
9	36° 46.53' N	121° 54.85' W
12	36° 46.80' N	121° 57.00' W
16	36° 46.21' N	121° 59.19' W
17	36° 49.50' N	121° 58.60' W
19	36° 48.40' N	121° 59.50' W
21	36° 47.47' N	121° 59.90' W
22	36° 46.52' N	122° 0.20' W
27	36° 46.85' N	122° 1.38' W
33	36° 46.23' N	122° 2.27' W
42	36° 43.79' N	122° 0.91' W
44	36° 42.60' N	122° 1.00' W

b. Microstructure VMP Time Series

Microstructure surveys were measured from the Vertical Microstructure Profiler (VMP) deployed by Eric Kunze and his team from University of Victoria from 7 am to 7 pm. The station occupations alternated with the CTD/LADCP time series. Ten stations were sampled along the canyon-axis and in Soquel Canyon (Table 3). Greater details about the methods used are found in Kunze et al. (*submitted*). For calculations of oscillatory bottom boundary layers, only stations that were also sampled for the CTD time series were considered. Not all of the microstructure surveys landed near the bottom, thus only surveys that approached the bottom were considered.

Table 3. VMP time series stations and nominal locations sampled from August 2008 cruise.

VMP Station #	Latitude	Longitude
7	36° 47.27' N	121° 54.22' W
12	36° 46.80' N	121° 57.00' W
17	36° 49.50' N	121° 58.60' W
19	36° 48.40' N	121° 59.50' W
22	36° 46.52' N	122° 0.20' W
27	36° 46.85' N	122° 1.38' W
31	36° 46.95' N	122° 2.33' W
33	36° 46.23' N	122° 2.27' W
41	36° 44.39' N	122° 1.18' W
42	36° 43.79' N	122° 0.91' W

c. XCP Time Series

XCP surveys consisted of approximately 6 occupations of 9 stations over a 12 – 14-hour period to represent one cycle of the semidiurnal tide (Table 4). The XCP sites were selected after initial analysis of LADCP/CTD and VMP data that identified a region of energy-flux convergence along the canyon-axis. XCPs provide measurements at depths up to 2000 m and have a high vertical resolution of 3 m and velocity uncertainty of about 0.5 cm s^{-1}. XCP data extended to the bottom seabed while shipboard ADCP and LADCP measurements were affected by reflection of acoustic beams off the canyon walls and the bottom. XCPs measure the local velocity, whereas the ADCP computes horizontal averages from its four beams. The XCP profiles thus were more precise for calculating shear ($\partial u/\partial z$).

Table 4. XCP time series stations and nominal locations from August 2008 cruise.

XCP Station #	Latitude	Longitude
26	36° 46.41' N	122° 1.28' W
27	36° 46.85' N	122° 1.38' W
28	36° 47.12' N	122° 1.44' W
30	36° 46.60' N	122° 1.90' W
32	36° 46.52' N	122° 2.50' W
35	36° 45.52' N	122° 2.69' W
36	36° 45.55' N	122° 2.21' W
37	36° 45.80' N	122° 1.72' W
38	36° 45.96' N	122° 1.18' W

d. Total Suspended Matter

On some of the casts, water samples were collected and filtered for suspended material. Two liters of water from the Niskin bottle were collected and vacuum filtered using 0.45 μm Millipore filters (Hunter 2006). After filtration, the filters were rinsed with deionized water to remove salt. After drying in an oven, the filters were weighed, and their weight was divided by the volume filtered to get the concentration.

e. Mooring Specifications

The mooring was designed by the mooring engineering group at University of Washington, Applied Physics Laboratory, and was deployed on August 19, 2008 (Figure 3) and retrieved on October 22, 2008. It included instruments from the University of Washington and Moss Landing Marine Laboratories; the transmissometer was on loan from USGS. The mooring was located on the Monterey Bend at 36° 46.188' N and 122° 02.255' W at a depth of 1097 m. The mooring extended up to 938 m depth, and provided

coverage of a significant portion of the water column. There were three ADCPs on the mooring. There was a downward-facing Workhorse ADCP (S/N 8064) at 1050 m, a downward-facing Workhorse ADCP (S/N/ 10010) at 940 m, and an upward-facing Longranger ADCP (S/N 11181) at 938 m (Table 5, Figure 4). The Workhorse ADCPs bin size was smaller, and these ADCPs provided greater detail than the Longranger ADCP that had greater spatial coverage. The transmissometer (Seatech S/N 21) was located at ~1045 m depth and the record interval was 5 seconds. The thermistor chain extended from 10-120 mab and included twelve temperature sensors at 10-m intervals.

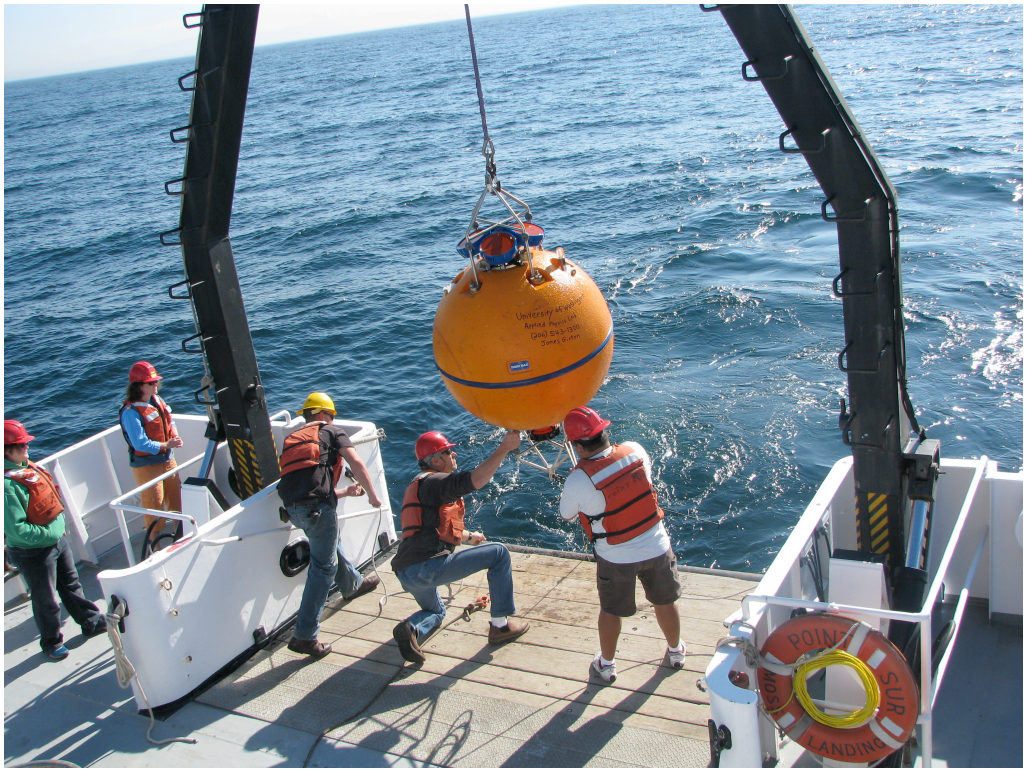

Figure 3. Scientists deploy mooring from R/V Point Sur on August 19, 2008.

Table 5. Instrument specifications for the ADCPs located along the mooring.

ADCP	**wh300 S/N 8064**	**wh300 S/N 10010**	**Longranger S/N 11181**
Depth	1050 m	940 m	938 m
Direction	down	down	up
Frequency	307.2 kHz	307.2 kHz	76.8 kHz
Bins	28	30	45
Bin Size	2.0 m	4.0 m	16.0 m
1st Bin	4.23 m	6.21	24.63 m
Ensembles	8,890	45,056	15,621
First Ens.	8/19/08 00:01:04.31	8/19/08 00:01:00.00	08/19/08 00:01:00.00
Last Ens.	8/31/08 09:59:48.67	10/20/08 13:50:59.96	10/23/08 02:01:00.00
Pings/Ens	28	19	13
Time/Ping	00:04.28 s	00:06.31 s	00:27.69 s

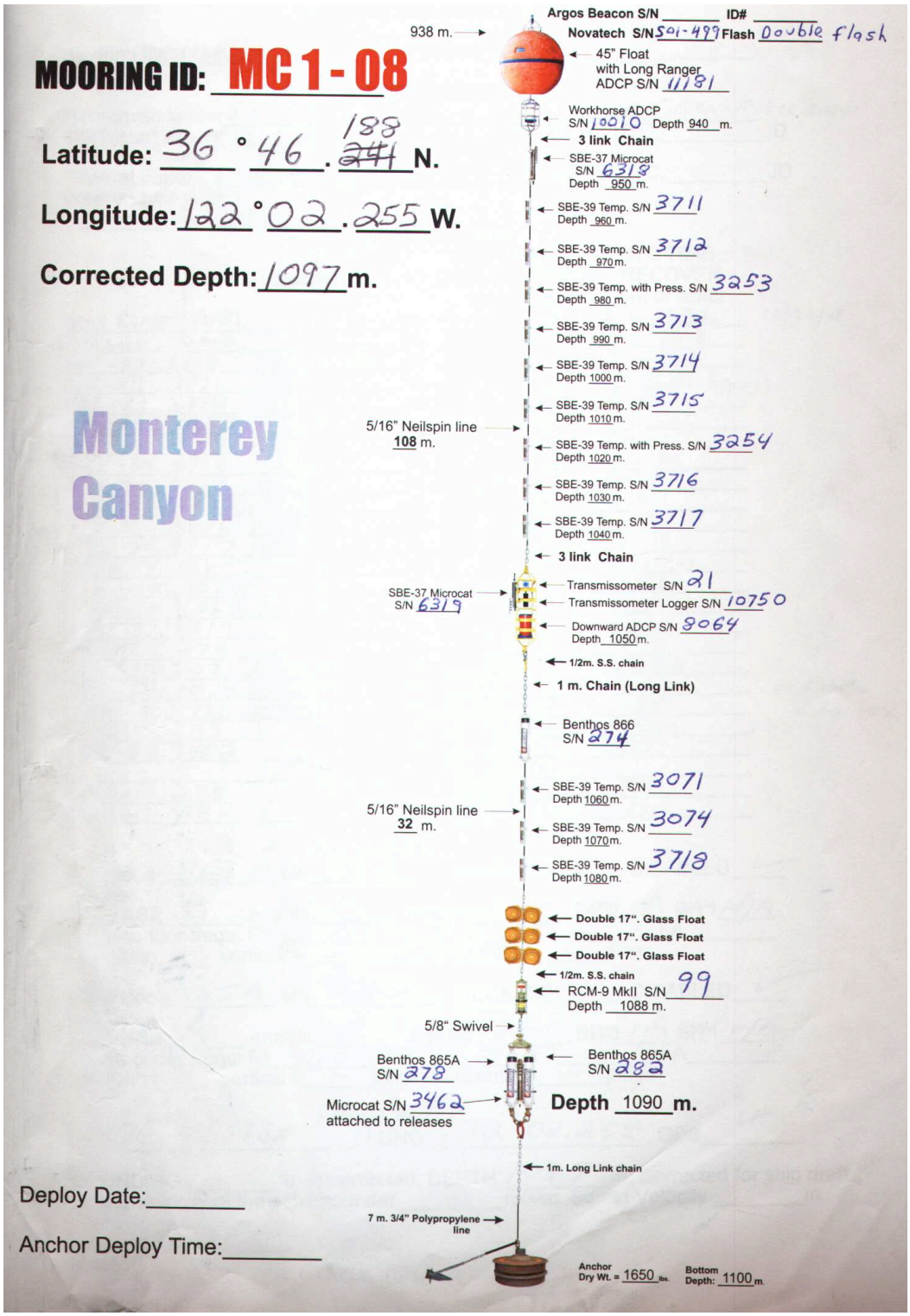

Figure 4. Mooring diagram with locations of ADCPs, transmissometer, and thermistor chain.

f. Data Analysis

The data collected were analyzed to determine bottom boundary layer heights for each cast for all the stations (typically 10 to 12 per site, spanning 12 hour M_2 tidal cycle). Since each station was occupied for one semidiurnal cycle, the effect of the oscillating tide on boundary layer structures was addressed. The internal tide phase was estimated from the thermistor chain deployed on the mooring. Cold temperatures were assumed to correspond with the upslope phase of the internal tide, and warm temperatures were assumed to correspond with the downslope phase of the internal tide. The boundary layer heights were analyzed based on baroclinic and barotropic tidal phase to identify the temporal variations in boundary layer dynamics and their association with the tide.

Density time series for each station were examined to identify isopycnal displacement near the bottom. Beam attenuation coefficient time series from the transmissometer were analyzed and compared to boundary layer thicknesses to address whether or not well-mixed bottom features corresponded with regions of high suspended particulate matter. The filtered sediment data provided an estimate of the mass of particulates in the water column.

1 DETERMINING THICKNESS OF OBSERVED HEIGHTS FROM DENSITY

Bottom mixed layer heights (H_{BML}) were determined from density profiles and calculations of the Brunt-Väisälä frequency. Layers of homogenous density that were weakly stratified were classified as bottom mixed layers. Using the Matlab seawater routine for the buoyancy frequency, temperature, salinity, pressure, and latitude data

collected from the CTD were used to determine the Brunt-Väisälä frequency (N^2). From initial analysis, I selected buoyancy frequency values of 10^{-6} s^{-1} as being weakly stratified, so this value was used to predict H_{BML}. A weakly stratified bottom boundary layer height (H_{WS}) was predicted from density profiles where $|\rho - \rho_{bottom}| < 0.03$ kg m^{-3}. This method defined a weakly stratified layer rather than a truly well-mixed layer. Figure 5 shows the difference between H_{BML} and H_{WS} and illustrates how well-mixed the bottom mixed layer is compared to the more weakly stratified layer above it. H_{WS} were also determined from smoothed VMP profiles.

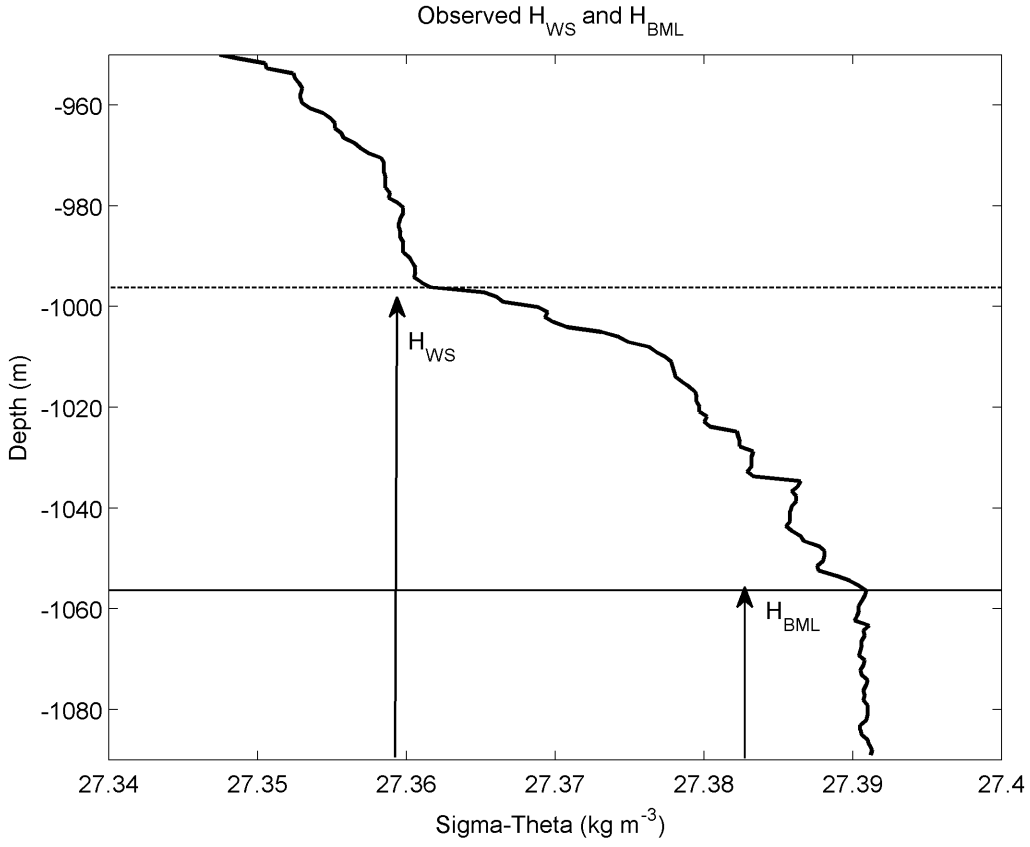

Figure 5. Bottom mixed layer height (H_{BML}) and weakly stratified layer height (H_{WS}) from sigma-theta (kg m^{-3}).

2 DETERMINING OBSERVED HEIGHTS FROM LADCP AND XCP DATA

To identify shear layer thickness based on near-bottom velocities, the maximum nose velocity was identified. The shear layer thickness was identified as the region where the velocity magnitude was 90% of this free-stream value (Figure 6). Profiles that did not exhibit this roll-off in the near-bottom velocity structure were not quantified. These profiles had increased velocities near the seafloor instead of decreased velocities with proximity to the seafloor.

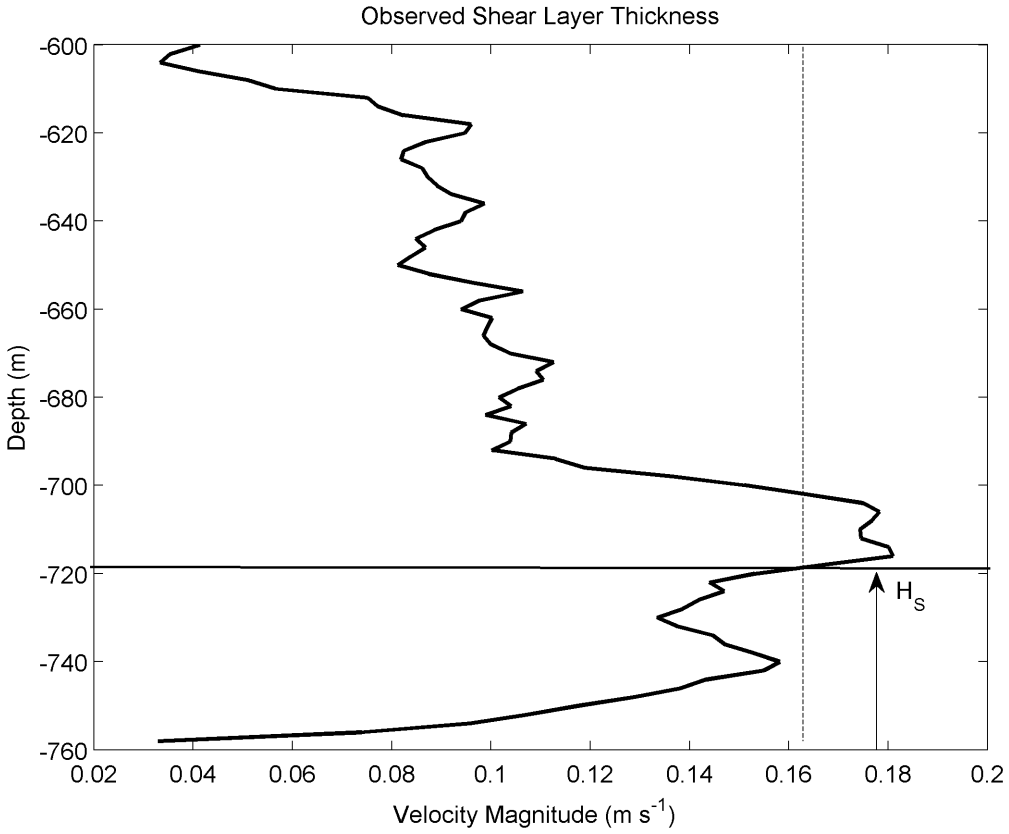

Figure 6. Observed shear layer thickness determined from velocity magnitude. The height (H_S) is indicated by the arrow, where the velocity reaches 90% of the free-stream value (dashed line).

3 CALCULATION OF EKMAN LAYER LIMITED BY ROTATION (H_{FBBL})

The LADCP and XCP measurements were used to determine H_{FBBL}. Using the more highly resolved XCP data, the shear velocity and roughness were found by fitting velocity u (z) to the law-of-the-wall (as described in Background and Theory),

$$u(z) = \frac{u_*}{\kappa} \ln\left(\frac{z}{z_0}\right).$$

Data points were selected from the bottom of the profile, about 16 m off the bottom (personal communication, J. Girton). Since the XCP's maximum depth was approximately 3 m off the bottom, this amount was added to the heights off the bottom (personal communication, J. Girton). The natural logarithm of these heights off the bottom was calculated and plotted against the horizontal velocity, showing a linear trend. A linear fit was assigned to this plot, and the slope of the line was used to calculate the shear velocity, u_* (Figure 7). The y-intercept may be used to find the roughness, z_0; however, in this study, only u_* was calculated.

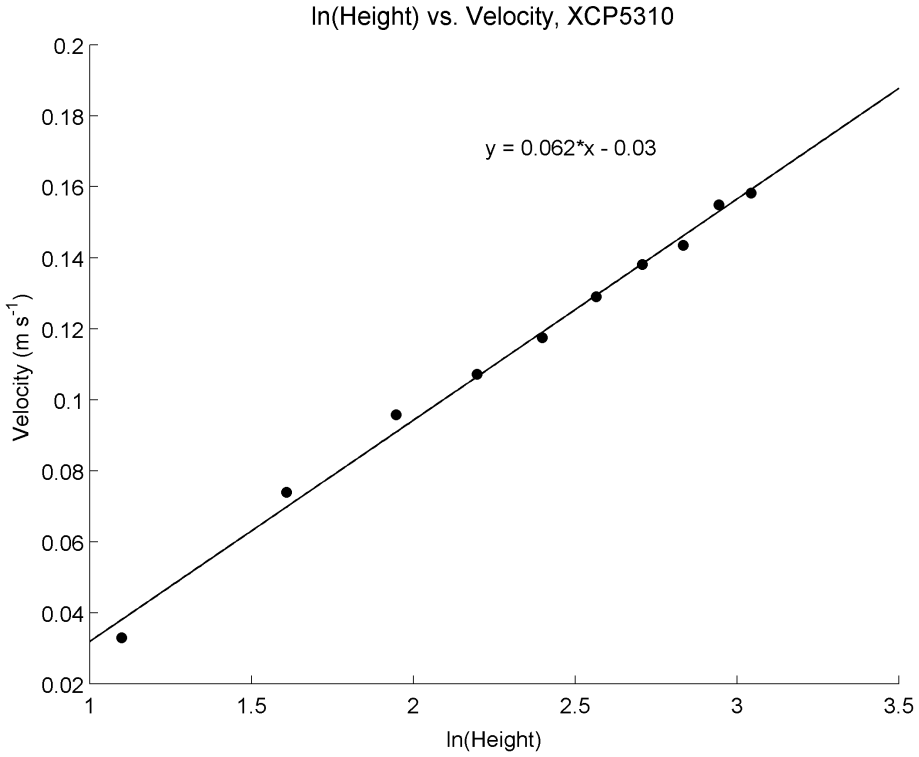

Figure 7. Velocity magnitude from 16 mab plotted against the natural logarithm of the height above bottom. The slope of this line is used to calculate u_*, the shear velocity.

Since the LADCP resolution was 8 m and not as highly resolved as the XCP data (3 m resolution), the shear velocity was predicted from the drag coefficient and the free-stream velocity

$$u_*^2 = C_d \cdot u^2 .$$

The free-stream velocity was taken as the maximum "nose" velocity near the bottom, assuming that the velocity was reduced at the bottom and increased to some maximum value at a certain height above the bottom. This method was also used to quantify the shear velocity for the XCP data, so the Law-of-the-Wall methods could be compared to the drag coefficient method. Once the shear velocities were calculated for the XCP and

LADCP data, the Coriolis parameter was quantified, and the height of the frictional bottom boundary layer was found

$$h = 0.4 \cdot \frac{u_*}{f}.$$

The XCP data were used to estimate H_{FBBL} concentrated around the second bend in the canyon axis (Monterey Bend), and the LADCP data were used to estimate H_{FBBL} along the canyon-axis corresponding with CTD surveys.

4 CALCULATION OF STRATIFIED BBL AND OSCILLATORY BBL

Bottom boundary layer heights were also calculated for a stratified bottom boundary layer, using equations from Pollard et al. (1973) and Taylor and Sarkar (2008). These height calculations used shear velocity, buoyancy frequency, and inertial frequency (Table 6). The buoyancy frequency used in these calculations was the stratification of the layer closest to the mixed layer (Taylor and Sarkar 2008). A bottom boundary layer constrained by tidal frequencies was determined from K_Z (Prandle 1982, Souza and Friedrichs 2005), calculated from ε and N^2 from microstructure data (e.g. Osborn 1980). An additional oscillatory bottom boundary layer was estimated from K_Z, tidal frequencies, and inertial frequencies (Maas and van Haren 1987). Values of ε and N^2 from the bottom 50 m in the microstructure profiles were used to calculate K_Z. The average K_Z was then calculated to determine the oscillatory bottom boundary layer height. These calculated heights were compared to observed heights. The tidal frequency used was the semidiurnal frequency, 1.4075×10^{-4} s^{-1}.

Table 6. Equations used for approximation of H_{BML} and calculation of H_{FBBL}, BLS, H_P, and H_O.

Description	Equation	Variables
Ekman Layer Thickness	$\delta_E = \left(\frac{2K_z}{f}\right)^{\frac{1}{2}}$	δ_E=Ekman layer height (m), K_z=eddy viscosity (m^2s^{-1}), f=Coriolis parameter (s^{-1})
Brunt-Väisälä Frequency	$N^2 = \frac{-g}{\rho_0} \cdot \frac{\partial \rho}{\partial z}$	N=buoyancy frequency (s^{-1}), g = $9.8ms^{-2}$, ρ_0=mean density (kgm^{-3}), $\partial\rho$=change in density, ∂z=change in depth
Law-of-the-Wall	$u(z) = \frac{u_*}{\kappa}\ln\left(\frac{z}{z_0}\right)$	u(z)=velocity (ms^{-1}), u_*=shear velocity (ms^{-1}), κ=von Karman constant (0.41), z=height off bottom (m), z_0=roughness (m)
Shear Stress	$u_*^2 = C_d \cdot u^2$	u_*=shear velocity (ms^{-1}), C_d = drag coefficient, u = velocity (ms^{-1})
Boundary Layer Height (H_{FBBL}) (Ekman)	$h = 0.4 \cdot \frac{u_*}{f}$	h=height (m), u_*=shear velocity (ms^{-1}), f=coriolis parameter (s^{-1})
Coriolis Parameter	$f = 2\Omega\sin(\theta)$	f=Coriolis parameter (s^{-1}), θ=latitude (°)
Stratified BBL (Pollard et al. 1973)	$H_P = \frac{u_*}{\sqrt{Nf}}$	H_P =height (m), u_*=shear velocity (ms^{-1}), N=buoyancy frequency (s^{-1}), f=Coriolis parameter (s^{-1})
Buoyancy Length Scale (Taylor and Sarkar 2008)	$l = \frac{u_*}{N}$	l=buoyancy length scale (m), u_*=shear velocity (ms^{-1}), N=buoyancy frequency (s^{-1})
Diapycnal Diffusivity	$K_Z = \frac{\Gamma\varepsilon}{N^2}$	K_z=eddy viscosity (m^2s^{-1}), Γ = mixing efficiency), ε = turbulent dissipation rate (m^2s^{-3}), N=buoyancy frequency (s^{-1})
Boundary Layer with Oscillatory Flow (Prandle 1982, Souza and Friedrichs 2005)	$H_{Oa} = \left(\frac{K_z}{i\omega}\right)^{\frac{1}{2}}$	H_{Oa}=height (m), K_z=eddy viscosity, ω=tidal frequency (s^{-1})
Boundary Layer with Oscillatory Flow (Maas and Van Haren 1987)	$H_{Ob} = \sqrt{2K/(\lvert f \pm \sigma \rvert)}$	H_{Ob}=height (m), K_z=eddy viscosity, σ=tidal frequency (s^{-1})

5. Results

From August 18, 2008, to August 31, 2008, twelve CTD/LADCP stations were sampled over a 12-hour sampling period (Figure 8, Table 7). Stations 42 and 27 were sampled twice. There were 174 CTD casts and 149 LADCP profiles. Some of the profiles were missing LADCP casts to preserve the life of the LADCP battery. On August 20-21, 2008, nine stations near Monterey Bend were sampled using the XCPs (Table 8). Out of the ten stations sampled using the VMP, only seven were considered (Table 9). The mooring was deployed from August 19 to October 22, 2008.

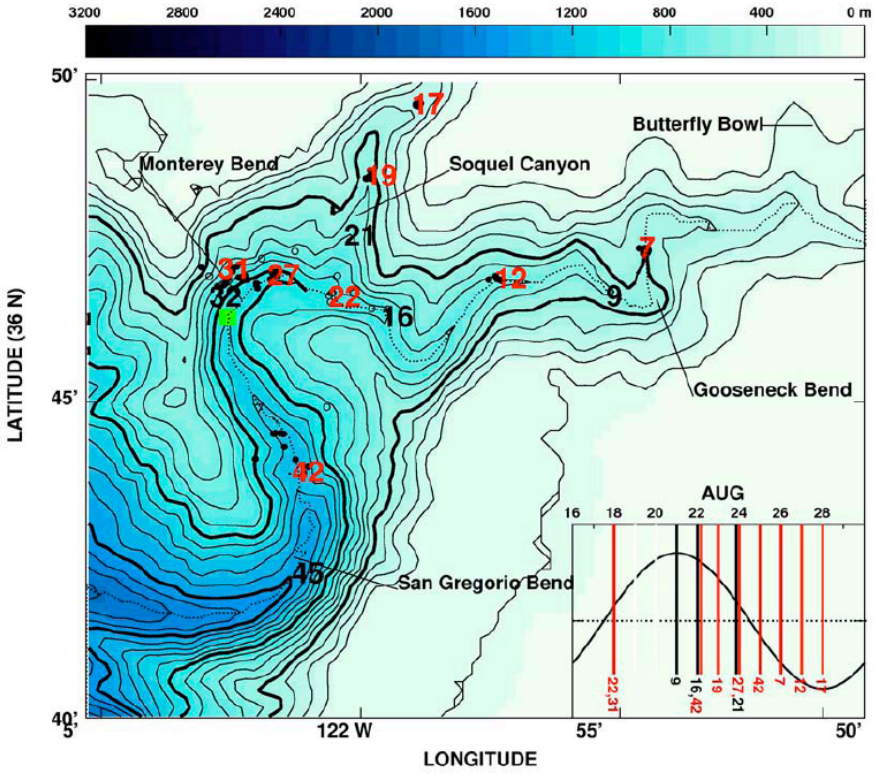

Figure 8. Locations of CTD and VMP time-series stations. Stations in red are microstructure VMP and CTD/LADCP time-series stations, and stations in black are CTD/LADCP time-series stations. The insert shows the spring-neap cycle. Reprinted with permission from Kunze et al. (*submitted*).

Table 7. CTD/LADCP time series stations, CTD casts, dates, nominal positions, distances from the canyon head, and average depths.

Station	CTD Profiles	Date	Nominal Latitude	Nominal Longitude	Distance (km)	Depth[1] (m)	Depth[2] (m)
33	1-11	8/18/08	36° 46.230' N	122° 02.275' W	36.9	1017	1099
22	12-21 169	8/19/08 8/31/08	36° 46.520' N	122° 00.200' W	32.0	907	964
42	23-32 72-80 124	8/20/08 8/23/08 8/28/08	36° 43.794' N	122° 00.912' W	43.1	1157	1221
44	34-43	8/21/08	36° 42.600' N	122° 01.000' W	45.6	1303	1388
9	44-59 158	8/21/08 8/31/08	36° 46.530' N	121° 54.850' W	19.9	508	556
16	60-71 168	8/22/08 8/31/08	36° 46.212' N	121° 59.194' W	29.2	752	792
21	81-92 170	8/24/08 8/31/0	36° 47.466' N	121° 59.898' W	31.0	720	745
27	94-102 146-156 174	8/25/08 8/30/08 8/31/08	36° 46.854' N	122° 01.380' W	34.5	983	1013
7	103-111	8/26/08	36° 47.268' N	121° 54.220' W	16.0	471	500
12	112-123, 165	8/27/08 8/31/08	36° 46.800' N	121° 57.000' W	24.0	708	733
17	131-145 (odd), 173	8/29/08 8/31/08	36° 49.500' N	121° 58.600' W	27.5	387	411
19	132-144 (even), 171	8/29/08 8/31/08	36° 48.400' N	121° 59.500' W	29.0	571	594

[1]CTD, [2]LADCP

Table 8. XCP time series including stations, XCP profiles, nominal positions, and distances from the canyon head.

Station	Profiles	Nominal Latitude	Nominal Longitude	Distance (km)
26	5302, 5311, 5321, 5332, 5343, 5357	36° 46.407' N	122° 01.278' W	34.3
27	5303, 5312, 5322, 5333, 5344, 5359	36° 46.854' N	122° 01.380' W	34.5
28	5304, 5313, 5323, 5334, 5346, 5358	36° 47.122' N	122° 01.441' W	34.6
30	5305, 5314, 5324, 5348	36° 46.602' N	122° 01.899' W	35.9
32	5306, 5315, 5327, 5336, 5349	36° 46.523' N	122° 02.504' W	36.6
35	5307, 5316, 5328, 5337, 5350	36° 45.517' N	122° 02.690' W	38.8
36	5308, 5317, 5329, 5339, 5352	36° 45.552' N	122° 02.214' W	39.0
37	5309, 5318, 5330, 5340, 5353	36° 45.798' N	122° 01.716' W	38.0
38	5301, 5310, 5319, 5331, 5341, 5355	36° 45.960' N	122° 01.176' W	37.6

Table 9. VMP time series including stations, profiles, nominal positions, and distances from the canyon head.

Station	Profile	Date	Time	Nominal Latitude	Nominal Longitude	Distance (km)	Depth (m)
22	7	8/18/08	19:36:00	36° 46.60' N	122° 0.27' W	32.0	914
42	16	8/22/08	21:19:00	36° 43.81' N	122° 0.81' W	43.1	1160
	35	8/25/08	17:09:00	36° 44.43' N	122°1.36' W	43.1	1209
	36	8/25/08	19:53:00	36° 44.21' N	122° 1.18' W	43.1	1206
	37	8/25/08	22:32:00	36° 44.42' N	122° 1.39' W	43.1	1281
	77	8/30/08	20:11:00	36° 44.41' N	122° 1.20' W	43.1	1202
19	25	8/23/08	23:02:00	36° 48.44' N	121° 59.48' W	29.0	601
27	29	8/24/08	17:53:00	36° 46.85' N	122° 1.39' W	34.5	950
	75	8/29/08	23:35:00	36° 46.87' N	122° 1.40' W	34.5	977
7	40	8/26/08	16:49:00	36° 47.27' N	121° 54.22' W	16.0	516
	44	8/26/08	20:33:00	36° 47.27' N	121° 54.16' W	16.0	530
12	50	8/27/08	14:37:00	36° 46.83' N	121° 57.09' W	24.0	751
	52	8/27/08	17:26:00	36° 46.80' N	121° 57.02' W	24.0	775
	53	8/27/08	19:07:00	36° 46.87' N	121° 57.11' W	24.0	754
	54	8/27/08	20:41:00	36° 46.80' N	121° 56.99' W	24.0	768
	55	8/27/08	21:03:00	36° 46.80' N	121° 57.02' W	24.0	680
	56	8/27/08	23:19:00	36° 46.81' N	121° 57.00' W	24.0	745
17	58	8/28/08	14:32:00	36° 49.51' N	121° 58.65' W	27.5	425
	59	8/28/08	15:29:00	36° 49.51' N	121° 58.62' W	27.5	424
	65	8/28/08	20:41:00	36° 49.53' N	121° 58.59' W	27.5	423
	69	8/28/08	23:55:00	36° 49.53' N	121° 58.56' W	27.5	433

a. Surface Tide Conditions

Surface tide measurements from the Monterey Harbor had a mixed diurnal and semidiurnal signature (Figure 9). The max spring tide occurred on August 20, and from August 18-21, the difference in height between the low and high tide was decreased. After August 22-31, the difference in tide heights increased.

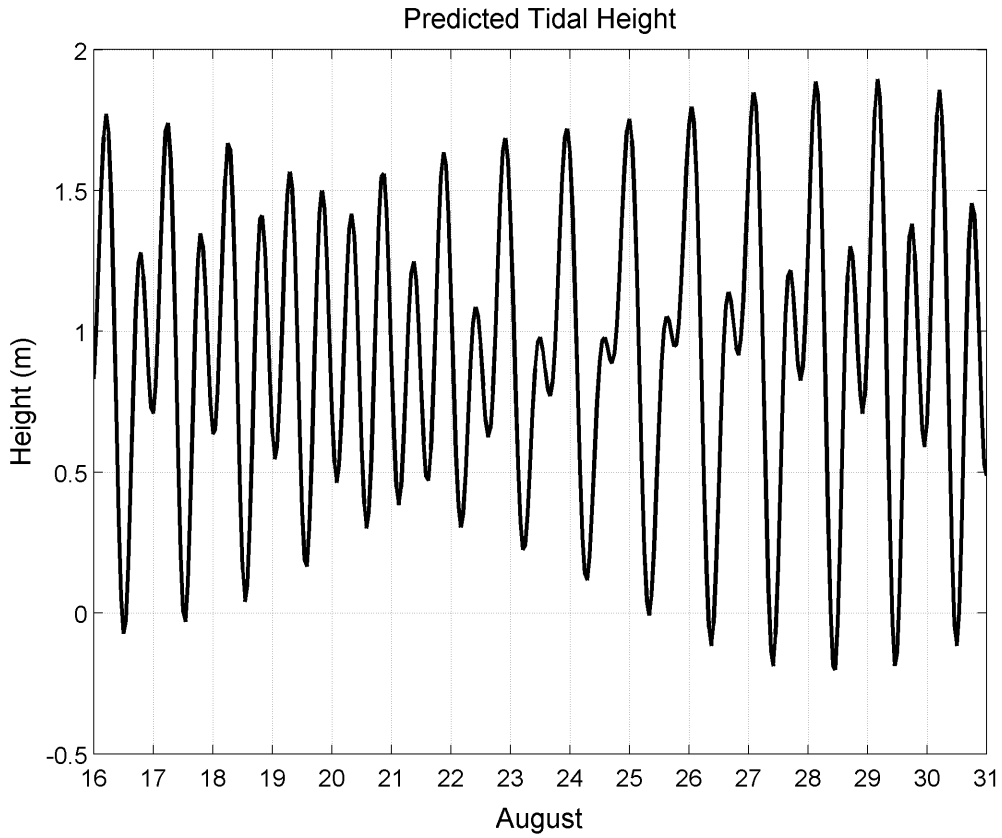

Figure 9. Surface tide from August 16-31, 2008 from the Monterey Harbor tide gauge.

b. Mooring Observations and Spectral Analysis

To better understand the internal tide, mooring temperatures from the thermistor 3071 at 1060 m depth were examined. The histogram plot identified the frequencies of different temperatures, and 3.59 °C was chosen as the bottom temperature threshold to identify cold pulses associated with the internal tide (Figure 10). The temperature record was fairly noisy, so the temperature was smoothed using a one-hour averaging. Spectrum of the unsmoothed temperature from August 19 – October 22, 2008 showed distinct peaks at the diurnal and semidiurnal frequencies (Figure 11).

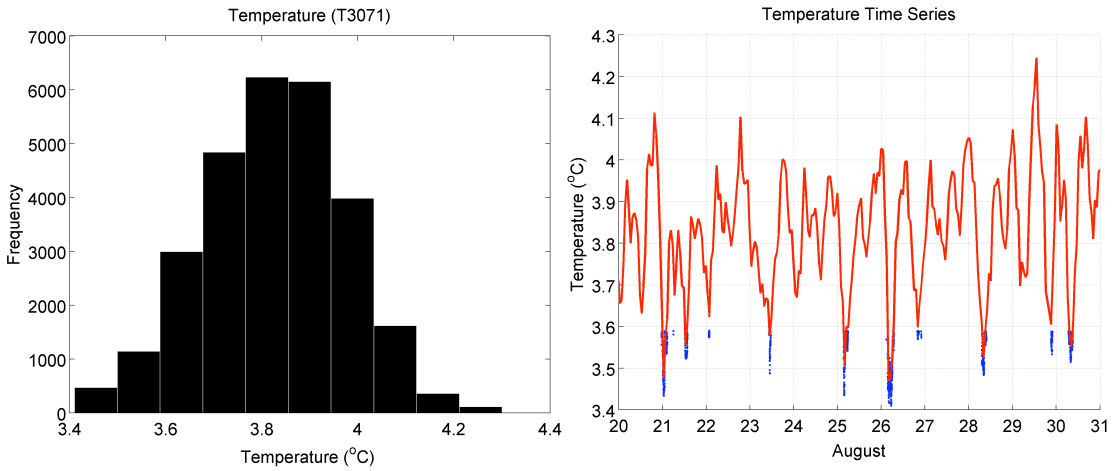

Figure 10. (*left*) Histogram of mooring temperatures from the thermistor 3071 (1060 m depth). (*right*) Temperature time series averaged over 1-hour. Temperatures less than 3.59° C are cold pulses (blue) associated with the upslope phase of the internal tide.

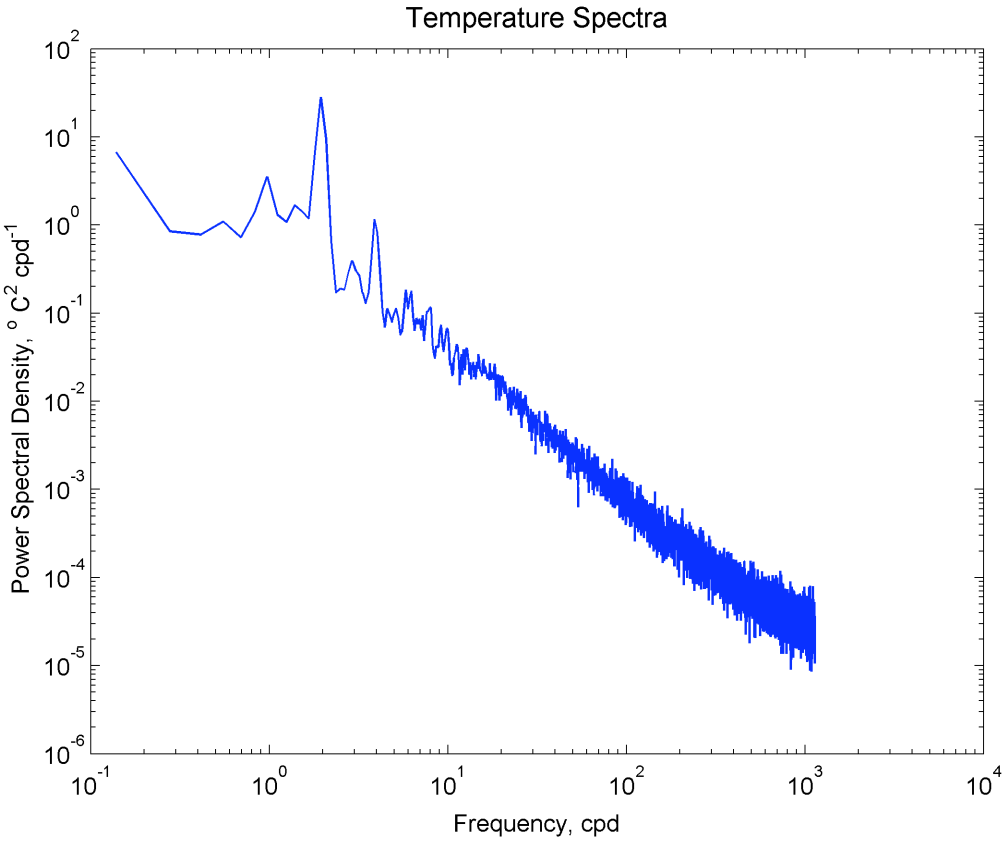

Figure 11. Spectrum of temperature from thermistor 3071 on mooring from August 19 to October 22, 2008.

The velocity magnitude was observed at the mooring by the three ADCPs and provided coverage of most of the water column, extending up to 890 m above the bottom (Figure 12). The downward ADCP S/N 8064 at 1050 m depth stopped working after August 31, so there was no near-bottom velocity coverage in September and October. Strong pulses were observed extending up to 200-300 m above the bottom. These episodes of elevated velocity lasted from six to ten days and the periods of decreased velocities between these pulses lasted from five to ten days. These pulses may be associated with the spring-neap cycle or another synoptic-scale forcing. Peak velocities observed by the downward-facing ADCP S/N 8064 at 47 mab were ~0.45 m s^{-1} (Figure 13). Velocities were decreased on August 25 and 28. Spectra of the v component, the dominant velocity vector, from 83 m showed diurnal and semidiurnal peaks (Figure 14).

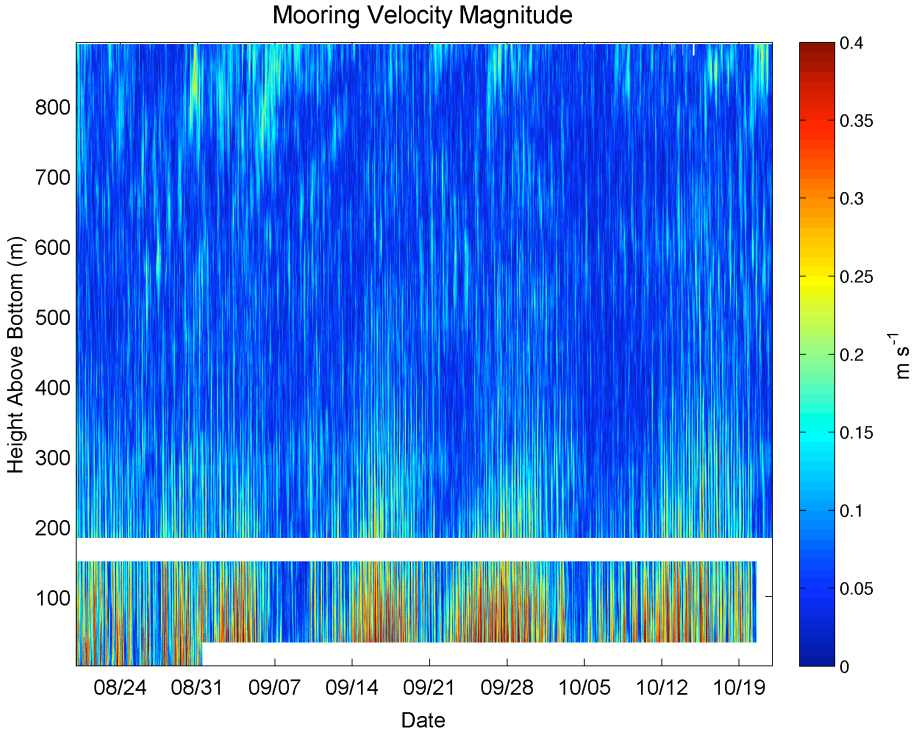

Figure 12. Mooring velocity magnitude (m s^{-1}) for duration of the mooring deployment.

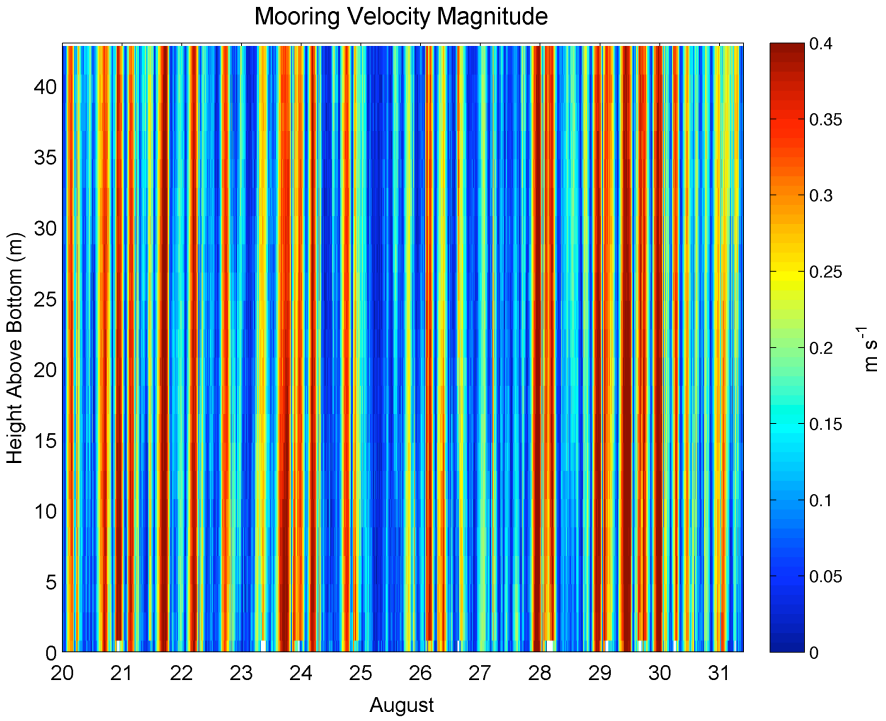

Figure 13. Velocity magnitude from the downward-facing ADCP at 1050 m depth (~47 mab) from August 20, 2008 – August 31, 2008.

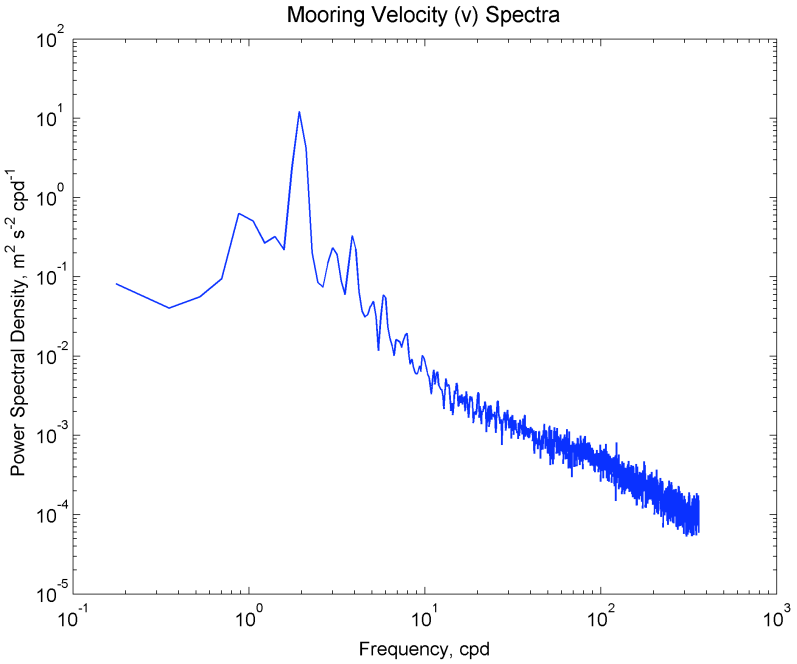

Figure 14. Spectrum of velocity from mooring from August 19 to October 22, 2008.

The transmissometer, located at ~50 mab, showed semidiurnal fluctuations and similar pulses as those observed in the velocity record (Figure 15). The stronger currents may have contributed to erosion, resulting in increased suspended sediment. The spectrum showed distinct peaks at the diurnal and semidiurnal frequencies (Figure 16).

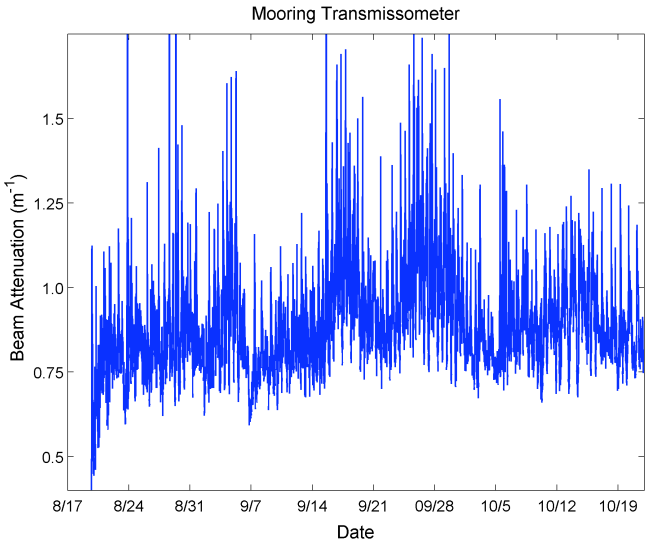

Figure 15. Beam attenuation coefficient (m^{-1}) from the transmissometer on the mooring at 1045 m depth from August 19 – October 22, 2008.

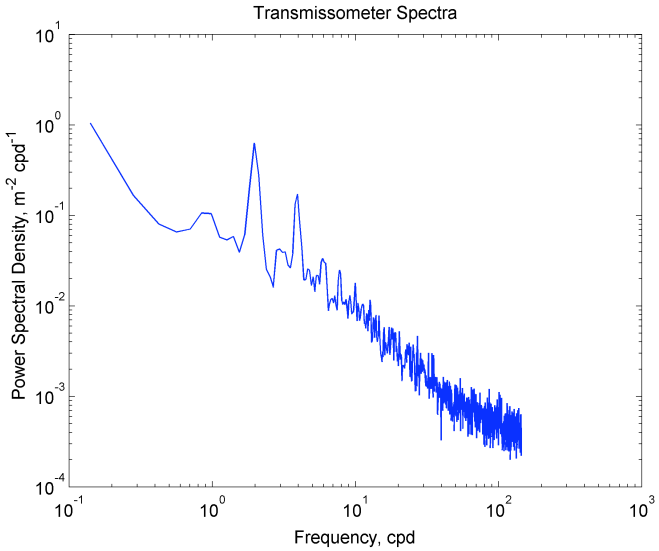

Figure 16. Spectrum of the mooring transmissometer from August 19, 2008 to October 22, 2008.

c. Station-Specific Temporal Variations of CTD/LADCP Time Series

This section explores station-specific temporal variations in density and beam attenuation from the CTD time series and velocity from the LADCP time series. Each station was sampled over a period of 12 hours. The stations are presented based on their distance, starting at the mouth of the canyon and leading up to the head of the canyon. Station distances were measured along the thalweg, and stations located in Soquel Canyon were relative to station 22. Density time series are described to show isopycnal displacements. Beam attenuation plots identify bottom nepheloid layers. Velocity magnitude from the LADCP shows how near-bottom velocities change over the 12-hour sampling period.

Observed bottom boundary layer heights are described, including bottom mixed layer heights, weakly stratified heights, and shear layer thicknesses. While all of the casts were considered for observations of H_{BML} and H_{WS}, only casts that came within 50 m of the bottom (as measured by the altimeter) were further analyzed. Shear layer thicknesses were described regardless of the proximity to the bottom since the LADCP collected data closer to the seafloor than the rosette was capable of reaching. For the stations that were within 50 m of the bottom, H_{BML} were 17 – 56 m, H_{WS} were 19 – 181 m. Shear layer heights were 13 – 294 m. During the 12 hour sampling period, isopycnals were displaced 40 to 160 m in 2 to 8 hours. Beam attenuation plots showed bottom nepheloid layers up to 200 m thick, and intermediate layers that were 100-200 m thick.

1 STATION 44

Station 44 was sampled on August 21, 2008 and included ten CTD profiles and five LADCP profiles (Table 10). The station was located at 36° 42.600' N and 122° 01.000' W, and was the farthest station from the canyon head (45.6 km). The average CTD depth was 1357 m, and the average LADCP depth was 1388 m. Over half of the casts did not come within 50 m of the bottom. Bottom mixed layers were not observed at this station, and H_{WS} were 59 – 177 m. Near-bottom velocities were increased during the first half of sampling, possibly indicating a tidal bore, and shear layers were not quantified. After that, shear layer thicknesses were 37 – 91 m.

The bottom isopycnal (27.4477 k gm^{-3}) was displaced 165 m (from 1295 m to 1130 m) in ~ 5 hours (Figure 17). An intermediate nepheloid layer was observed between 800 and 900 m depth. Bottom nepheloid layers were present at depths greater than 1100 m, where beam attenuation coefficient values were 0.5 – 0.7 m^{-1}. Above 800 m and between 950 and 1100 m, the water was clear and distinct from the nearby turbid water. Near-bottom velocities were greatest at the start and end of the time series; however velocities in this region were weaker than velocities higher up in the water column.

Table 10. CNV profile, LADCP profile, time, depth, and bottom boundary layer heights at Station 44.

CNV	LADCP	Time	Depth[1] (m)	Depth[2] (m)	H_{BML} (m)	H_{WS} (m)	H_S (m)
34	34	3:00:00	1403	1500	-	-	*
35	-	4:15:00	1430	-	-	-	-
36	36	5:21:00	1322	1429	-	-	*
37	-	6:24:07	1351	-	-	177	-
38	38	7:31:29	1378	1390	-	-	*
39	-	8:47:00	1324	-	-	-	-
40	40	9:59:00	1229	1233	-	95	37
41	-	11:08:00	1327	-	-	115	-
42	42	12:34:00	1382	-	-	-	91
43	-	13:39:00	1423	-	-	59	-

Casts in blue did not reach within 50 m of the bottom.

* Shear layer not quantified due to strong near-bottom velocities.

[1]: CTD, [2]: LADCP

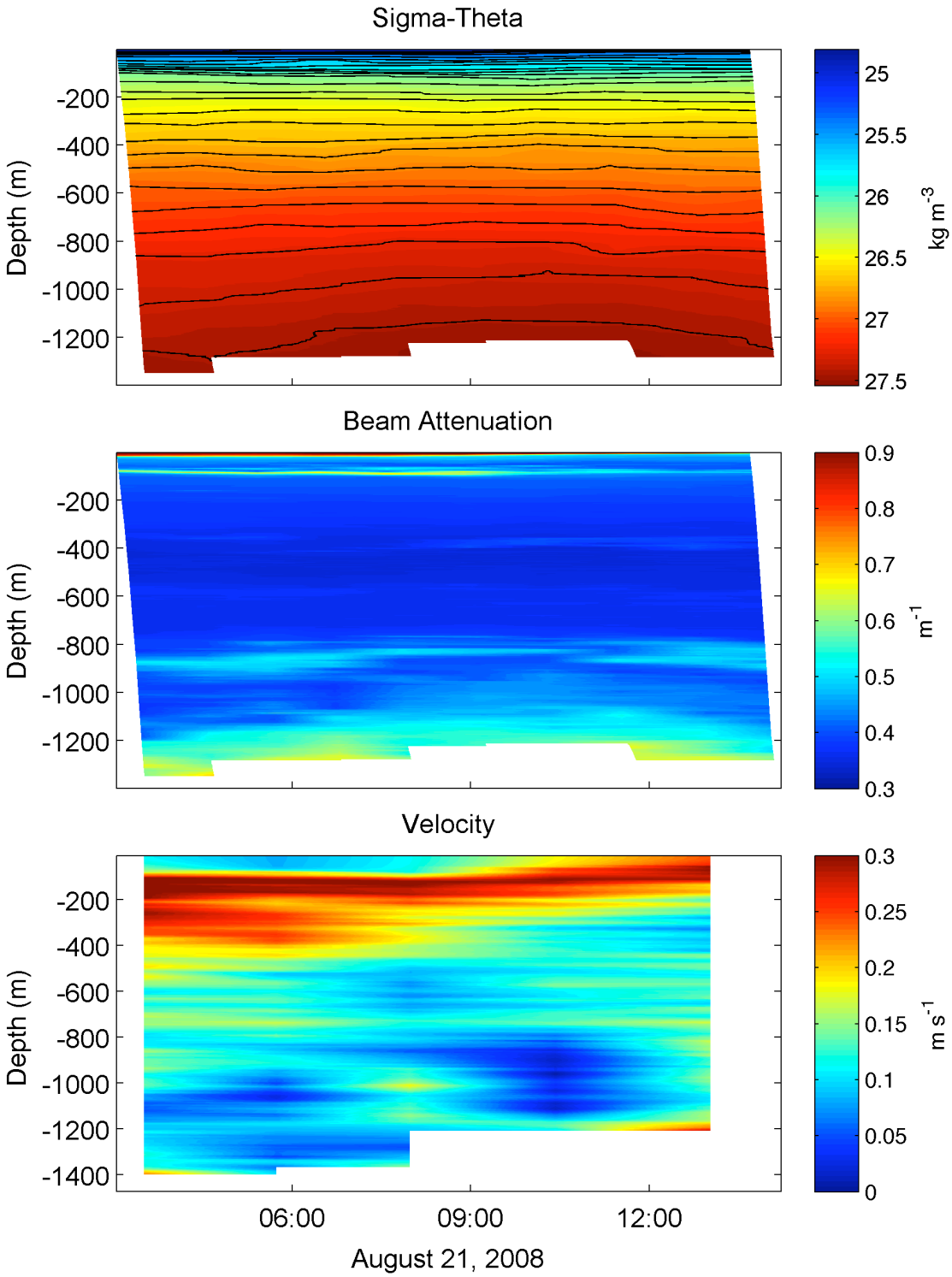

Figure 17. (*top*) Sigma-theta (kg m^{-3}), (*middle*) beam attenuation (m^{-1}), and (*bottom*) velocity magnitude (m s^{-1}) time series at Station 44.

2 STATION 42

There were twelve casts completed during the first occupation of station 42 on August 20, 2008, and nine casts sampled during the second occupation on August 23, 2008 (Table 11). An additional cast was done on August 31, 2008. The station was located at 36° 43.794' N and 122° 00.912' W, 43.1 km from the head of the canyon. The average CTD depth was 1201 m, and the average LADCP depth was 1221 m. At the first occupation of station 42, LADCP profiles were collected on half of the casts and only three of these profiles detected the bottom. For the casts that reached the bottom during the first occupation, H_{BML} were 29 – 41 m, H_{WS} were 51 – 153 m, and H_S were 13 – 188 m.

On August 20, 2008, the bottom isopycnal (27.3534 kg m^{-3}) was displaced 120 m from 1050 to 930 m in 4.5 hours (Figure 18). Beam attenuation values were higher (~0.6 m^{-1}) near the surface at 100 m depth, and an intermediate nepheloid layer (0.55 – 0.6 m^{-1}) was observed at 800 – 900 m depth (Figure 18, Table 12). Suspended sediment was also increased (0.6 – 0.7 m^{-1}) near the bottom 100 m, especially in casts 28 and 31. LADCP velocities were greatest at the start of the time series and decreased near the bottom from 05:00 – 08:00.

On August 23, 2008, the bottom isopycnal (27.3534 kg m^{-3}) was displaced from 1030 to 950 m in ten hours (Figure 19). Beam attenuation values were high (0.6 – 0.7 m^{-1}) between 800 and 1000 m and also from 1100 to 1250 m. Bottom velocities were greatest from 05:00 – 07:00 and also at the end of sampling.

Table 11. CNV profile, LADCP profile, time, depth, and bottom boundary layer heights at Station 42. Profiles 23-32 are from the first occupation; profiles 72-80 are from the second occupation.

CNV	LADCP	Time	Depth[1] (m)	Depth[2] (m)	H_{BML} (m)	H_{WS} (m)	H_S (m)
23	23	3:55:00	1146	-	-	-	13
24	-	4:57:50	1310	-	-	-	-
25	25	5:57:00	1197	1295	-	-	134
26	-	7:32:00	1229	-	-	-	-
27	27	8:29:00	1287	1287	-	78	*
28	-	9:41:00	1170	-	38	71	-
29	29	10:38:00	1126	-	-	-	57
30	-	11:30:30	1209	-	-	57	-
31	31	12:33:00	1241	1246	29	52	188
32	-	13:36:00	1208	-	-	-	-
72	72	3:04:00	1255	1257	-	92	-
73	73	4:24:00	1186	-	-	-	25
74	74	5:32:00	1167	1275	-	-	*
75	75	6:36:00	1337	1334	-	-	25
76	76	9:12:00	1283	1283	-	105	-
77	77	10:34:00	1237	1238	41	153	113
78	78	11:42:00	1135	1140	-	72	98
79	79	12:42:00	1046	1047	-	51	141
80	80	13:37:00	960	962	-	57	52
124	124	2:31:26	1288	1290	-	111	34

Casts in blue did not reach within 50 m of the bottom.
* Shear layer not quantified due to strong near-bottom velocities.
[1]: CTD, [2]: LADCP

Table 12. CNV, sample depth, concentration, beam attenuation coefficient and transmission at Station 42.

CNV	Depth (m)	Concentration (mg L^{-1})	Attenuation (m^{-1})	Transmission %
24	1197	0.12	0.60	86.1
	1099	0.47	0.48	88.8
	947	0.31	0.45	89.4
	872	0.30	0.49	88.4
	699	0.67	0.38	91.0
	399	0.21	0.34	91.7
	300	0.74	0.37	91.1
	201	0.25	0.39	90.7
75	1256	0.21	0.62	85.6
	888	0.08	0.50	88.3
	849	3.35	0.47	89.0
	798	0.69	0.42	90.0
	601	0.18	0.37	91.1
	499	0.21	0.36	91.4
	449	6.10	0.36	91.4
	390	0.09	0.40	90.6

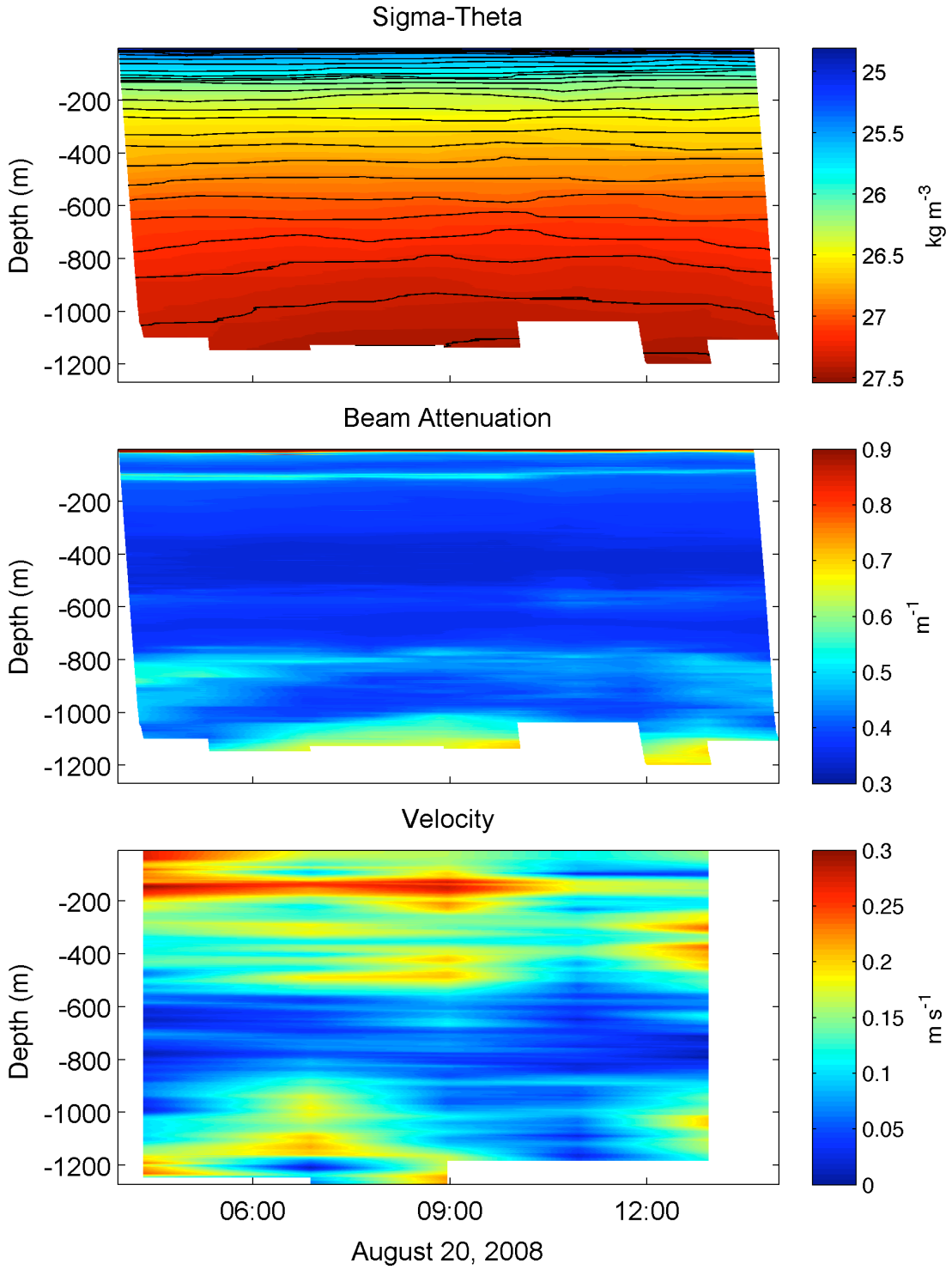

Figure 18. (*top*) Sigma-theta (kg m^{-3}), (*middle*) beam attenuation (m^{-1}), and (*bottom*) velocity magnitude (m s^{-1}) time series at the first occupation of station 42.

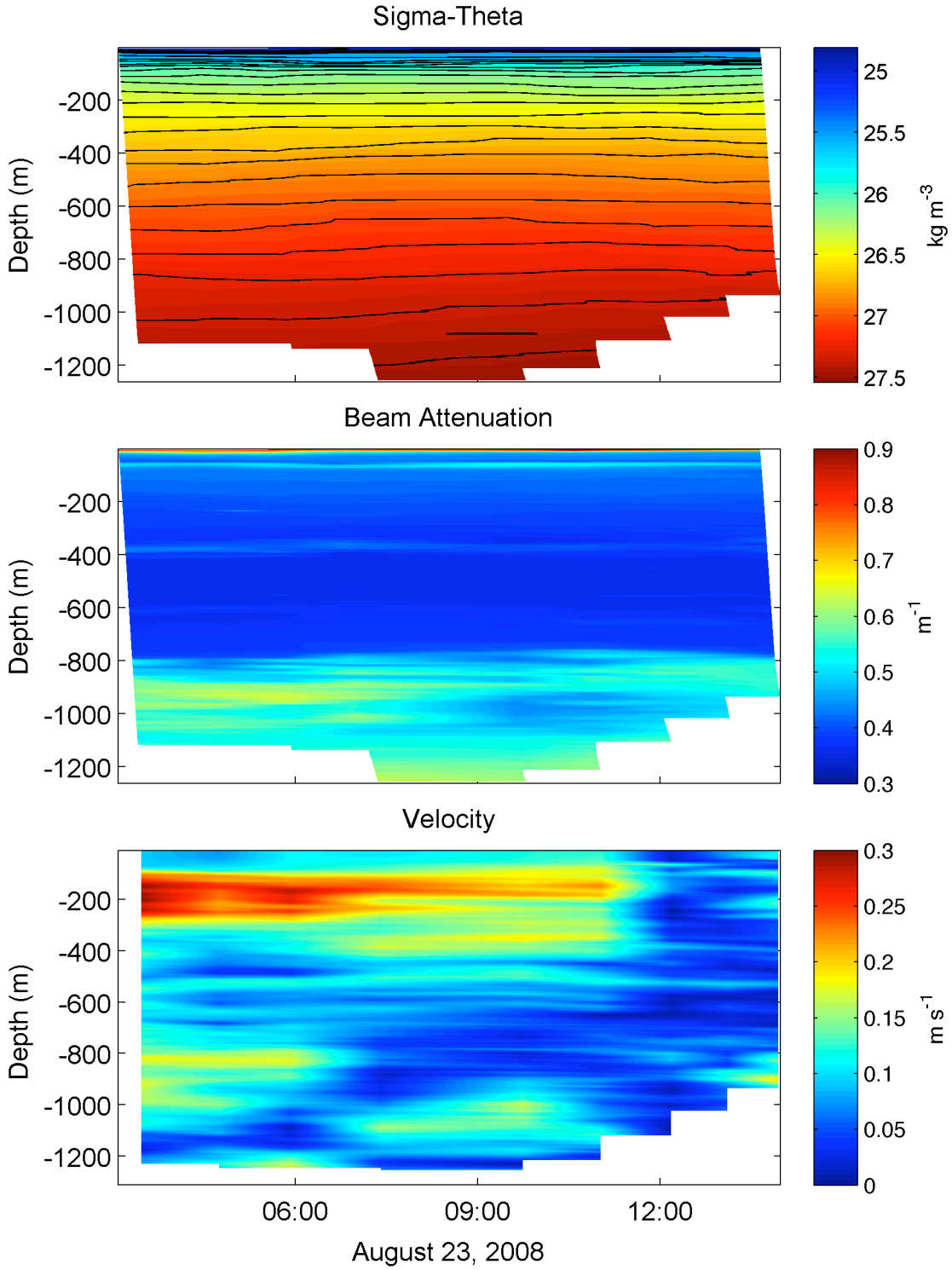

Figure 19. (*top*) Sigma-theta (kg m^{-3}), (*middle*) beam attenuation (m^{-1}), and (*bottom*) velocity magnitude (m s^{-1}) time series at second occupation of station 42.

3 STATION 33

There were eleven casts sampled at station 33 on August 18, 2008 (Table 13). The station was located at 36° 46.230' N and 122° 02.275' W, 36.9 km from the head of the canyon. The average CTD depth was 1082 m, and the average LADCP depth was 1099 m. H_{BML} were 20 – 48 m, and H_{WS} were 39 – 108 m. Shear layer heights from the LADCP data were 41 – 294 m.

The deepest isopycnal (27.3534 kg m^{-3}) was displaced 30 m in 3 hours (from 08:00 – 11:00) (Figure 20). The 27.259 kg m^{-3} isopycnal was displaced 70 m in the first 7 hours and back down 60 m after 6 hours. Suspended sediment was greatest in the 200 – 300 m above the bottom (Table 14). Beam attenuation coefficients were greatest (0.6 – 0.8 m^{-1}) at depths greater than 850 m, particularly during the first half of sampling. Velocity magnitudes were greatest from 04:00 – 08:00 and after 12:00, and values were 0.18 – 0.25 m s^{-1} at depths greater than 900 m.

Table 13. CNV profile, LADCP profile, time, depth, and bottom boundary layer heights at Station 33.

CNV	LADCP	Time	Depth[1] (m)	Depth[2] (m)	H_{BML} (m)	H_{WS} (m)	H_S (m)
1	-	2:21:00	1100	-	-	-	-
2	2	3:38:00	1096	1117	-	-	61
3	3	5:01:41	1088	1115	-	-	75
4	4	6:06:00	1088	1113	-	-	83
5	5	7:26:00	1088	1110	-	-	71
6	6	8:23:32	1047	1047	35	64	41
7	7	9:18:00	1109	1128	-	-	294
8	8	10:38:00	1104	1105	48	108	251
9	9	11:42:56	1050	1125	-	-	62
10	10	12:41:00	1104	1103	20	78	*
11	11	13:36:00	1025	1025	-	39	*

Casts in blue did not reach within 50 m of the bottom.
* Shear layer not quantified due to strong near-bottom velocities.
[1]: CTD, [2]: LADCP

Table 14. CNV, sample depth, concentration, beam attenuation coefficient and transmission at Station 33.

CNV	Depth (m)	Concentration (mg L^{-1})	Attenuation (m^{-1})	Transmission %
4	947	0.57	0.70	84.0
	897	1.63	0.71	83.7
	848	0.06	0.65	85.0
	798	0.18	0.60	86.0
	599	0.17	0.45	89.3
	498	0.11	0.37	91.1
	395	0.31	0.35	91.6
	300	0.59	0.39	90.8
7	849	0.94	0.63	85.3
	699	0.32	0.46	89.0
	600	0.25	0.45	89.3
	399	0.08	0.35	91.7
	300	1.09	0.37	91.1
	250	0.35	0.38	90.9

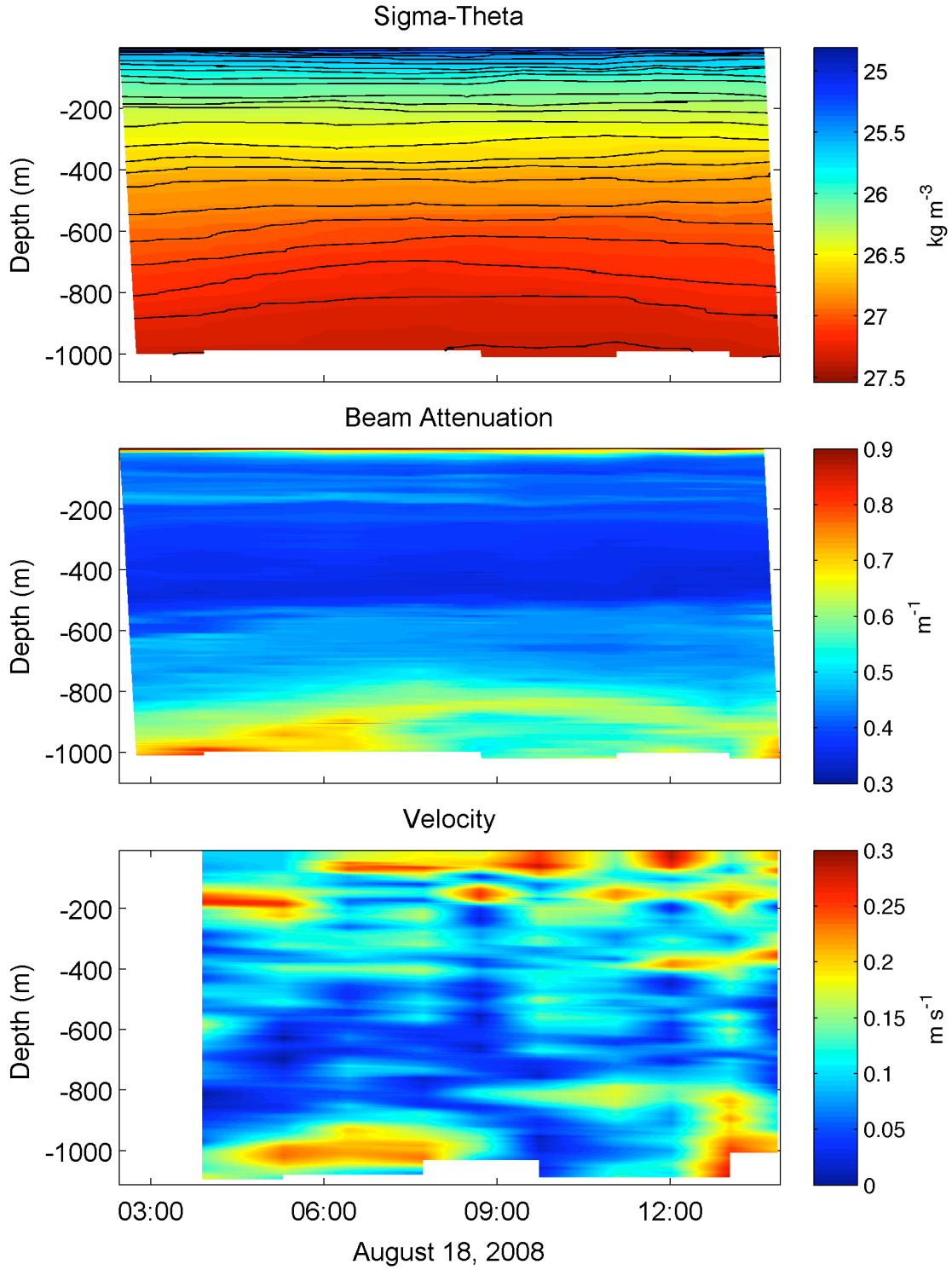

Figure 20. (*top*) Sigma-theta (kg m^{-3}), (*middle*) beam attenuation (m^{-1}), and (*bottom*) velocity magnitude (m s^{-1}) time series at Station 33.

4 STATION 27

There were nine casts sampled during the first occupation of station 27 on August 25, 2008, and ten casts were sampled during the second occupation on August 30, 2008 (Table 15). An additional profile was sampled on August 31, 2008. The station was located at 36° 46.854' N and 122° 01.380' W, 34.5 km from the head of the canyon, on the Monterey Bend. The average CTD depth was 1008 m and the average LADCP depth was 1013 m. Bottom mixed layers were observed in nearly half of the casts; heights were 28 – 50 m. H_{WS} were 42 – 154 m, and H_S were 22 – 235 m.

During the first occupation of station 27, the deepest isopycnal (27.2592 kg m^{-3}), dropped 70 m from 820 to 890 m in 8 hours (Figure 21). The isopycnal then rose to 795 m in 2 hours. Beam attenuation coefficient values were greater at depths below 650 m, especially at depths past 900 m, where values were 0.7 – 0.85 m^{-1}. Near-bottom velocities were small and less than 0.1 m s^{-1}.

At the second occupation of station 27, the bottom isopycnal (27.3534 kg m^{-3}) was displaced to 945 m in 3 hours (Figure 22). The isopycnal at 27.2592 kg m^{-3} was displaced from 825 to 915 m in 6 hours. Beam attenuation coefficient values were greater during this second occupation, particularly near the bottom at depths greater than 900 m, where values were 0.8 – 1 m^{-1} and sediment concentrations were greater (Table 16). Near-bottom velocities were greater than the velocities during the first occupation, and values were 0.15 – 0.3 m s^{-1}. Velocities were greatest at 3:00, 7:00, and from 11-13:00.

Table 15. CNV profile, LADCP profile, time, depth, and bottom boundary layer heights at Station 27. Profiles 94-102 are from the first occupation; profiles 146-156 are from the second occupation.

CNV	LADCP	Time	Depth[1] (m)	Depth[2] (m)	H_{BML} (m)	H_{WS} (m)	H_S (m)
94	94	3:56:00	1046	1048	48	142	235
95	95	5:05:00	933	1043	-	-	141
96	96	6:09:38	1055	1060	45	94	47
97	97	7:27:00	992	991	45	66	*
98	98	8:53:00	989	989	-	51	90
99	99	9:57:00	1000	1001	31	72	117
100	100	11:45:27	987	987	36	79	143
101	101	12:51:00	991	992	-	83	125
102	102	13:38:39	1011	1011	50	111	128
146	146	2:12:00	1013	1014	35	54	43
147	147	3:14:26	1014	1015	-	58	*
148	148	4:22:00	1009	1009	-	47	175
149	149	5:37:00	1047	1048	-	66	147
150	150	6:37:00	1020	1020	-	70	*
151	151	7:46:42	1044	1046	28	63	225
152	152	8:53:00	1017	1017	-	67	22
153	153	9:57:00	996	996	-	52	124
154	154	11:27:17	938	938	-	76	*
155	155	12:25:00	969	972	36	74	*
156	156	13:25:00	1042	1040	34	154	45
174	174	15:36:00	1048	1050	-	42	*

Casts in blue did not reach within 50 m of the bottom.
* Shear layer not quantified due to strong near-bottom velocities.
[1]: CTD, [2]: LADCP

Table 16. CNV, sample depth, concentration, beam attenuation coefficient and transmission at Station 27.

CNV	Depth (m)	Concentration (mg L^{-1})	Attenuation (m^{-1})	Transmission %
97	938	0.76	0.65	85.1
	878	0.20	0.62	85.6
	838	0.38	0.67	84.7
	797	0.41	0.57	86.7
	639	0.38	0.45	89.3
	450	0.60	0.33	92.0
148	978	2.59	1.04	77.2
	958	2.02	0.94	79.0
	848	0.84	0.58	86.5
	769	1.20	0.53	87.5
	599	0.47	0.47	88.9
	489	0.40	0.41	90.4
	360	0.27	0.34	91.8
	130	0.14	0.38	90.9

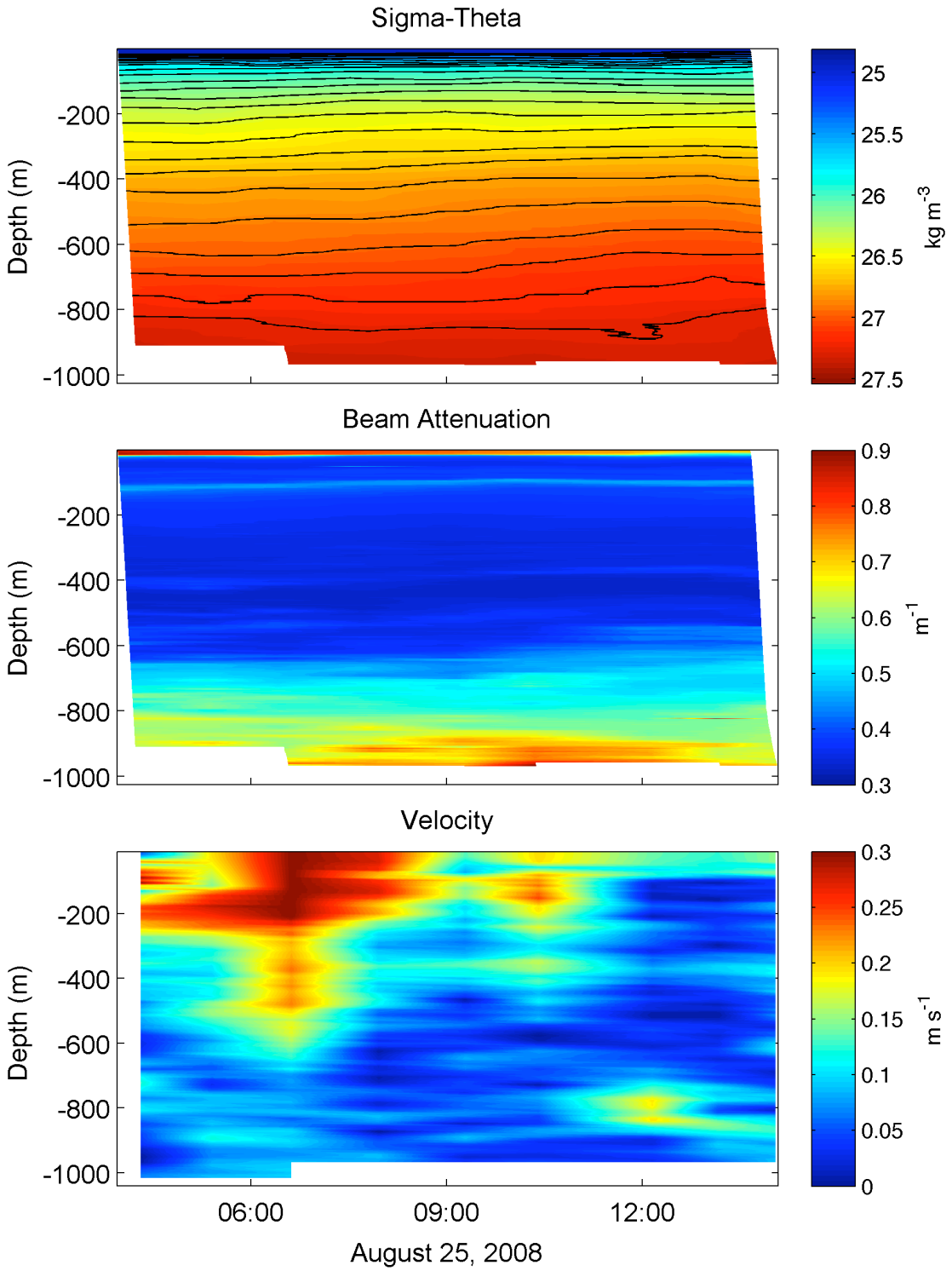

Figure 21. (*top*) Sigma-theta (kg m^{-3}), (*middle*) beam attenuation (m^{-1}), and (*bottom*) velocity magnitude (m s^{-1}) time series at the first occupation of Station 27.

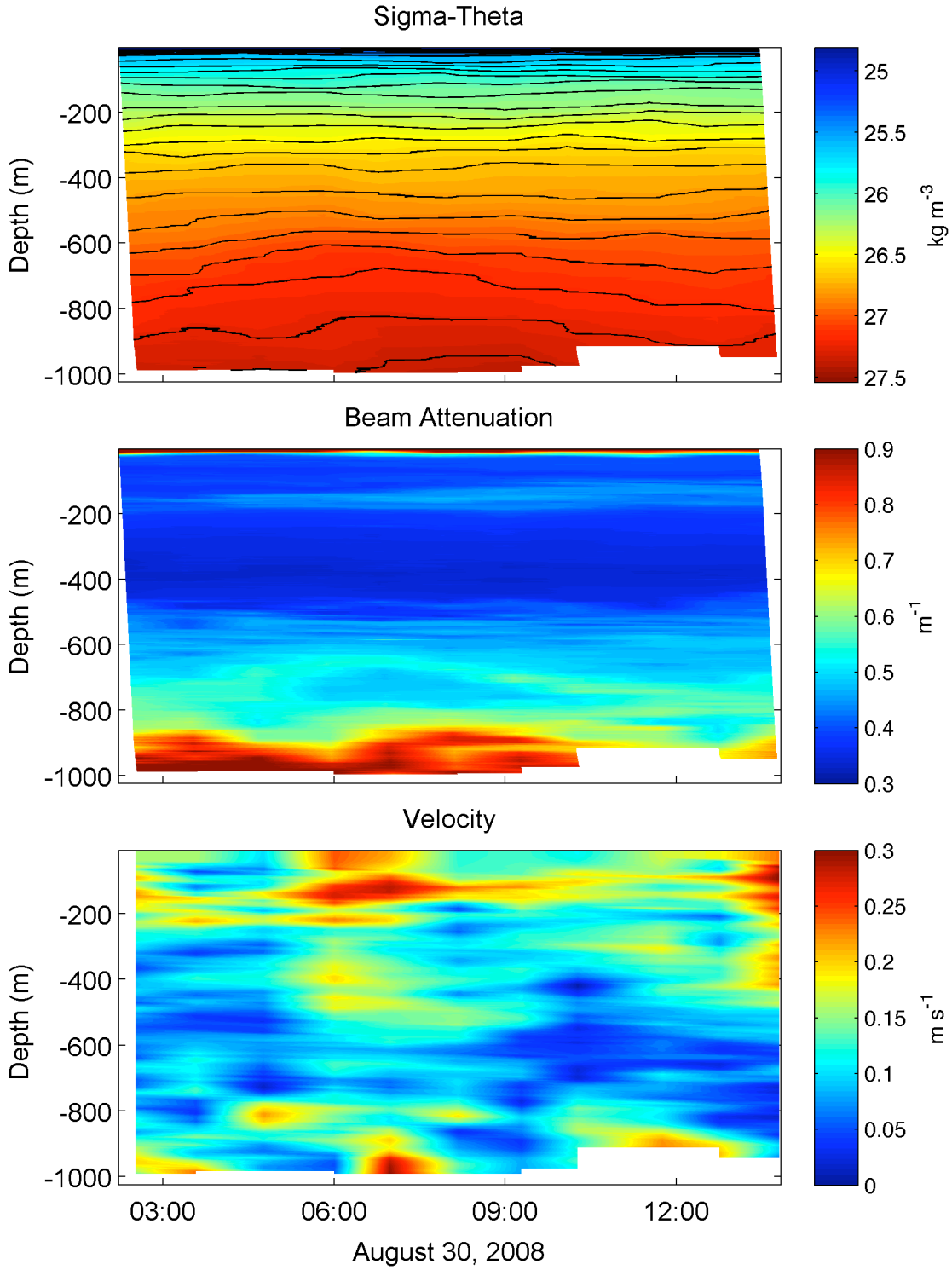

Figure 22. (*top*) Sigma-theta (kg m^{-3}), (*middle*) beam attenuation (m^{-1}), and (*bottom*) velocity magnitude (m s^{-1}) time series at the second occupation of Station 27.

5 STATION 22

There were ten casts sampled at station 22 on August 19, 2008, and an additional cast on August 31, 2008 (Table 17). The station was located at 36° 46.520' N and 122° 00.200' W, 32.0 km from the head of the canyon. The average CTD depth was 943 m, and the average LADCP depth was 964 m. Bottom mixed layers were 4 – 15 m, weakly stratified layers were 24 – 123 m, and shear layer thicknesses were 22 – 205 m.

The bottom isopycnal (27.2592 kg m^{-3}) was displaced 40 m upwards in one hour starting around 08:00 (Figure 23). The isopycnal above that, at 27.1649 kg m^{-3} was displaced 120 m upward in five hours starting at 06:00. Beam attenuation coefficients were greater in the casts after 09:00. Only two of the casts before this came close enough to the bottom to detect elevated suspended matter associated with bottom nepheloid layers. Values ranged from 0.65 – 0.95 m^{-1}. Sediment samples were taken from a profile that did not reach near the bottom (Table 18). Velocity magnitudes were greatest between 07:00 and 10:00, and values were 0.15 – 0.3 ms^{-1}. The increased velocities coincided with displaced isopycnals.

Table 17. CNV profile, LADCP profile, time, depth, and bottom boundary layer heights at Station 22.

CNV	LADCP	Time	Depth[1] (m)	Depth[2] (m)	H_{BML} (m)	H_{WS} (m)	H_S (m)
12	12	02:35:00	949	951	47	56	145
13	13	04:29:00	949	983	-	-	131
14	14	05:25:23	929	983	-	-	205
15	15	06:43:00	921	922	-	52	22
16	16	07:47:00	861	970	-	-	39
17	17	09:00:00	939	940	-	107	*
18	18	10:20:00	956	958	56	78	57
19	19	11:14:53	1015	1015	-	148	35
20	20	12:06:00	938	938	-	76	107
21	21	12:55:59	967	967	22	89	147
169	169	11:18:00	972	974	-	78	164

Casts in blue did not reach within 50 m of the bottom.
* Shear layer not quantified due to strong near-bottom velocities.
[1]: CTD, [2]: LADCP

Table 18. CNV, sample depth, concentration, beam attenuation coefficient and transmission at Station 22.

CNV	Depth (m)	Concentration (mg L^{-1})	Attenuation (m^{-1})	Transmission %
14	846	0.25	0.65	85.0
	797	0.26	0.53	87.6
	698	1.99	0.46	89.2
	601	0.15	0.46	89.1
	501	0.80	0.41	90.2
	401	0.52	0.36	91.3
	300	0.96	0.38	91.0
	200	1.26	0.41	90.3

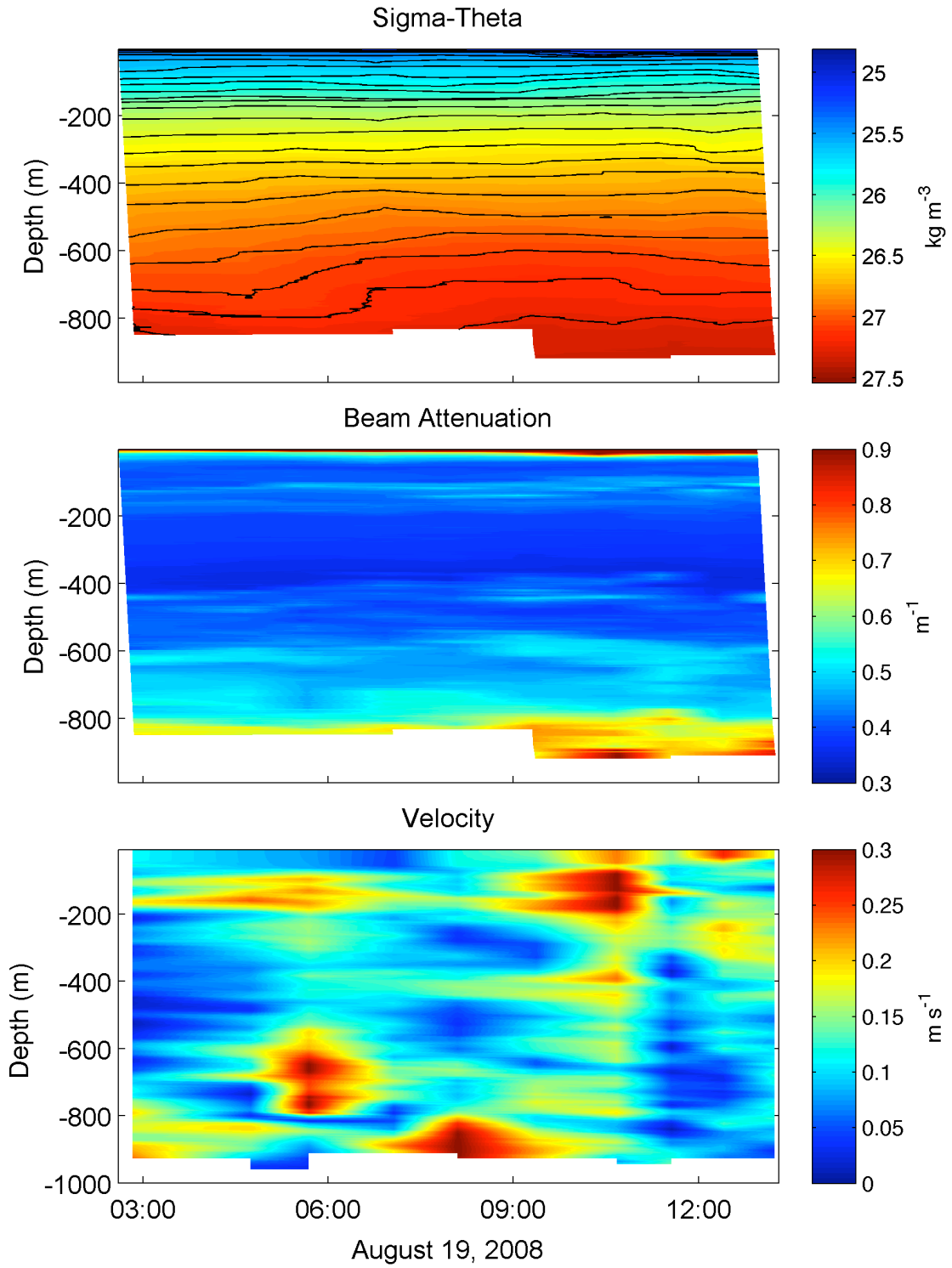

Figure 23. (*top*) Sigma-theta (kg m^{-3}), (*middle*) beam attenuation (m^{-1}), and (*bottom*) velocity magnitude (m s^{-1}) time series at Station 22.

6 STATION 21

There were twelve casts sampled at station 21 on August 24, 2008, and an additional cast was sampled on August 31, 2008 (Table 19). The station was located at the mouth of Soquel Canyon, at 36° 47.466' N and 121° 59.898' W, 31.0 km from the head of the canyon. The average CTD depth was 745 m, and the average LADCP depth was 745 m. Bottom mixed layers were observed in four casts and heights ranged from 28 – 32 m. H_{WS} were 19 – 91 m, and H_S were 30 – 162 m.

The bottom isopycnal (27.0706 kg m^{-3}) was displaced 85 m (from 720 m to 635 m) in 7 hours starting around 7:00 (Figure 24). The isopycnal at 26.9763 kg m^{-3} was displaced from 645 to 555 m in 8 hours. The isopycnals dropped from 3 – 07:00, and after that the isopycnals continued to rise. The beam attenuation coefficient values were greater (0.6 – 0.7 m^{-1}) at the start and end of the time series, and values were greater at depths > 600 m (Table 20). Near-bottom velocities from the LADCP were greatest (0.15 – 0.2 m s^{-1}) between 3 and 4:00 and 6 and 8:00.

Table 19. CNV profile, LADCP profile, time, depth, and bottom boundary layer heights at Station 21.

CNV	LADCP	Time	Depth[1] (m)	Depth[2] (m)	H_{BML} (m)	H_{WS} (m)	H_S (m)
81	81	2:23:00	771	771	-	26	106
82	82	3:26:00	748	749	-	19	60
83	83	4:30:00	760	758	29	37	57
84	84	5:28:12	748	744	-	64	77
85	85	6:28:00	775	775	-	38	120
86	86	7:33:30	744	758	-	32	103
87	87	8:31:41	730	733	-	91	106
88	88	9:32:00	774	769	-	57	30
89	89	10:44:00	638	640	28	50	32
90	90	11:35:08	742	743	31	61	35
91	91	12:38:00	767	765	-	45	162
92	92	13:29:00	753	750	32	74	148
170	170	12:20:00	734	736	-	58	147

[1]: CTD, [2]: LADCP

Table 20. CNV, sample depth, concentration, beam attenuation coefficient and transmission at Station 21.

CNV	Depth (m)	Concentration (mg L^{-1})	Attenuation (m^{-1})	Transmission (%)
82	709	0.27	0.60	86.1
	679	0.49	0.55	87.2
	599	0.52	0.43	89.9
	518	0.15	0.44	89.7
	479	0.60	0.40	90.6
	401	0.42	0.42	90.1
	360	0.07	0.40	90.6
	200	0.21	0.37	91.3

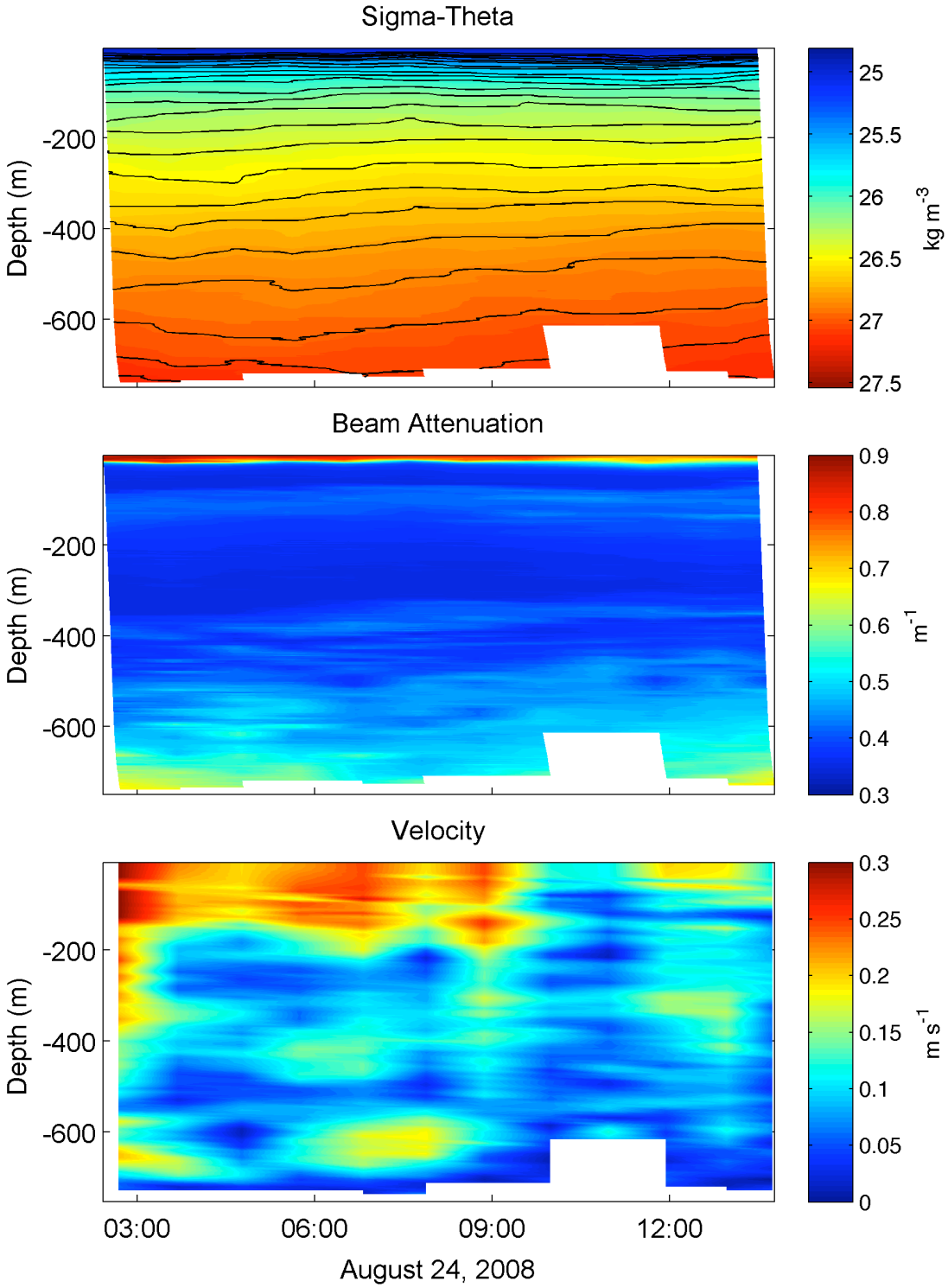

Figure 24. (*top*) Sigma-theta (kg m^{-3}), (*middle*) beam attenuation (m^{-1}), and (*bottom*) velocity magnitude (m s^{-1}) time series at Station 21.

7 STATION 16

Twelve casts were completed at station 16 on August 22, 2008, and an additional cast was sampled on August 31, 2008 (Table 21). The station was located at 36° 46.212' N and 121° 59.194' W, 29.2 km from the head of the canyon. The average CTD depth was 778 m, while the average LADCP depth was 792 m. Bottom mixed layers were not present at this station. H_{WS} were 28 – 77 m, and shear layer thicknesses were 23 – 67 m.

The bottom isopycnal (27.1649 kg m^{-3}) was displaced 20 m (from 700 m to 680 m) in 1 hour (Figure 25). The isopycnal above that (27.0706 kg m^{-3}) was displaced 95 m (from 710 to 615 m) in 6 hours. Beam attenuation coefficient values were greater at the start and end of the time series. Greater amounts of suspended sediment were observed higher in the water column associated with increased velocities. Bottom velocities were greater from 07:00 until the end of the sampling period.

Table 21. CNV profile, LADCP profile, time, depth, and bottom boundary layer heights at Station 16.

CNV	LADCP	Time	Depth[1] (m)	Depth[2] (m)	H_{BML} (m)	H_{WS} (m)	H_S (m)
60	60	3:01:36	750	750	-	56	60
61	-	4:05:00	804	-	-	36	-
62	62	4:55:58	776	777	-	44	28
63	-	5:49:00	774	-	-	51	-
64	64	6:37:00	749	750	-	58	24
65	-	7:25:48	635	-	-	68	-
66	66	8:09:00	876	877	-	73	67
67	-	9:09:00	705	-	-	28	-
68	68	9:59:00	703	706	-	50	53
69	-	10:57:00	832	-	-	39	-
70	70	11:52:00	771	770	-	57	23
71	-	12:54:53	835	-	-	77	-
168	168	10:30:00	907	911	-	48	-

[1]: CTD, [2]: LADCP

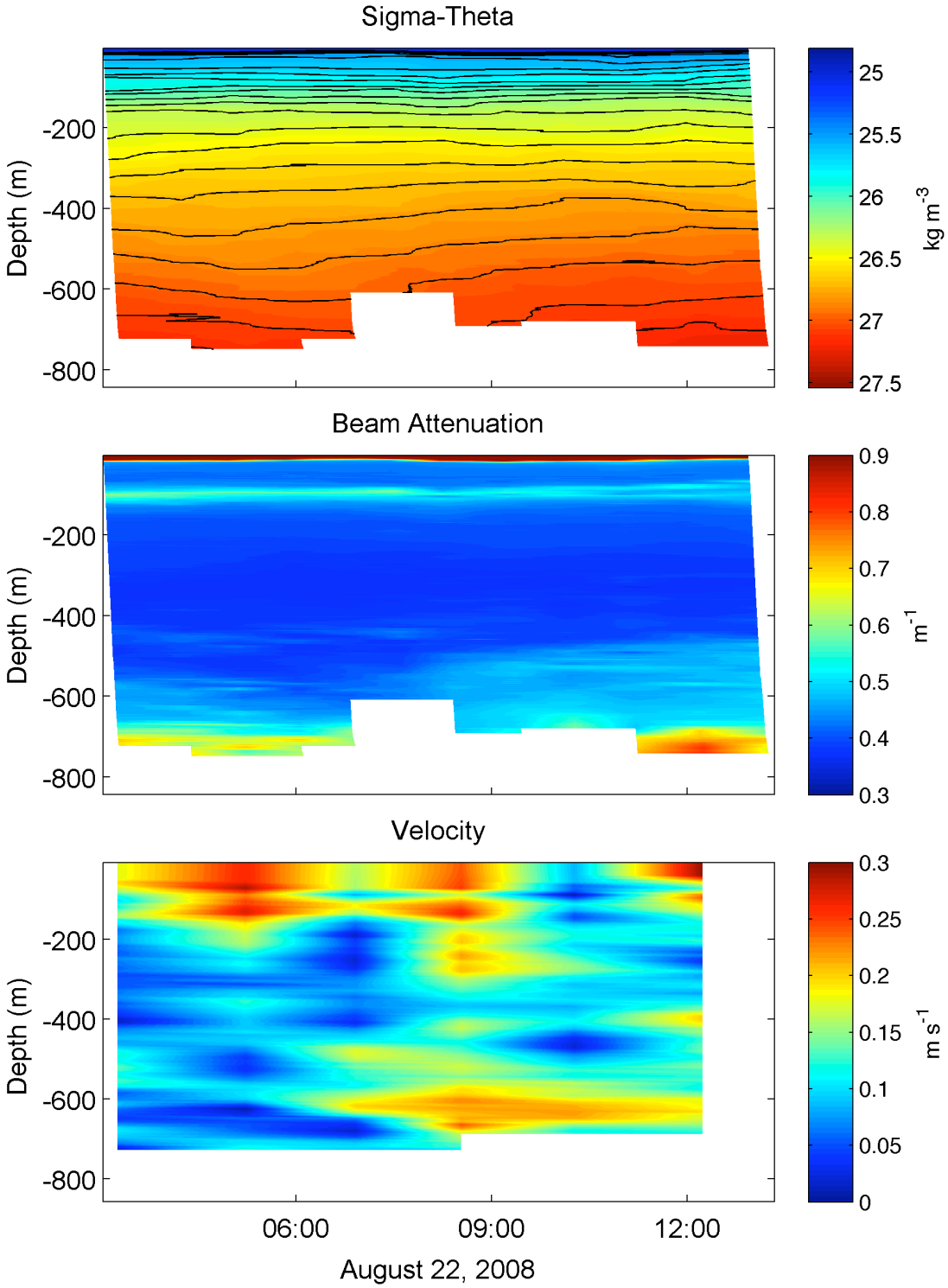

Figure 25. (*top*) Sigma-theta (kg m^{-3}), (*middle*) beam attenuation (m^{-1}), and (*bottom*) velocity magnitude (m s^{-1}) time series at Station 16.

8 STATION 19

There were seven profiles sampled at station 19 on August 29, 2008, and an additional profile sampled on August 31, 2008 (Table 22). The station was located in the Soquel Canyon at 36° 48.400' N and 121° 59.500' W, at an along-canyon distance of 29.0 km, which was the distance relative to station 22 at the mouth of Soquel Canyon. This station was the fourth shallowest station; the average CTD depth was 592 m and the average LADCP depth was 594 m. H_{BML} were observed in two profiles and measured 26 and 31 m. H_{WS} were 29 – 57 m, and H_S were 22 – 153 m.

The isopycnal 26.8821 kg m^{-3} was displaced 70 m from 540 to 470 m after 1.5 hours at the start of the survey (Figure 26). The isopycnal was then displaced back down to 545 m after 8 hours. Beam attenuation coefficient values were high between 75 and 150 m, measuring 0.5 – 0.6 m^{-1}. This layer corresponds with sediment transport from the continental shelf. Beam attenuation values were greater at depths below 450 m and were around 0.6 m^{-1} (Table 23). Velocity magnitude from the LADCP showed increased velocities near the bottom between 03:00 and 05:00 and 07:00 and 09:00. Velocities were also increased near the bottom towards the end of the sampling interval, around 12:00.

Table 22. CNV profile, LADCP profile, time, depth, and bottom boundary layer heights at Station 19.

CNV	LADCP	Time	Depth[1] (m)	Depth[2] (m)	H_{BML} (m)	H_{WS} (m)	H_S (m)
132	132	02:45:51	597	598	-	29	68
134	134	04:17:00	596	597	-	47	40
136	136	05:48:00	603	603	31	52	-
138	138	07:14:50	606	606	-	57	22
140	140	08:47:00	599	600	-	56	24
142	142	10:44:00	579	581	26	33	49
144	144	12:29:00	571	578	-	40	*
171	171	13:21:00	588	590	-	45	153

* Shear layer not quantified due to strong near-bottom velocities.
[1]: CTD, [2]: LADCP

Table 23. CNV, sample depth, concentration, beam attenuation coefficient and transmission at Station 19.

CNV	Depth (m)	Concentration (mg L^{-1})	Attenuation (m^{-1})	Transmission (%)
140	579	0.30	0.62	85.6
	549	0.40	0.64	85.3
	499	0.44	0.56	87.0
	479	0.45	0.52	87.7
	440	0.27	0.52	87.8
	400	0.88	0.46	89.2
	300	0.50	0.36	91.4
	130	0.65	0.54	87.4

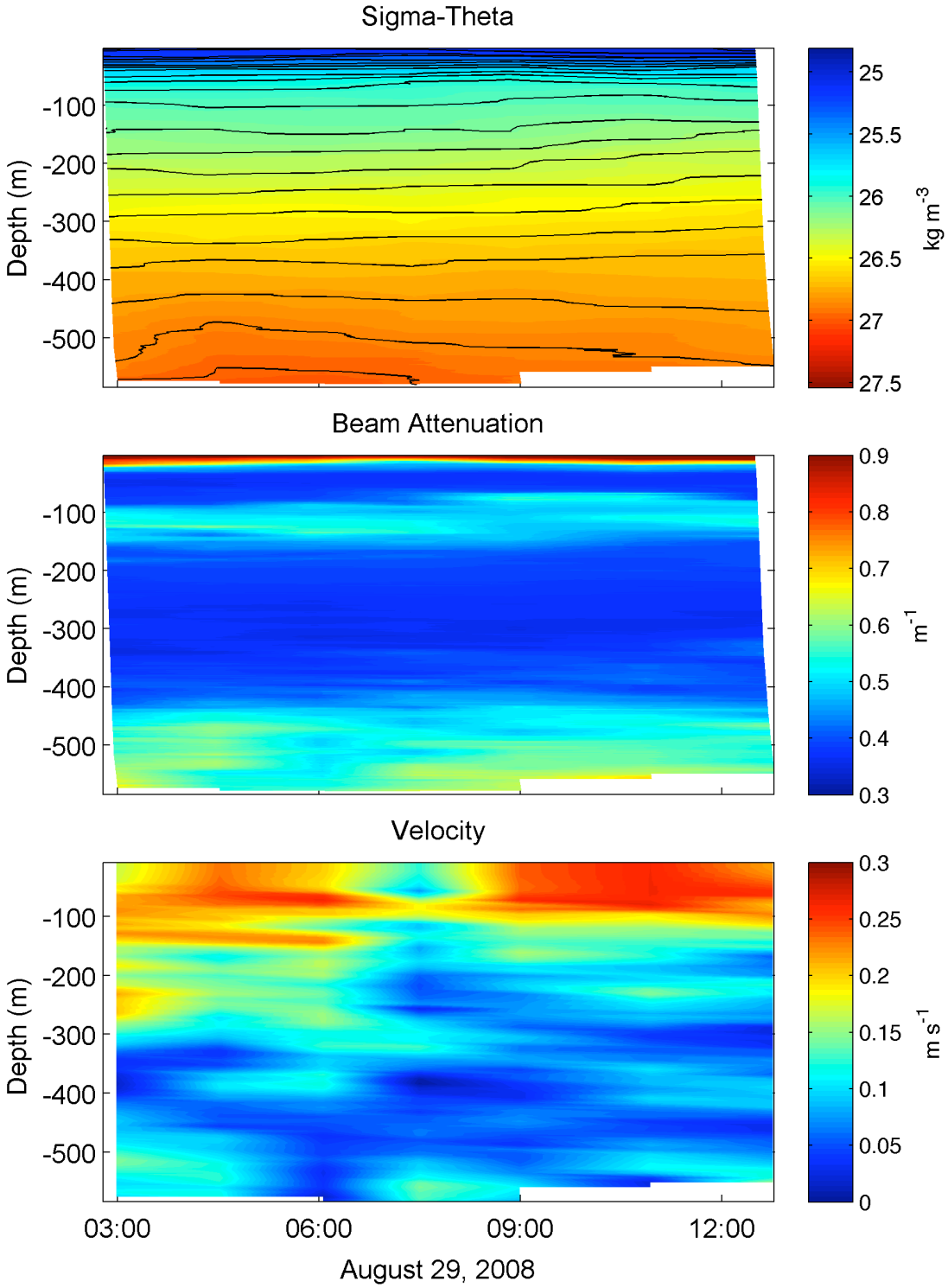

Figure 26. (*top*) Sigma-theta (kg m^{-3}), (*middle*) beam attenuation (m^{-1}), and (*bottom*) velocity magnitude (m s^{-1}) time series at Station 19.

9 STATION 17

There were eight casts sampled at station 17 on August 29, 2008, and an additional profile sampled on August 31, 2008 (Table 24). The station was located at the head of the Soquel Canyon at 36° 49.500' N and 121° 58.600' W, at an along-canyon distance of 27.5 km, which was the distance relative to station 22 at the mouth of the Soquel Canyon. It was the shallowest station measured; the average CTD depth was 407 m, and the average LADCP depth was 411 m. Bottom mixed layers were not observed at this station, and H_{WS} were between 24 and 59 m. H_S were 26 – 92 m.

The bottom isopycnal (26.6935 kg m^{-3}) was displaced 50 m, from 400 m to 350 m in 4 hours from 02:00-06:00 (Figure 27). The isopycnal at 26.5992 kg m^{-3} was displaced 40 m from 345 to 305 m at the start of the sampling period in about 4 hours and was displaced back down to 340 m after 3.5 hours. Beam attenuation coeffficient values were low near the bottom and were greatest between 03:00 and 07:00 and were around 0.6 m^{-1}. Beam attenuation values were greater between 80 m and 180 m and were 0.6 – 0.8 m^{-1}, likely resulting from sediment transport off the continental shelf. Velocities reported from the LADCP were reduced near the bottom, reaching maximum values of ~0.15 m s^{-1} at the start of the time series. Velocities were slightly greater again around 08:00.

Table 24. CNV profile, LADCP profile, time, depth, and bottom boundary layer heights at Station 17.

CNV	LADCP	Time	Depth[1] (m)	Depth[2] (m)	H_{BML} (m)	H_{WS} (m)	H_S (m)
131	131	02:03:00	430	430	-	31	26
133	133	03:36:00	422	423	-	50	28
135	135	05:04:01	427	428	-	59	33
137	137	06:34:00	383	410	-	30	40
139	139	08:05:00	425	426	-	32	*
141	141	09:56:00	377	385	-	33	*
143	143	11:32:00	396	390	-	24	71
145	145	13:21:00	420	421	-	38	27
173	173	14:44:00	382	384	-	50	92

* Shear layer not quantified due to strong near-bottom velocities.
[1]: CTD, [2]: LADCP

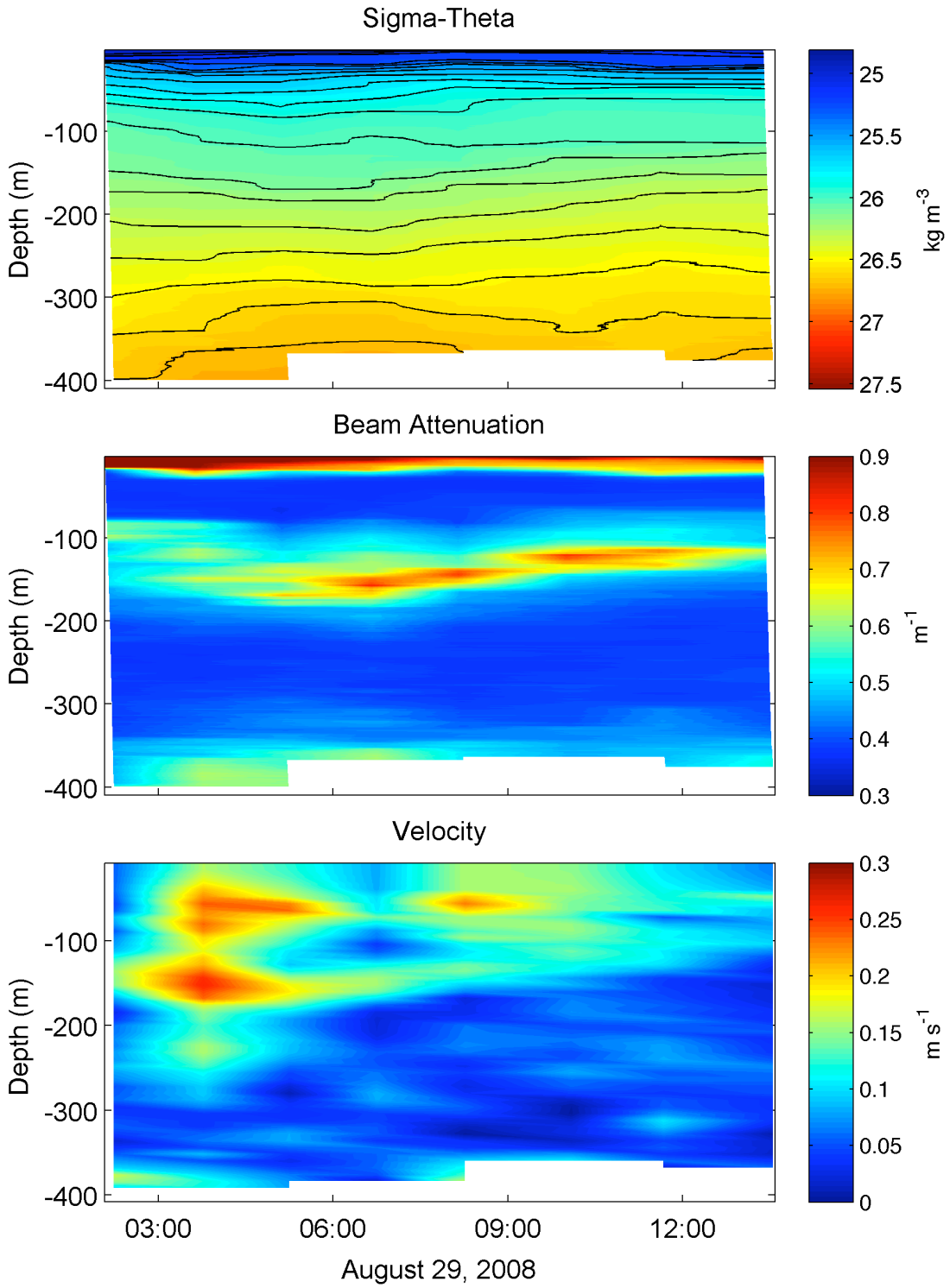

Figure 27. (*top*) Sigma-theta (kg m^{-3}), (*middle*) beam attenuation (m^{-1}), and (*bottom*) velocity magnitude (m s^{-1}) time series at Station 17.

10 STATION 12

There were twelve casts sampled at station 12 on August 27, 2008, and an additional cast was sampled on August 31, 2008 (Table 25). The station was the third closest to the canyon head (24.0 km) and was located at 36° 46.800' N and 121° 57.000' W. The average CTD depth was 732 m, while the average LADCP depth was 733 m. Bottom mixed layers were observed at only two of the stations, reaching a maximum of 29 m. H_{WS} were 35 – 101 m, and H_S were 13 – 240 m.

The deepest isopycnal (27.0706 kg m^{-3}) was displaced by 40 m from 660 to 700 m in 3 hours (Figure 28). After 2 hours, the isopycnal was displaced 70 m to 630 m and back down to 665 m in 2.5 hours. Suspended sediment concentrations were high near the bottom (depths > 450 m), where values were 0.8 – 1.2 m^{-1}, and concentrations were up to 2.16 mg L^{-1} (Table 26). Near-bottom velocities were small, usually less than 0.1 m s^{-1}. Values were greatest around 10:30, and due to the increased velocities at that time, shear layer thickness was not measured.

Table 25. CNV profile, LADCP profile, time, depth, and bottom boundary layer heights at Station 12.

CNV	LADCP	Time	Depth[1] (m)	Depth[2] (m)	H_{BML} (m)	H_{WS} (m)	H_S (m)
112	112	2:40:00	720	722	-	65	13
113	113	3:35:00	689	692	-	40	210
114	114	4:28:00	758	759	-	48	*
115	115	5:29:18	720	722	29	44	*
116	116	6:28:00	755	757	-	69	50
117	117	7:37:00	755	756	-	62	49
118	118	8:37:00	754	755	-	49	197
119	119	9:48:54	714	717	-	54	*
120	120	10:40:00	746	746	-	101	*
121	121	11:33:00	745	745	-	35	112
122	122	12:24:41	747	747	28	80	38
123	123	13:24:00	757	758	-	53	240
165	165	8:06:00	657	659	-	83	78

* Shear layer not quantified due to strong near-bottom velocities.
[1]: CTD, [2]: LADCP

Table 26. CNV, sample depth, concentration, beam attenuation coefficient and transmission at Station 12.

CNV	Depth (m)	Concentration (mg L^{-1})	Attenuation (m^{-1})	Transmission (%)
116	730	2.11	1.15	75.0
	730	1.76	1.16	74.8
	719	2.16	1.04	77.2
	699	1.99	1.08	76.3
	676	1.67	0.94	79.2
	639	1.01	0.70	83.9
	599	0.50	0.57	86.7
	479	0.43	0.48	88.7

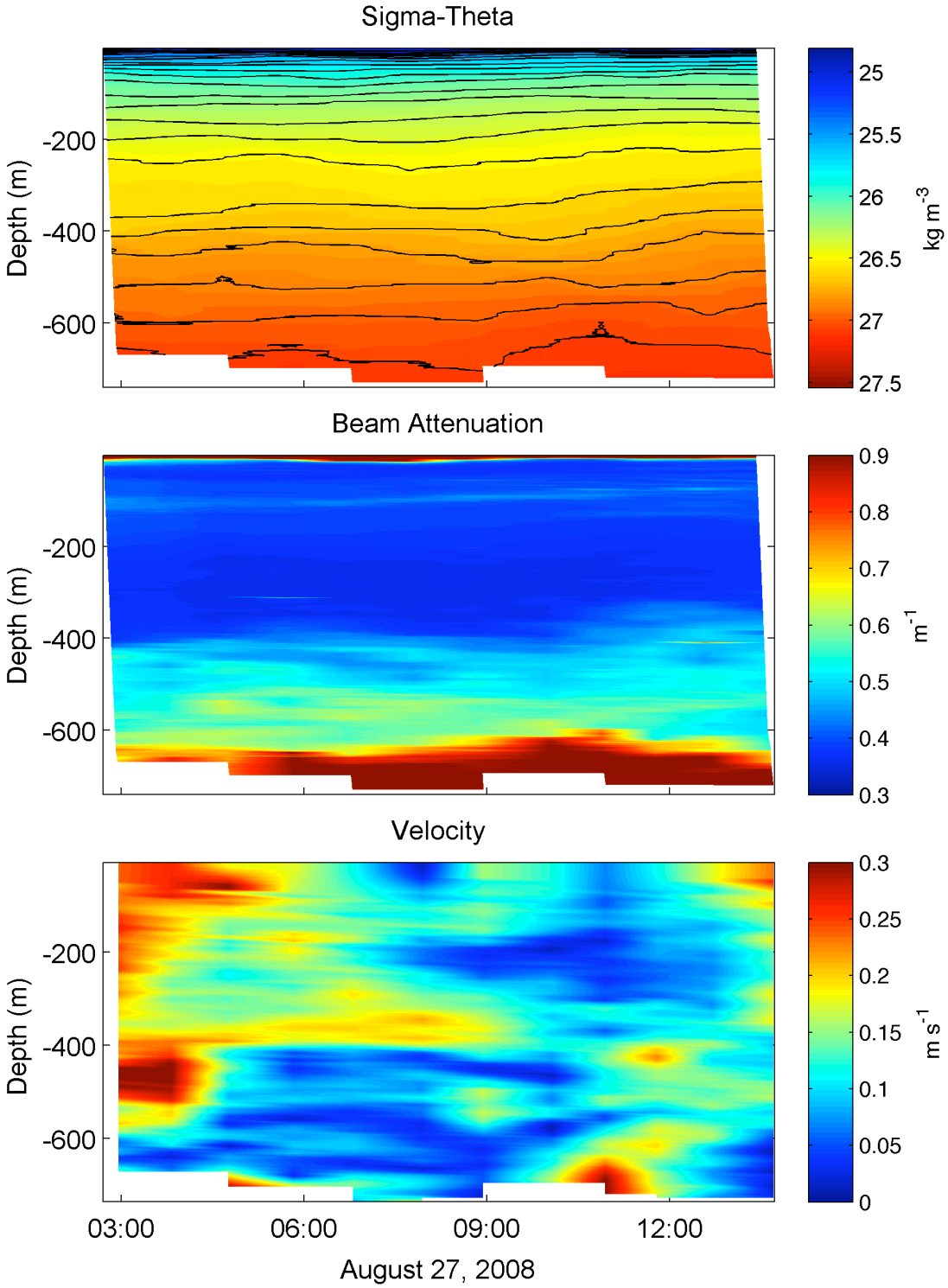

Figure 28. (*top*) Sigma-theta (kg m^{-3}), (*middle*) beam attenuation (m^{-1}), and (*bottom*) velocity magnitude (m s^{-1}) time series at Station 12.

11 STATION 9

There were sixteen casts completed at station 9 from August 21-22, 2008 and an additional cast sampled on August 31, 2008 (Table 27). The station was located at 36° 46.530' N and 121° 54.850' W, 19.9 km from the head of the canyon, making it the second closest station to the canyon head. The average CTD depth was 542 m, while the average LADCP depth was 556 m. Bottom mixed layers were 32 - 46 m, and H_{WS} were 33 – 79 m. Shear layer heights were 20 – 253 m.

The bottom isopycnal (26.8821 kg m^{-3}) was displaced 40 m (from 460 to 500 m) in two hours (Figure 29), and the isopycnal at 26.7878 kg m^{-3} was displaced 60 m (from 455 m to 395) m in 2 hours. Beam attenuation values were greater (0.6 – 0.9 m^{-1}) around 80 m, and values were greatest at the end of the time series. Beam attenuation values were also elevated (0.6 – 0.9 m^{-1}) near the bottom at depths below 450 m. The deeper casts at this station had greater suspended sediment. Velocities were typically less than 0.15 m s^{-1} near the bottom. At depths between 350 and 425 m and from 20:00 – 22:00, velocities were increased, and after this period, isopycnals were more displaced.

Table 27. CNV profile, LADCP profile, time, depth, and observed bottom boundary layer heights at Station 9.

CNV	LADCP	Time	Depth[1] (m)	Depth[2] (m)	H_{BML} (m)	H_{WS} (m)	H_S (m)
44	44	15:50:00	598	606	-	-	*
45	-	16:30:00	580	-	-	47	-
46	46	17:01:00	624	626	-	53	153
47	-	17:45:00	552	-	-	36	-
48	48	18:16:00	554	559	-	-	20
49	-	18:55:00	470	-	-	33	-
50	50	19:32:00	455	460	35	46	63
51	-	20:07:00	619	-	33	36	-
52	52	21:05:00	579	582	34	62	*
53	-	21:47:00	399	-	46	50	-
54	54	22:18:00	597	603	32	49	253
55	-	23:00:00	526	-	-	50	-
56	56	23:47:00	506	496	-	-	*
57	-	0:32:00	544	-	-	68	-
58	58	1:14:00	484	490	-	61	36
59	-	1:54:00	542	-	-	79	-
158	158	3:11:00	578	581	-	53	*

Casts in blue did not reach within 50 m of the bottom.

* Shear layer not quantified due to strong near-bottom velocities.

[1]: CTD, [2]: LADCP

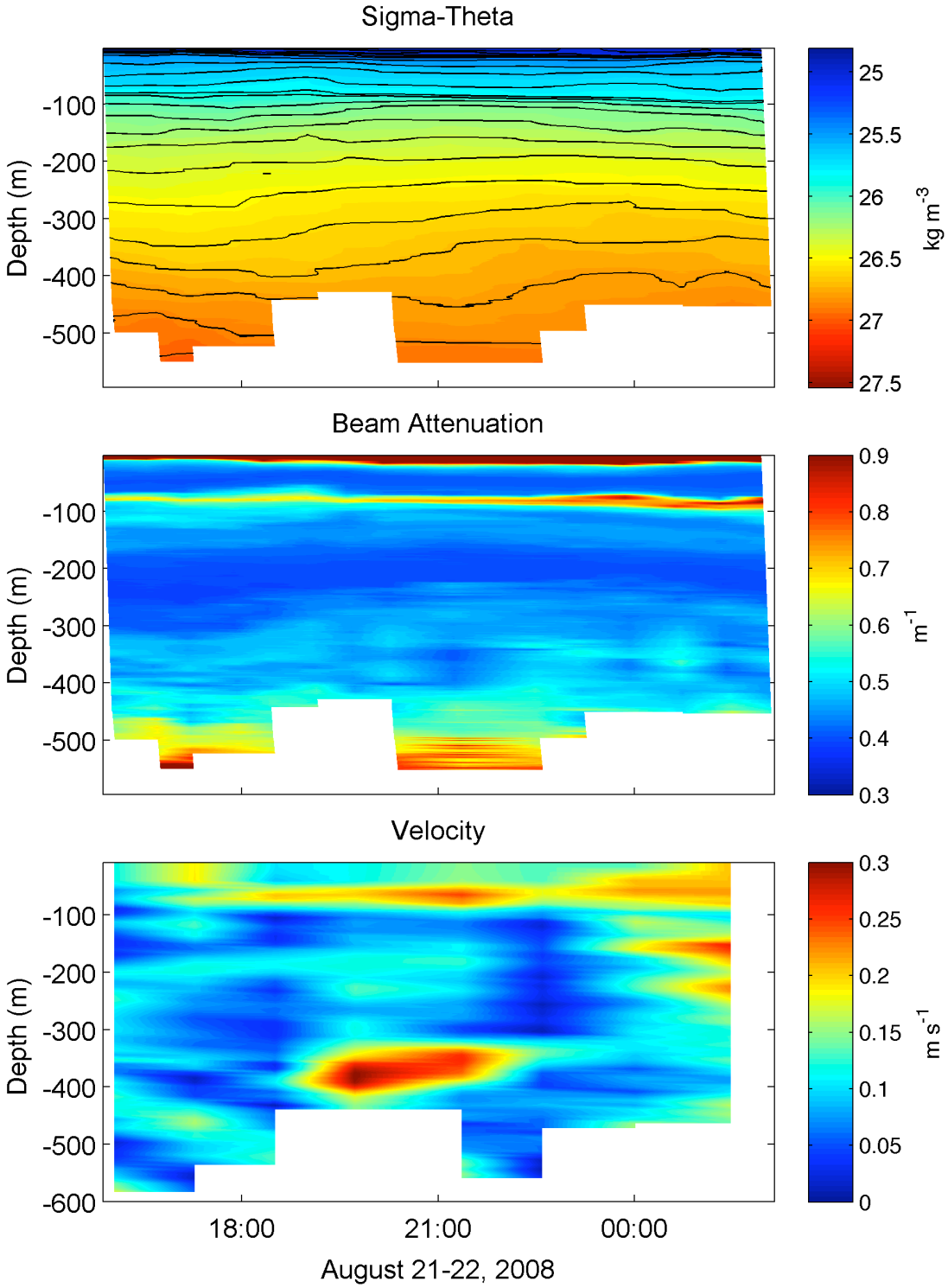

Figure 29. (*top*) Sigma-theta (kg m^{-3}), (*middle*) beam attenuation (m^{-1}), and (*bottom*) velocity magnitude (m s^{-1}) time series at Station 9.

12 STATION 7

There were nine casts sampled at station 7 on August 26, 2008 (Table 28). The station was the closest to the canyon head (16.0 km) and was located at 36° 47.268' N and 121° 54.220' W. The average CTD depth was 496 m, while the average LADCP depth was 500 m. Neglecting the stations sampled in Soquel Canyon, this was the shallowest station along the main axis. Bottom mixed layers were observed in only two of the profiles. Weakly stratified layers were 13 – 39 m, and shear layer thicknesses were 33 – 94 m.

The bottom isopycnal (26.8821 kg m^{-3}) was displaced 15 m (from 475 m to 460 m) in 2 hours and back down 15 m in 1.5 hours (Figure 30). The isopycnal at 26.7878 kg m^{-3} was displaced ~20 m back and forth between 405 and 425 m depth at several points in the time series. Beam attenuation was greater at depths below 400 m. Velocities from the LADCP were greatest from 07:00 – 11:00 corresponding with thicker bottom boundary layer features.

Table 28. CNV profile, LADCP profile, time, depth, and observed bottom boundary layer heights at Station 7.

CNV	LADCP	Time	Depth[1] (m)	Depth[2] (m)	H_{BML} (m)	H_{WS} (m)	H_S (m)
103	103	6:53:00	464	522	-	-	33
104	104	7:49:33	475	477	-	27	*
105	105	8:31:00	492	495	-	42	*
106	106	9:19:28	530	528	-	54	52
107	107	10:13:00	484	486	-	49	*
108	108	10:57:00	503	508	-	42	41
109	109	11:53:41	535	493	-	-	82
110	110	12:52:00	493	498	-	36	94
111	111	13:30:43	491	496	7	49	85

Casts in blue did not reach within 50 m of the bottom.
* Shear layer not quantified due to strong near-bottom velocities.
[1]: CTD, [2]: LADCP

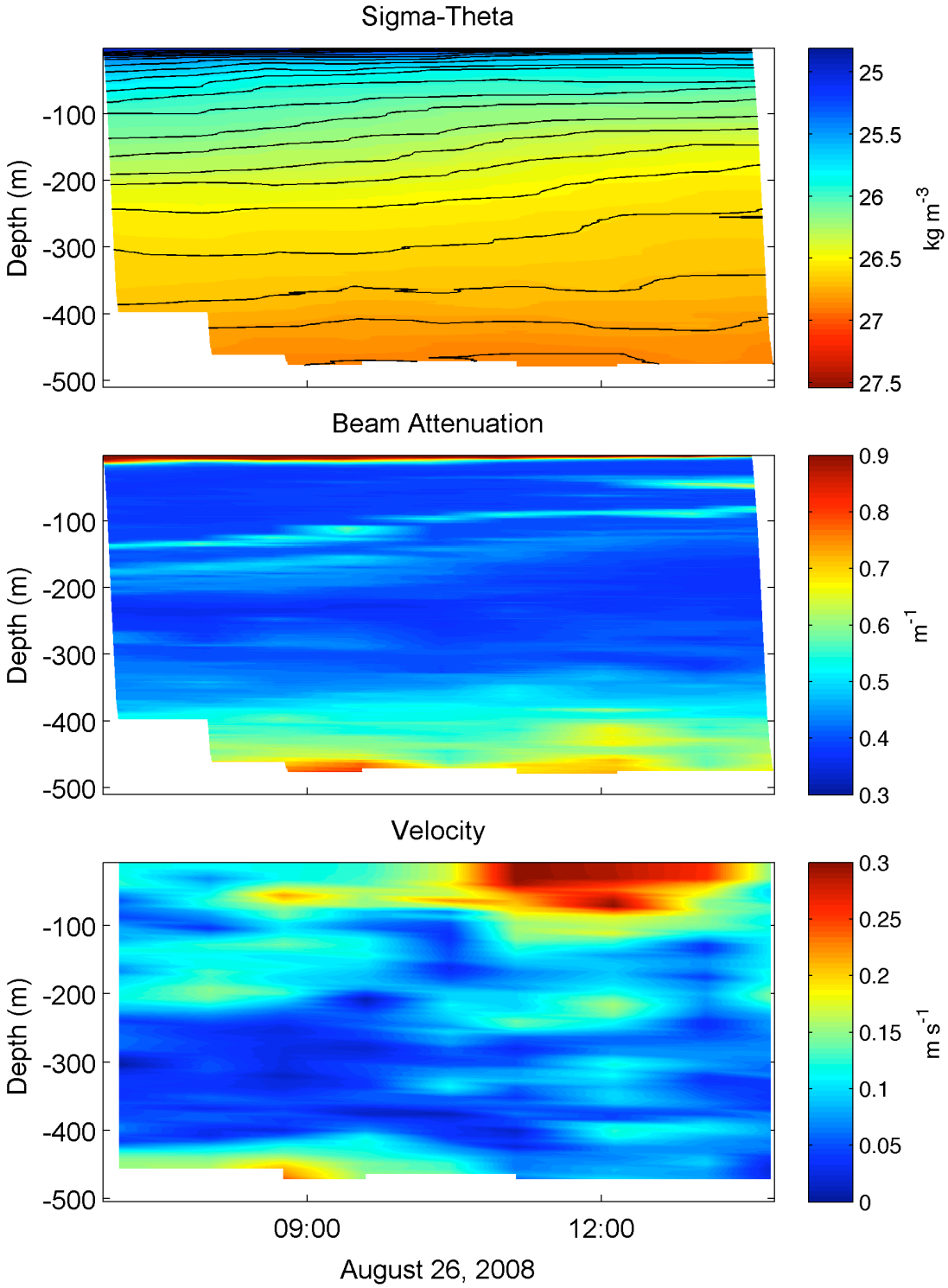

Figure 30. (*top*) Sigma-theta (kg m^{-3}), (*middle*) beam attenuation (m^{-1}), and (*bottom*) velocity magnitude (m s^{-1}) time series at Station 7.

d. Overview of Observations

The observed bottom boundary layer heights from the CTD time series, including H_{BML} and H_{WS} varied spatially and temporally. Isopycnal displacements were often associated with changes in near-bottom velocities. After velocities increased, isopycnals were displaced upwards, and heights also changed in response to the increased velocities and displaced isopycnals.

Beam attenuation coefficient patterns often followed isopycnals. At some stations, clearer water snuck in below water masses with elevated suspended particulate matter. Stations farther out along the canyon axis, past the Monterey Bend, had an intermediate nepheloid layer between 800 and 1000 m depth. Station 12 had the greatest suspended sediment near the bottom, and it was unique among the shallower stations. Stations 9 and 7, which were near Station 12, and at shallower depths, did not have as much suspended sediment near the bottom. The shallow stations in Soquel Canyon, Stations 19 and 17, did not show distinct bottom nepheloid characteristics, but did show a distinct intermediate nepheloid layer around 100 m depth, likely corresponding with suspended sediment originating from the continental shelf. Figure 31 shows the filter weights plotted against the beam attenuation coefficient. The weights were not closely related to beam attenuation coefficient ($R^2 = 0.4472$).

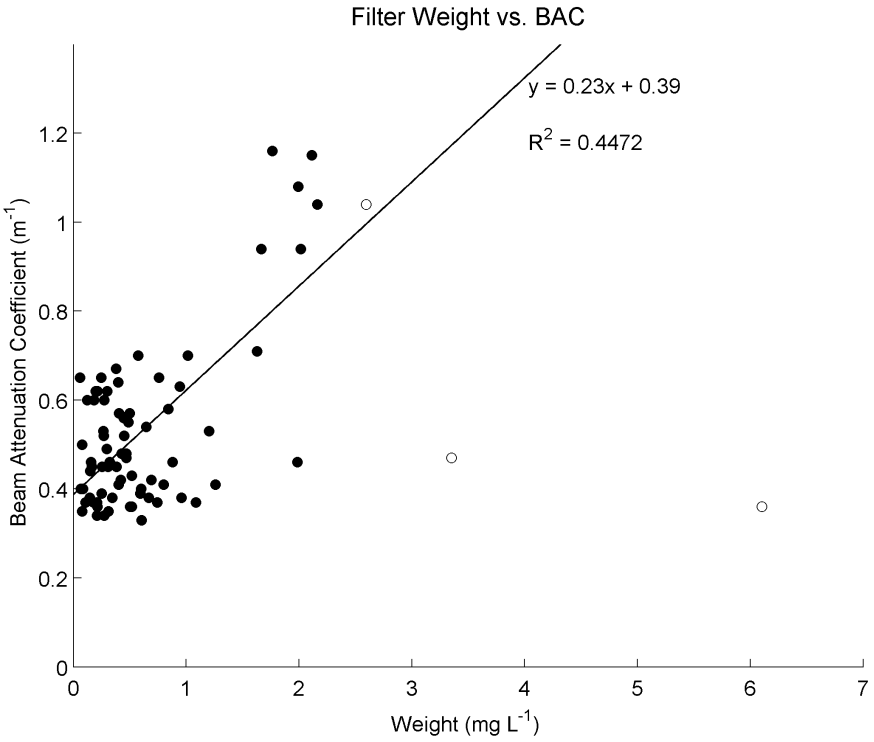

Figure 31. Filter weight (mg L^{-1}) and beam attenuation coefficient. Open dots are two standard deviations from mean. Trendline fitted to closed dots.

Shear velocities estimated from the Law-of-the-Wall were greater than shear velocities calculated from the free-stream velocity and drag coefficient methods. The values were not closely related ($R^2 = 0.00358$) (Figure 32). Shear velocities from the Law-of-the-Wall method were more widely distributed; the mean was 0.01307 ± 0.01084 m s^{-1}. The mean of u_* from XCPs and the drag coefficient method was 0.01106 m s^{-1} ± 0.004471 m s^{-1}. The LADCP data mean u_* from the drag coefficient method was 0.00865 ± 0.003497 m s^{-1}. Shear velocities from the XCP data were greater than shear velocities from the LADCP data. This may be due to the increased vertical resolution of the XCPs, and greater shear over small scales. It may also be due to the fact that the XCP

grid site was selected based on preliminary analysis that identified this region as having greater mixing and increased velocity magnitudes.

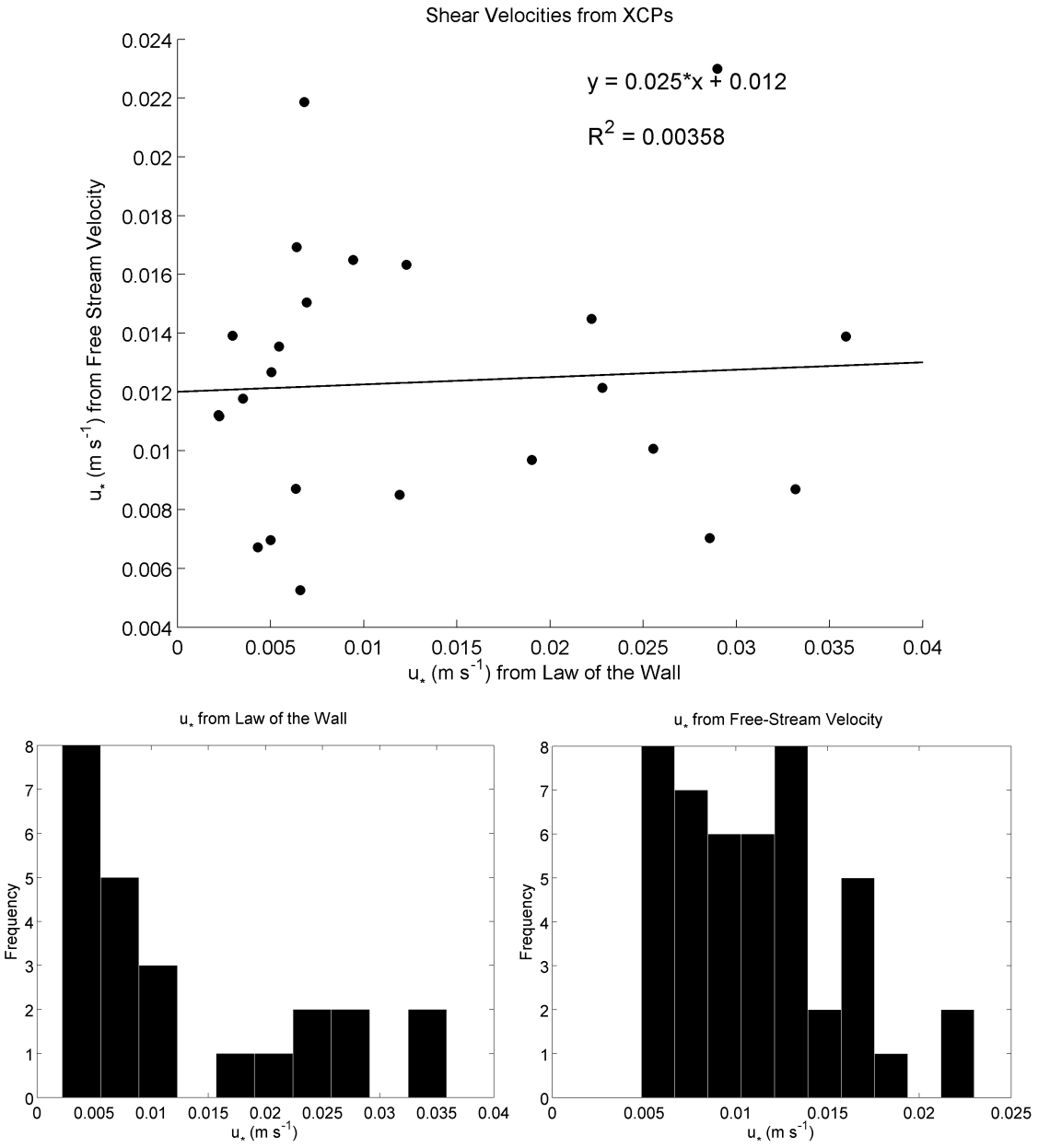

Figure 32. Shear velocities (m s^{-1}) from XCP data. (*top*) Shear velocity calculated from the Law of the Wall versus the shear velocity calculated from the free-stream velocity and $C_d = 3.01 \times 10^{-3}$. (*bottom, left*) Histogram of u_* magnitudes from log fits of XCP profiles. (*bottom, right*) Histogram of u_* magnitudes from drag coefficient and free-stream velocity of XCP profiles.

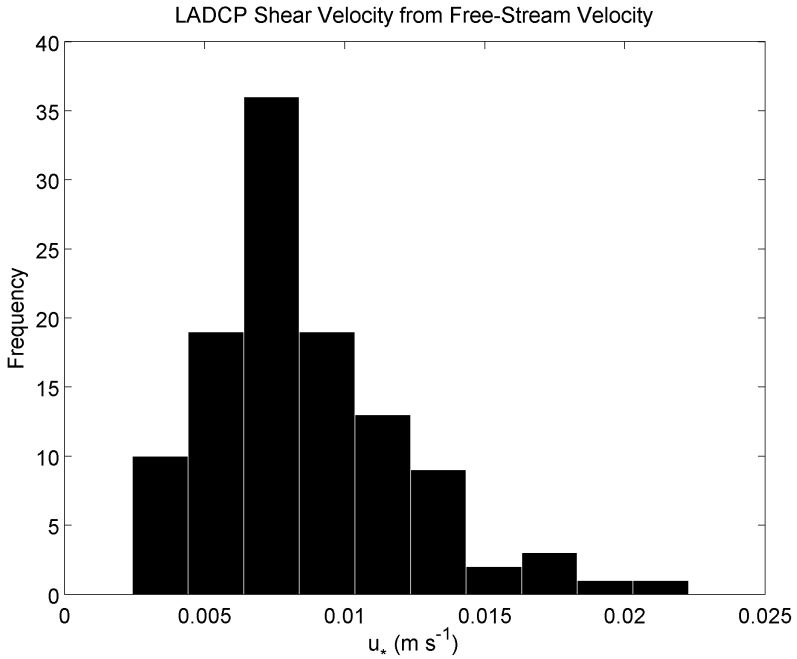

Figure 33. Histogram of u_* magnitudes from LADCP data.

e. Spatial Variations of Observed Heights from Density

Previously the observed bottom boundary layer thicknesses were described for each station; however, this did not address the spatial variations in bottom boundary layer thickness along the canyon axis. The bottom mixed layers, weakly stratified layers, and observed shear layers were plotted against the along canyon-axis distance (Figures 34 – 36). The shear velocities from XCP and LADCP data were also plotted against canyon-axis distance (Figure 37).

Bottom mixed layers were thin or absent along the canyon. Heights were 17 – 56 m (Figure 34). Heights observed along Soquel Canyon and at Station 7, the shallowest station, were thinner than heights observed in deeper portions of the canyon. There were

no bottom mixed layers observed at stations 17, 16, or 44. Overall, H_{BML} were thicker near the Monterey Bend and were reduced in shallower regions of the canyon.

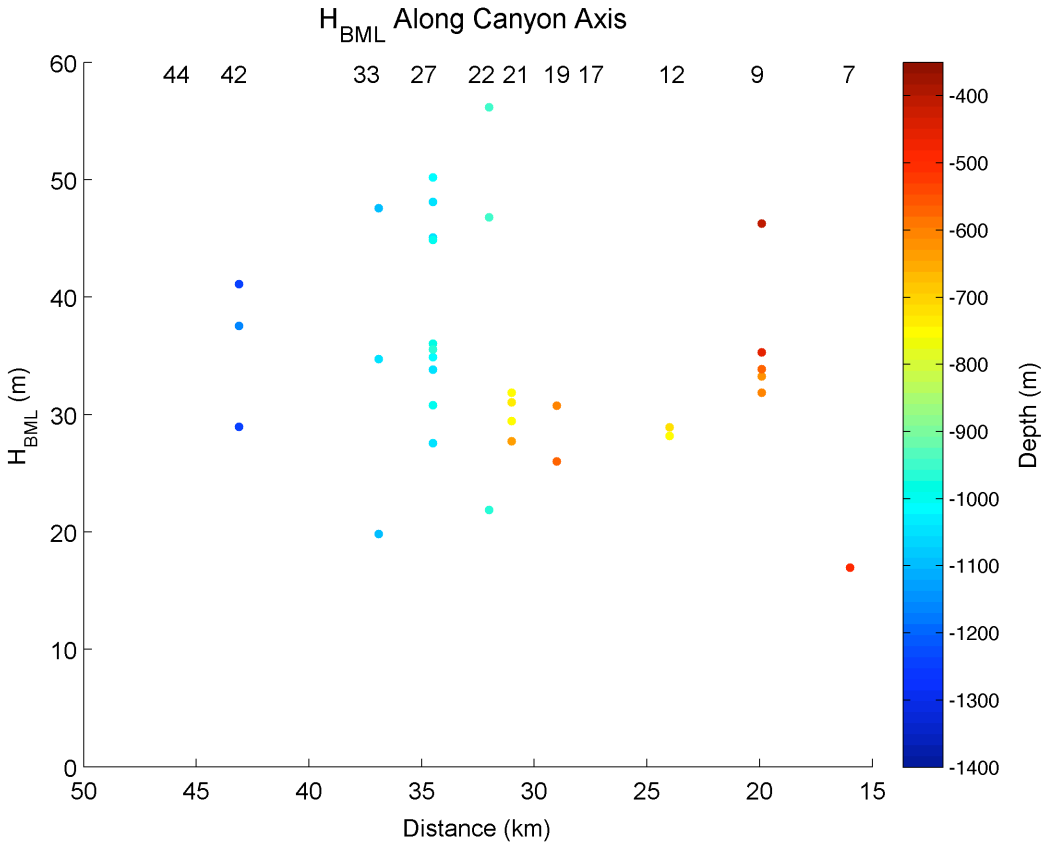

Figure 34. Bottom mixed layer heights along canyon axis. Colorbar represents bottom depth. Station numbers are indicated at top.

H_{WS}, where $[\rho-\rho_b] < 0.03$ kg m^{-3}, were 19 – 181 m for the CTD time series. H_{WS} observed from the VMP profiles were thinner (4 – 78 m). There was an obvious spatial pattern: deeper stations (>900 m) along the canyon axis had thicker weakly stratified layers than stations closer to the head of the canyon (Figure 35). Stations located within the first 31 km along the canyon axis were 4 – 75 m. The shallowest station in the main axis (station 7) and the shallowest stations in Soquel Canyon (stations 17 and 19) were

less than 60 m. The overall trend showed thicker H_{WS} near the canyon mouth and thinner H_{WS} near the heads of Monterey and Soquel Canyon.

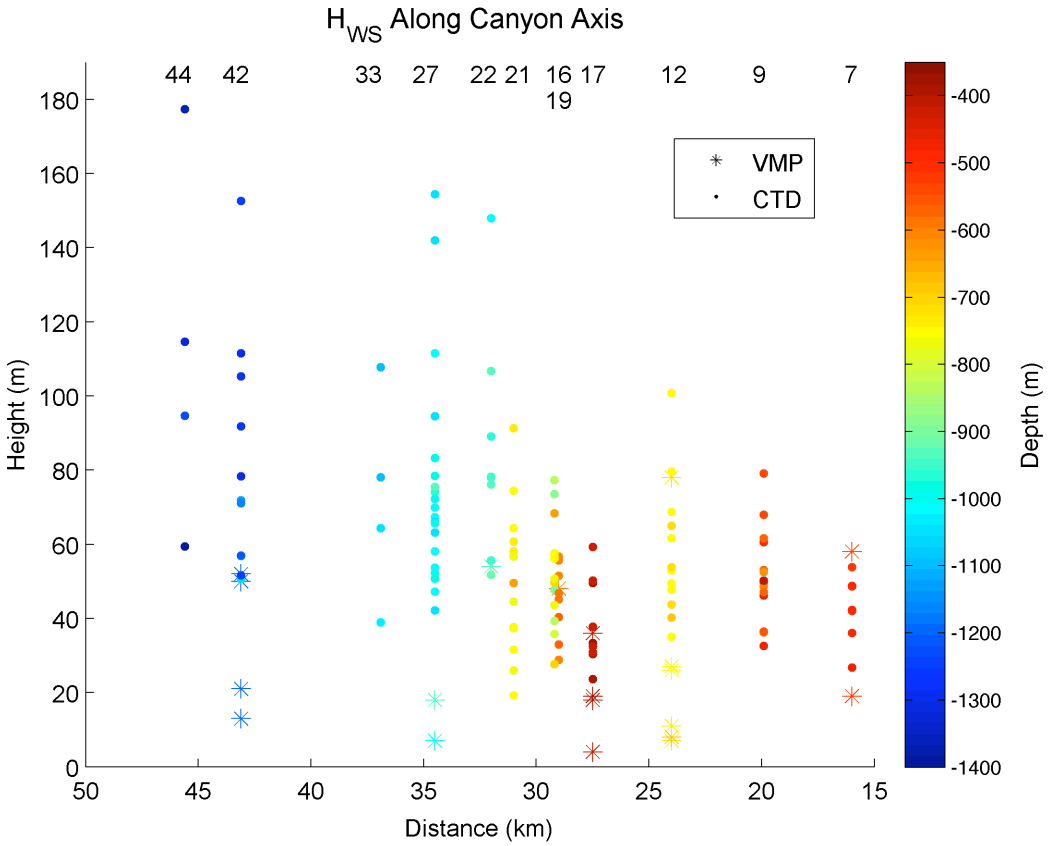

Figure 35. Weakly stratified bottom boundary layers ($[\rho-\rho_b]<0.03$ kg m^{-3}) observed along the canyon axis from VMP and CTD time series. Colorbar represents bottom depth. Station numbers are indicated at top. Each station has multiple casts. Variation at one station reflects temporal variability.

f. Observed Heights and Shear Velocities from LADCP and XCP Time Series

The shear layer heights were determined from the LADCP and XCP profiles and were defined as the height above the bottom where the velocity magnitude was 90% of the free-stream velocity. The heights from the LADCP observations were 13-295 m, and the heights from the XCP observations were 5-130 m (Figure 36). There were no clear

spatial variations. Some of the shallower stations (stations 12 and 9) had thick heights; however, the deeper stations near the Monterey Bend were thicker on average than shallower stations. Heights near the canyon mouth at station 44 were decreased. The LADCP data provided greater spatial coverage than the XCP data for differences along the canyon axis because velocity measurements were collected at each CTD time series station throughout the duration of the cruise from August 18-31, 2008. The XCP data were confined to the bend around the canyon axis from ~34 – 39 km from the head of the canyon. The shear velocities, calculated from the maximum "nose" velocity near the bottom, using a drag coefficient of 3.1×10^{-3} were greater near the Monterey Bend (Figure 37). The general trend shows increasing shear velocities from the canyon head to the mouth.

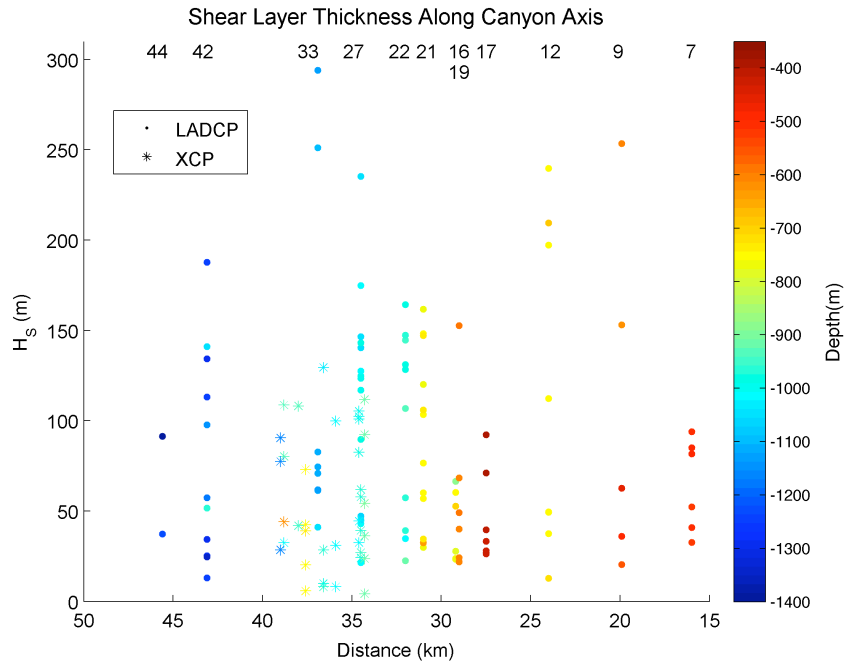

Figure 36. Observed shear layer thicknesses from LADCP and XCP data and canyon-axis distances. Colorbar represents bottom depth. Station numbers are indicated at top.

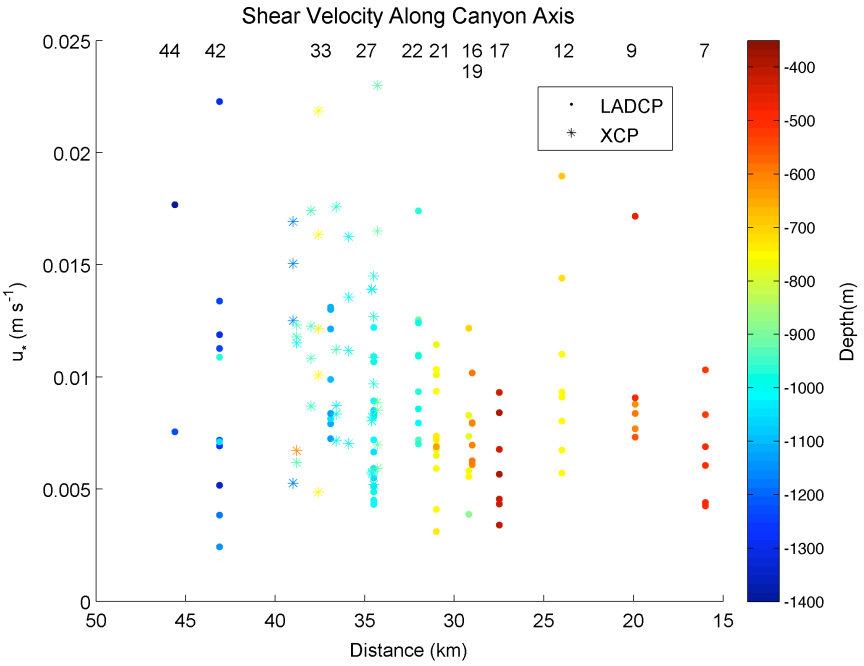

Figure 37. Shear velocities calculated from LADCP and XCP data using the drag coefficient method and $C_d = 3.01 \times 10^{-3}$ and canyon-axis distances. Colorbar represents bottom depth. Station numbers are indicated at top.

g. Observed BBL Heights and Internal Tide

The bottom mixed layer and weakly stratified layer heights from the CTD time series and shear layer heights from the LADCP and XCP time series were plotted against the temperature recorded at the mooring at thermistor 3071 at 1060 m depth to see how heights varied according to the phase of the internal tide. As discussed previously, the spectrum of the temperature time series showed clear diurnal and semidiurnal peaks. Weakly stratified heights were thick when temperatures were cold (Figure 39). Bottom mixed layers did not show any major patterns with phase of the internal tide. Since there were so few observed heights, it was difficult to assess how they varied with the internal tide. Shear layer thicknesses were also thicker when temperatures were at a minimum, and occasionally when temperatures were at a maximum (Figure 40). In some cases, heights were smallest during cold-water pulses. While the heights varied over the 12-hour sampling period, the heights did not show an obvious relationship with the internal tide as recorded by the thermistor.

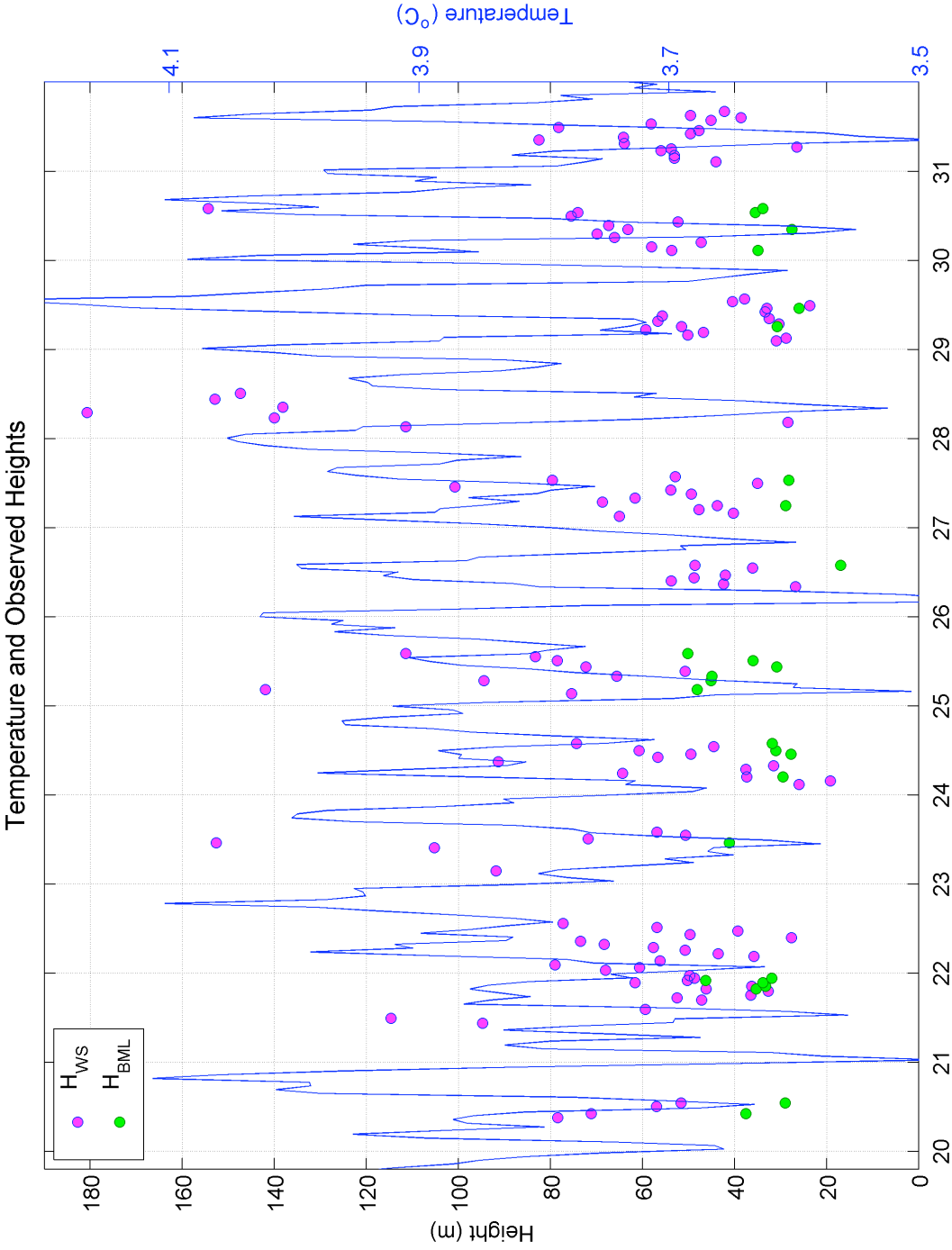

Figure 38. Mooring temperature (°C) and H_{WS} and H_{BML} from CTD.

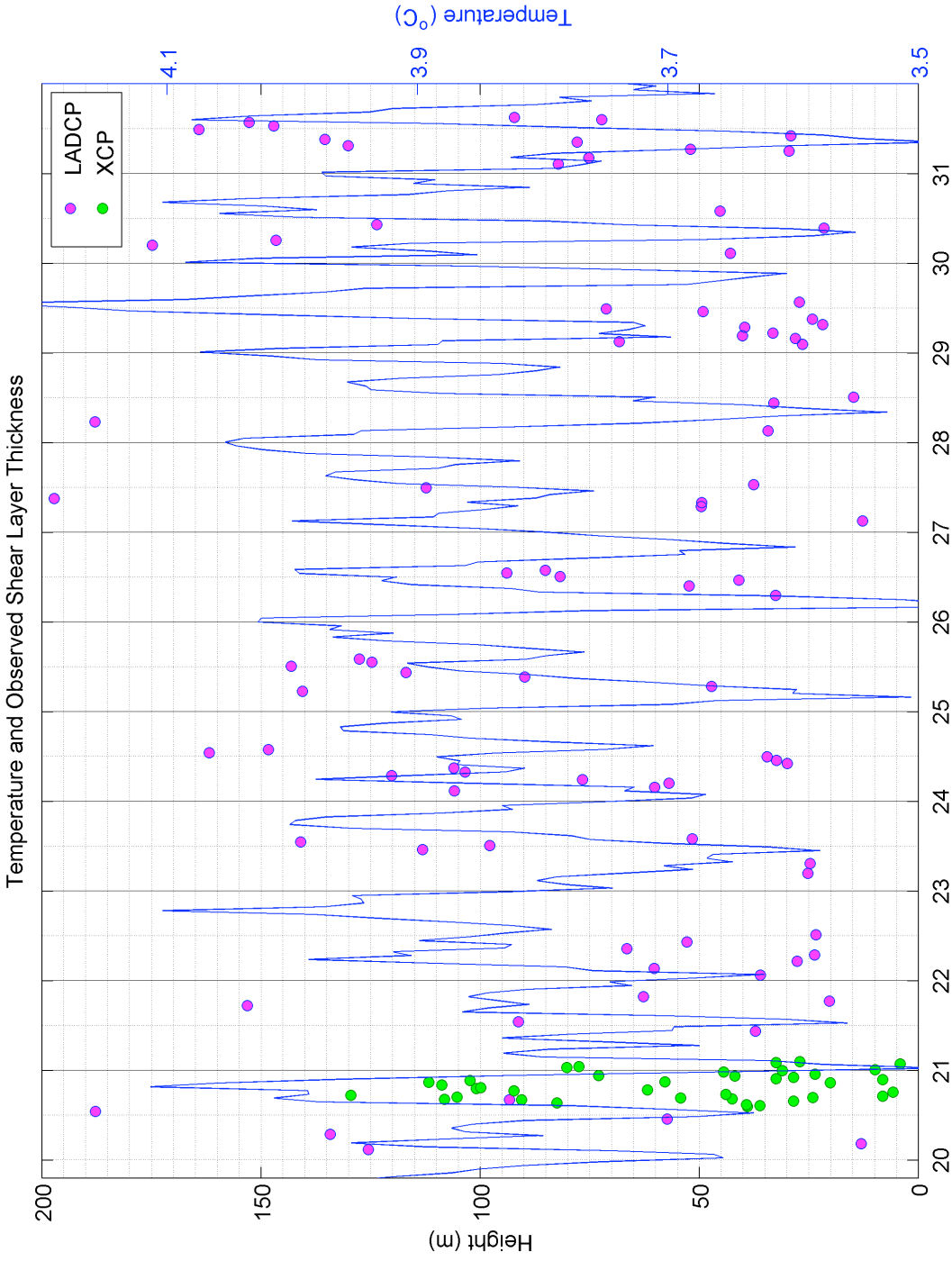

Figure 39. Mooring temperature (°C) and H_S from XCP and LADCP.

6. Discussion

a. Spatial Variations in Bottom Boundary Layers

Density, beam attenuation, and velocity time series were used from the CTD/LADCP time series to investigate the spatial variations in bottom boundary layer structures. Velocity data were used from the XCP time series to describe observed shear layer thicknesses and shear velocities. Smoothed density profiles from the VMP were used to describe weakly stratified layers. The CTD/LADCP time series provided greater spatial coverage of the canyon dynamics than other instrument measurements. The general trend showed thicker observed boundary layers, particularly H_{WS}, at deeper stations (depths > 900 m) at distances greater than 31 km from the canyon head, between the canyon mouth and the Monterey Bend. The shallower stations located near the heads of Monterey Canyon (stations 9 and 7) and Soquel Canyon (stations 17 and 19) had thinner bottom boundary layers than stations at greater depths. Water depth likely limited bottom boundary layer thickness resulting in thicker boundary layer structures at greater depths and thinner heights at shallower depths.

Although we had intended to look at changing bottom boundary layer structures over spatial and temporal scales, false detections of the bottom due to reflections from the canyon walls made it difficult to successfully get within 50 m of the bottom. Since the rosette did not get close enough to the bottom, it was challenging to describe the bottom mixed layer. Of the casts that did get within 50 m or less from the bottom, the altimeter distances were anywhere from 10 – 40 m, which created quite a bit of uncertainty in H_{BML} and H_{WS} estimates.

Despite the rosette's limitations, H_{BML} were thin or mostly absent. They were slightly thicker around the Monterey Bend, particularly at stations 33, 27, and 22, where they were up to 55 m thick. H_{WS} from the CTD time series were also thicker in this region (up to 140 m), especially stations 27 and 22; the greatest heights (up to 180 m) were observed near the canyon mouth in the deepest waters of the study site. H_{WS} from the VMP data were not as thick as H_{WS} from the CTD, and maximum heights were 78 m. Since there were not many VMP profiles that landed near the bottom to capture the bottom boundary layer structures, there were few observed heights. It was thus difficult to make any conclusions about spatial variations in H_{WS} from the VMP data.

The region along the canyon where there were thicker H_{WS} from the CTD time series is associated with the area identified as having enhanced energy dissipation as observed by Kunze et al. (2002). However, it is also important to note that weakly stratified layers may be thicker in deeper regions offshore because the background stratification is decreased in deeper, less stratified waters. Figure 40 shows the background stratification measured from the CTD time series. Stations farther offshore were less stratified than stations closer to the canyon head. The buoyancy frequencies from the region above the bottom mixed layer, representing the background stratification were $0.5 – 5.0 \times 10^{-3}$ s^{-1}. The shallow stations were likely constrained by the water depth and increased stratification, resulting in less fully developed bottom boundary layers. The decreased buoyancy frequencies near the canyon mouth also suggest that mixing was intensified farther offshore.

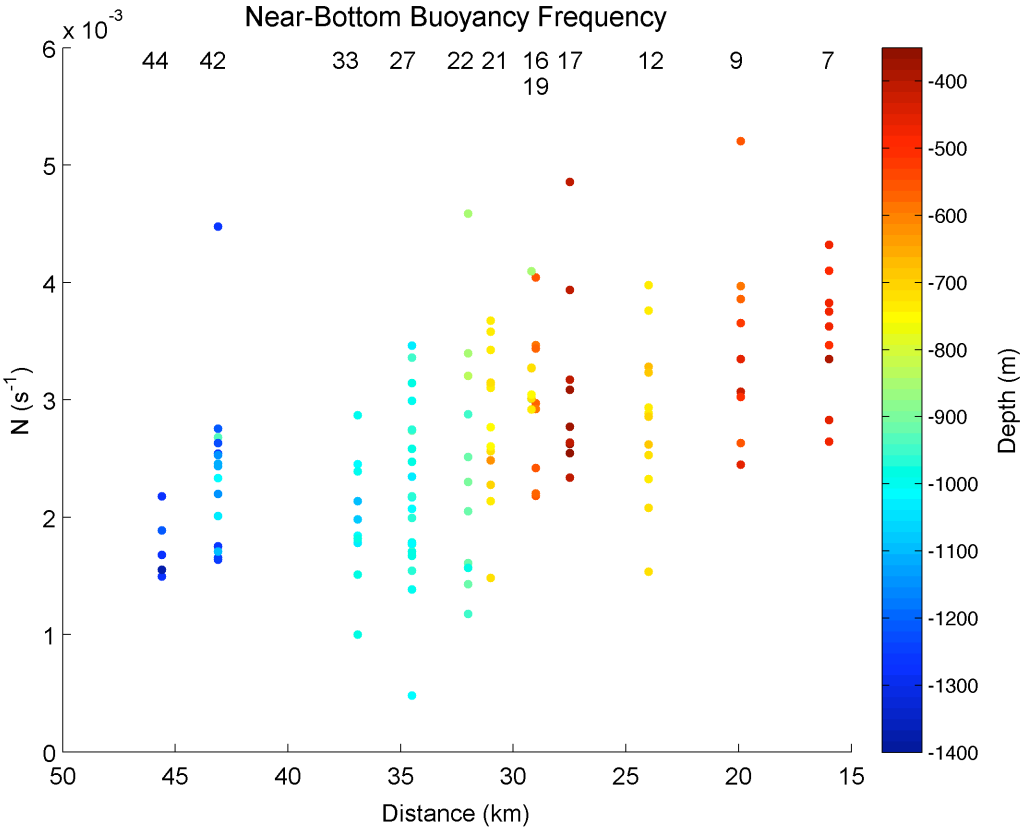

Figure 40. Buoyancy frequencies (s^{-1}) calculated from CTD time series along the canyon axis. The values describe the stratification of the layer just above the bottom mixed layer. Colorbar represents bottom depth. Station numbers are indicated at top.

Shear layer thicknesses from the LADCP showed a similar trend of increasing heights at greater depths centered around the Monterey Bend. Heights were decreased at station 44, the station closest to the canyon mouth. Stations 12 and 9 were the exceptions among shallower stations because H_S were just as thick as heights near the bend. Stations 33 and 27 in particular had thicker layers and these stations were located at the beginning of the Monterey Bend. Heights increased from station 42 to 33 and from stations 22 to station 27, which may suggest that this is an area of convergence.

Since the XCP data were confined to the Monterey Bend, they did not provide detailed information about spatial variations in H_S. In addition, shear layer thicknesses observed from the XCP data were typically less than heights observed from the LADCP data. This may have been due to the resolution of the LADCP (8 m) versus the resolution of the XCP (3 m). The XCPs also came much closer to the bottom, so it is also possible that the LADCP profiles were missing the near-bottom structure, thereby affecting the observed maximum nose velocity observed.

Shear velocities from the XCP data were greater than shear velocities from the LADCP. Since the LADCP collected data along the entire canyon axis and the XCPs were centered around a region of known energy dissipation, it makes sense that the XCPs would find greater shear velocities. Alternatively, greater shear velocities for the XCP data may be a function of the higher vertical resolution of the XCP velocity data. The stations farther offshore and station 12 had the greatest shear velocities. Shear velocities were decreased at stations in the Soquel Canyon (21, 19, 17) as well as at stations 16 and 7. As the internal tide passed along the canyon, shear velocities were greatest up until the Monterey Bend. In this region, energy is dissipated. This may also result in decreased shear velocities and shear layer thicknesses just past the Monterey Bend, which was observed. It is unknown what may cause the increased shear velocities and shear layer thicknesses observed at stations 12 and 9.

While the comparison of bottom boundary layer heights along the canyon axis did not always show a definitive pattern of increased heights from the canyon head to the canyon mouth, the overall trend showed increased observed heights centered around the

Monterey Bend. In Monterey Bay, the M_2 baroclinic tidal energy is restricted to the canyon, and energy magnitudes increase as much as 5 times in the bends along the canyon axis; topographic focusing is likely responsible for this intensification (Carter 2010). Figure 41 shows the energy fluxes observed by Kunze et al. (2002) and model energy fluxes from Carter (2010) and shows that energy fluxes are greater at the San Gregario Meander as well as the before the Monterey Meander (Monterey Bend). This region of energy flux convergence and energy loss might explain thicker bottom boundary layer features farther offshore. Kunze et al. (2002) found energy fluxes directed upcanyon at the mouth of the canyon that decreased from 5 kW m^{-1} near the mouth and ~1 kW m^{-1} closer to the head. The spatial patterns in weakly stratified heights and shear velocities showed a similar pattern. They were greater near the San Gregario Meander and Monterey Meander. Values were reduced past the Monterey Meander and were increased near station 12. While the figure shows this region as having decreased energy magnitudes, the energy was greater in this area compared to other shallower regions near the canyon head.

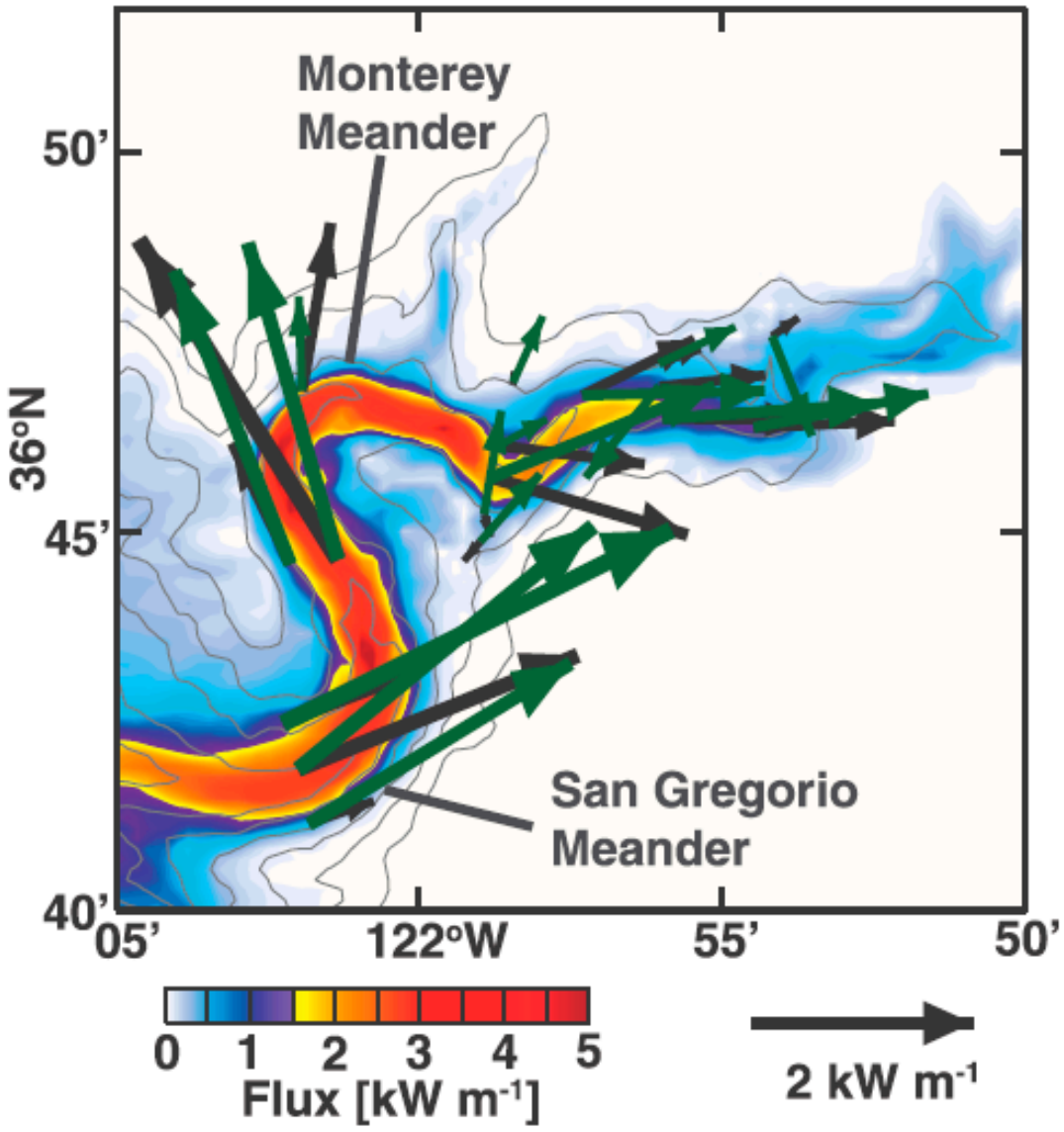

Figure 41. Energy fluxes from Kunze et al. (2002) in green and model energy fluxes from Carter (2010). Color is depth-integrated M_2 baroclinic energy flux (Carter 2010). © American Meteorological Society. Reprinted with permission.

b. Turbulence and Energy Dissipation and Implications from Boundary Layer Dynamics

One of the most important findings of this overall study was elevated turbulence extending several hundred meters above the seafloor all along the canyon-axis. Turbulent kinetic energy dissipation rate measurements from the Vertical Microstructure Profiler showed thick turbulent layers, h_ε, extending 200 – 300 m above the bottom (Figure 42). Turbulence was greatest near the bottom, where average dissipation rates were 4×10^{-8} W kg^{-1} and N^2 was 1.2×10^{-5} s^{-2}. At mid-water depths, 300-400 mab, dissipation rates were 4×10^{-9} W kg^{-1} (Kunze et al., *submitted*). Values from mid-water depths were similar to dissipation rates observed in the ocean interior, whereas values observed in the 200-300 m above the bottom were significantly greater. Eddy diffusivities were 16×10^{-4} m^2 s^{-1} (Kunze et al., *submitted*), where mixing efficiency was assumed to be 0.2 (Osborn 1980). The increased diffusivities help to explain some of the mixing discrepancy described earlier, where open ocean diffusivities are an order of magnitude less than predicted diffusivities. Canyons may make up for 10% of this missing mixing (Kunze et al., *submitted*).

Despite energetic turbulence, the bottom few hundred meters remained stratified, and bottom mixed layers and even weakly stratified layers were thin or nonexistent. Shear layer thicknesses from the LADCP and XCP were also not as thick as the turbulent layers measured by Kunze et al. (*submitted*). Although there were spatial variations in observed boundary layer heights, Kunze et al. (*submitted*) found no major spatial variations in near-bottom turbulence. However, turbulent dissipation rates varied over the tidal cycle (Kunze et al., *submitted*).

While the weakly stratified heights were thicker than the bottom mixed layer heights, they were nowhere near as thick as these turbulent layers. This suggests that there is intense exchange between the boundary and offshore waters that inhibits the development and persistence of bottom mixed layers. Perlin et al. (2007) discussed how stratification complicates Ekman theory by suppressing turbulence in the bottom boundary layer. While there is intense turbulent mixing near the bottom, the absence of well-mixed layers indicates that restratification, i.e. replenishment of stratification must occur to maintain the stratified conditions near the bottom. Thorpe et al. (1990) argued that the time for restratification of mixed fluid was less than a tidal period.

The major implication of this collaborative effort is that the water column remains stratified despite energetic turbulence. Over time, the elevated mixing should homogenize deep water masses; however, well mixed bottom boundary layers were not observed. Due to this constant restratification, there must be exchange between the boundary and ocean interior. Our research group (Kunze et al, *submitted*) found evidence for such exchange from mass conservation arguments and additional evidence from intermediate nepheloid layers marking a zone of persistent convergent, offshore transport around 1000-m depth. Further details are beyond the scope of this thesis, but are explained here to show the importance of properly measuring stratification and mixed layers in addition to studying energetics. Rapid restratification in the face of constant energetic turbulent mixing has repercussions for our understanding of outcropping and ventilation of mid-depth abyssal waters that, although not yet well understood, may be profound.

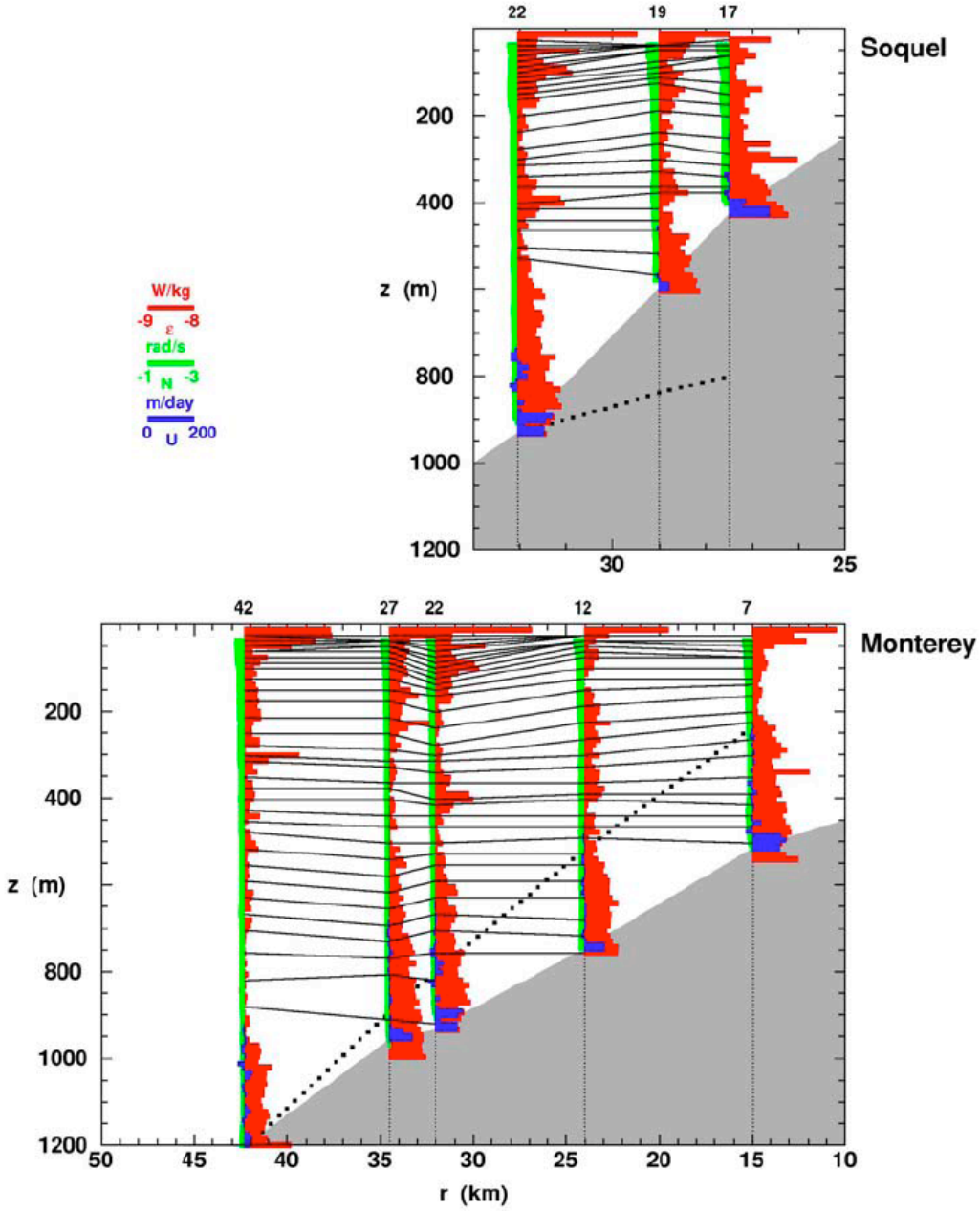

Figure 42. Tidally-averaged dissipation rate ε (red) and buoyancy frequency N (green) profiles from the Soquel and Monterey Canyon. Horizontal upcanyon velocity U (blue) are from tidally-averaged isopycnals (reprinted with permission from Kunze et al., *submitted*).

c. Temporal Variations and the Effect of Internal Tides on Bottom Boundary Layers

1 MOORING OBSERVATIONS

The mooring helped to address temporal variability during the study, particularly regarding the internal tide phase. More specifically, it provided a continuous record of near-bottom temperatures and velocities to describe temporal variations at the Monterey Bend. Cold pulses identified by the thermistor at 1060 m depth were used to identify the upslope phase of the internal tide. Velocity magnitudes recorded by the downward-facing ADCP at 1050 m depth were used to distinguish periods of increased mixing.

The mooring velocity time series showed intense semidiurnal velocities near the bottom that extended up to 200-300 mab. Pulses of increased velocities were seen throughout the record and lasted four to eight days. These pulses were likely associated with the spring-neap tide, but may also be the result of other synoptic-scale forcing. Strong semidiurnal fluctuations were also observed in the transmissometer record, as were the four to eight day pulses. The mooring showed a fortnightly signal of increasingly intense currents that matched the fortnightly energy of the surface tide (Kunze et al., *submitted*). The group velocities for the internal tides are ~100 km/day, so there should be minimal phase lag (Carter 2010) between locations. However, some studies (Carter 2010) show a difference between the mid- and deep canyon and the shallower canyon head in the phase between the internal and surface tide. Since there is minimal phase lag, the mooring can be used to represent conditions at other locations along the canyon axis.

Since H_{BML} were mostly absent, it was difficult to assess how this thickness varied over time. It appears that due to unsteady conditions and restratification of the near-boundary flow, these layers did not fully develop. The difficulty of reaching the bottom also made it hard to capture the bottom mixed layer. H_{WS} were often thickest during cold water pulses associated with the upslope phase of the internal tide. Some of the stations showed a clear oscillatory pattern in bottom boundary layer heights; however, the pattern was not necessarily closely associated with internal tide phase.

Although there was not a clear definitive pattern associated with the internal tide, bottom boundary layers varied over the 12-hour sampling period. Weakly stratified layer heights varied by as much as 120 m, and observed shear layer thicknesses varied as much as 200 m. The deeper stations especially had a lot of variation. Similarly, bottom isopycnals were displaced up to a hundred meters at some of the stations during the 12-hour sampling period.

Even though this study may not have shown a clear signature between tide phase and bottom boundary layer height, other studies have shown that bottom boundary layer dynamics are affected by tides and internal waves. Perlin et al. (2007) found that the greatest variations in near-bottom turbulence corresponded with tidal periods. Armi and D'Asaro (1980) observed wavelike oscillations in velocity and temperature data that were assumed to be caused by internal waves. One study that looked at bottom mixed layers in the Florida Current saw frequent variations in their development at a given location. The bottom mixed layers varied such that thicker layers occurred during cold-water pulses,

suggesting that the upslope advection of cooler water led to the formation of these layers (Weatherly and Niiler 1974). However, other studies have observed thicker bottom mixed layers during coastal downwelling (Moum et al. 2004). We expected to see such oscillations in mixed layer and shear layer thicknesses, but did not.

Lentz and Trowbridge (1991) looked at the bottom boundary layer thickness in the Northern California Shelf on a sloping bottom and predicted that the thickness be affected by the flow direction. High shear near the seabed results in greater turbulence, which over time creates a well-mixed homogenous boundary layer. Their results suggested that the boundary layer thickness was correlated with the flow direction; boundary layer heights were thicker during downwelling, and smaller when the flow was upwelling.

Although there were no clear associations between internal tide phase and bottom boundary layer heights, observed heights, particularly H_{WS}, were thick when temperatures were cold. This is the opposite of what Lentz and Trowbridge (1991) found. Instead, it suggests that bottom mixed layers are more affected by an influx of deep water masses, perhaps "bore-like" wave behavior, than by mixing and buoyancy, as discussed by Lentz and Trowbridge

d. Relationship Between Observed and Predicted Layer Thickness

As discussed in section 2, various dynamical balances were considered for predictions of bottom boundary layer heights. These modeled predictions were compared

to observed bottom boundary layer thicknesses. The accuracy of these predictions is discussed in this section.

The bottom boundary layer was initially modeled as a turbulent Ekman layer affected by shear velocity and Coriolis frequencies. Using the shear velocities from the LADCP and XCP data, these frictional bottom boundary layer heights were calculated. The heights from the LADCP observations were 8 – 102 m. Figure 43 shows observed bottom boundary layer heights, including weakly stratified heights (H_{WS}) observed from the CTD data and shear layer thicknesses (H_S) observed from the LADCP data plotted versus H_{FBBL} calculated from the LADCP shear velocities. There was no clear relationship between H_{FBBL} and H_{WS} or H_S. Although H_{WS} and H_{FBBL} were of similar magnitude, they were not closely related.

Figure 44 shows H_{FBBL} calculated from the XCP data and shows the two methods: (1) heights calculated from shear velocities using the Law-of-the-Wall, and (2) heights calculated from shear velocities using the drag coefficient method. The shear velocities from the Law-of-the-Wall were greater than shear velocities from the drag coefficient method. Heights were thus also greater following method (1). Neither method produced H_{FBBL} that agreed with observed shear layer thicknesses from the XCP data. Thus, modeling the bottom boundary layer as a frictional bottom boundary layer, or a turbulent Ekman layer, does not accurately predict bottom boundary layer heights for this environment.

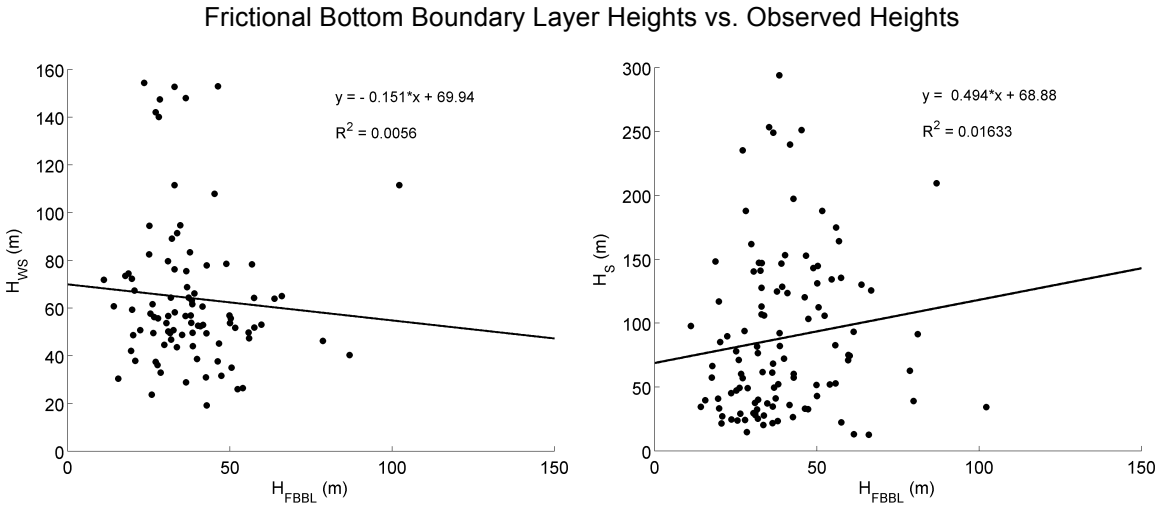

Figure 43. (*left*) Weakly stratified heights (m) from CTD time series versus frictional bottom boundary layer heights (m) calculated from LADCP data. (*right*) Shear layer thickness (m) from LADCP time series versus frictional bottom boundary layer heights (m).

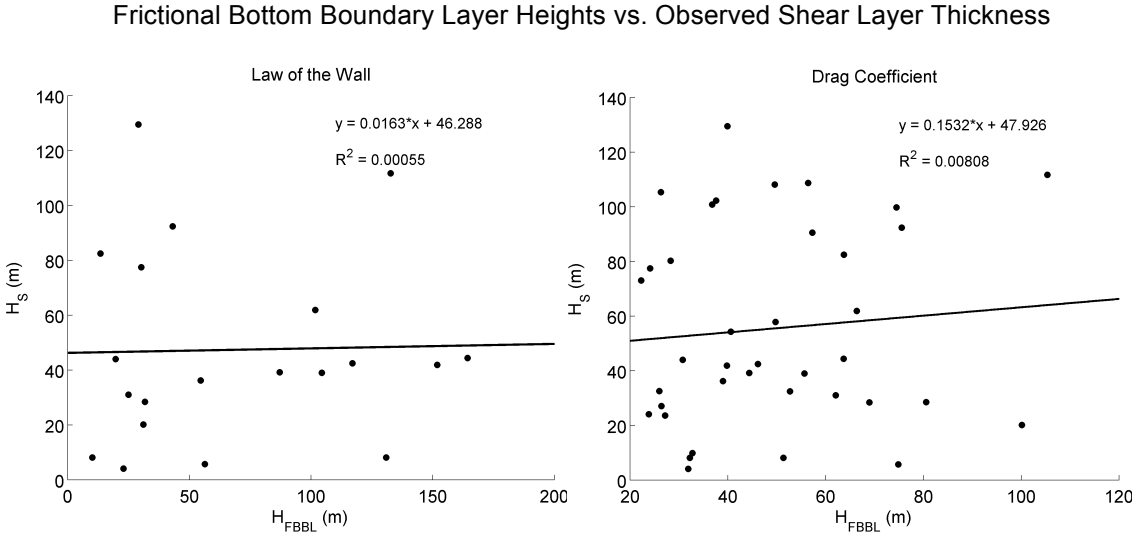

Figure 44. (*left*) Shear layer thickness (m) from XCP time series versus frictional bottom boundary layer heights (m) calculated from shear velocities from the Law-of-the-Wall. (*right*) Shear layer thickness (m) versus frictional bottom boundary layer heights calculated from shear velocities from the drag coefficient method.

Theoretical predictions for boundary layers whose growth is limited by tidal oscillations (e.g. Prandle 1982, Maas and Van Haren 1987) and stratification (e.g. Pollard et al. 1973, Taylor and Sarkar 2008) were considered. No clear tendencies were found, leading to no real progress in understanding whether any single one of these dynamics (stratification, tidal oscillations, or earth rotation) dominated over others. Figure 45 shows the two different types of oscillatory boundary layer heights. Heights predicted from Prandle (1982), H_{Oa}, do not differ substantially from heights predicted from Maas and van Haren (1987), H_{Ob}. The observed weakly stratified layers from the VMP profiles are plotted against the modeled oscillatory boundary layers, and these models prove to be more closely related to the observed heights than for other modeled predictions. These observed heights came from the VMP data, and it is likely that the VMP captured the near-bottom structure more accurately than the CTD rosette.

Comparing the observed heights against the stratified BBL height based on Pollard's equation ($H_P = \frac{u_*}{\sqrt{Nf}}$) did not show a close relationship (Figure 46). While this equation more accurately described the observed heights than the equation for H_{FBBL}, the trend was not significant. The bottom boundary layer based on Taylor and Sarkar's buoyancy length scale ($l = \frac{u_*}{N}$) (2008), was more closely related to observed weakly stratified heights; however, it was not significant. Figure 47 shows the positive trend between H_{WS} and H_S and buoyancy length scale. Testing these various models against observed heights did not accurately predict the observed thicknesses. It is likely that the dynamics going on in the Monterey Canyon are much more complicated than can be

predicted by most of these models. Typically these models are used to describe steady-state flow regimes, and the Monterey Canyon is not steady-state.

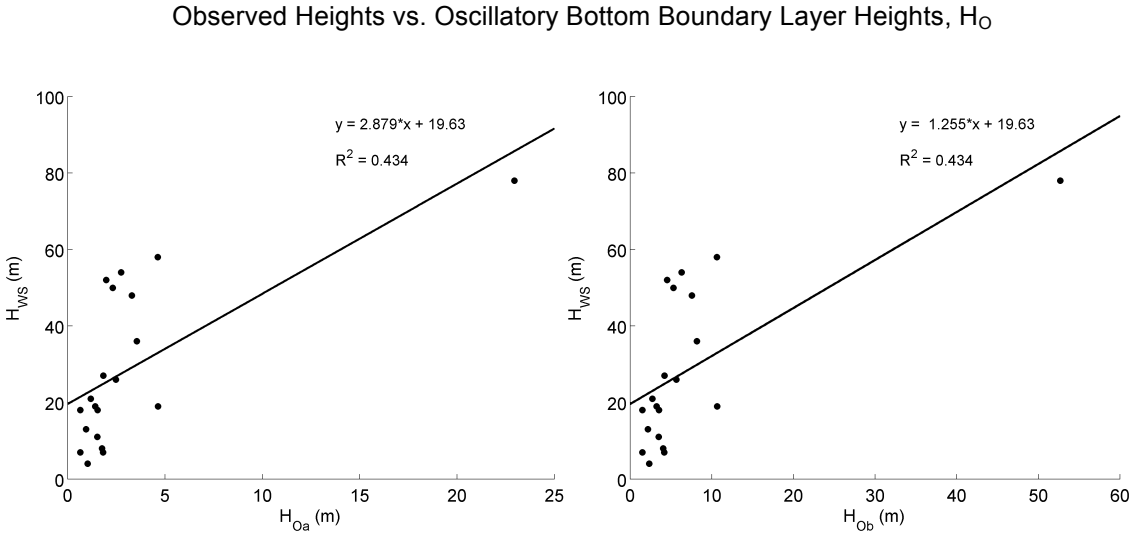

Figure 45. Weakly stratified heights (m) from microstructure data versus oscillatory bottom boundary layer heights (m) constrained by tidal frequencies. (*left*) Heights calculated from Prandle (1982). (*right*) Heights calculated from Maas and van Haren (1987).

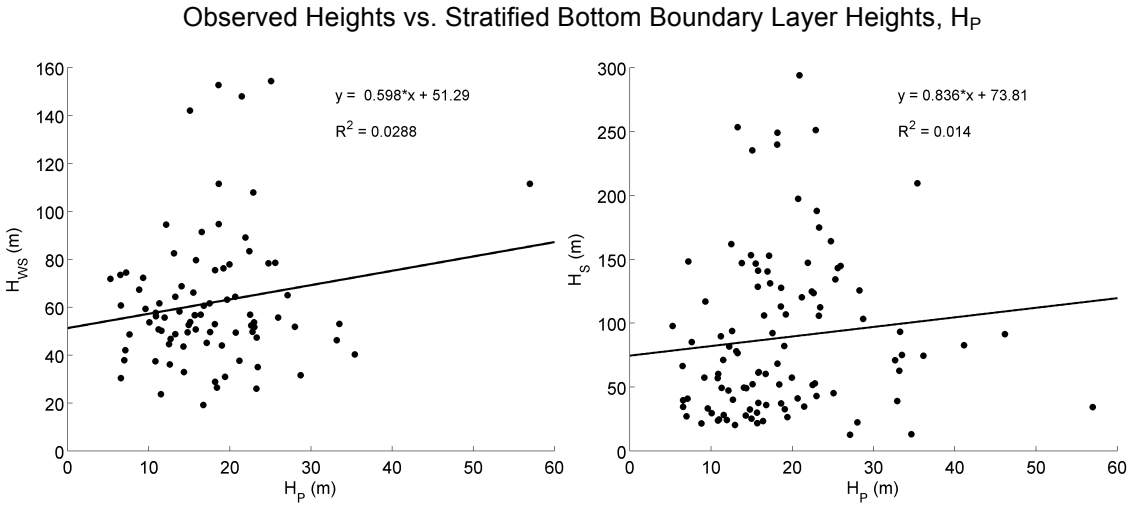

Figure 46. (*left*) Weakly stratified heights (m) from CTD time series versus stratified bottom boundary layer heights (m), H_P, calculated from CTD/LADCP data. (*right*) Shear layer thickness (m) from LADCP time series versus H_P (m).

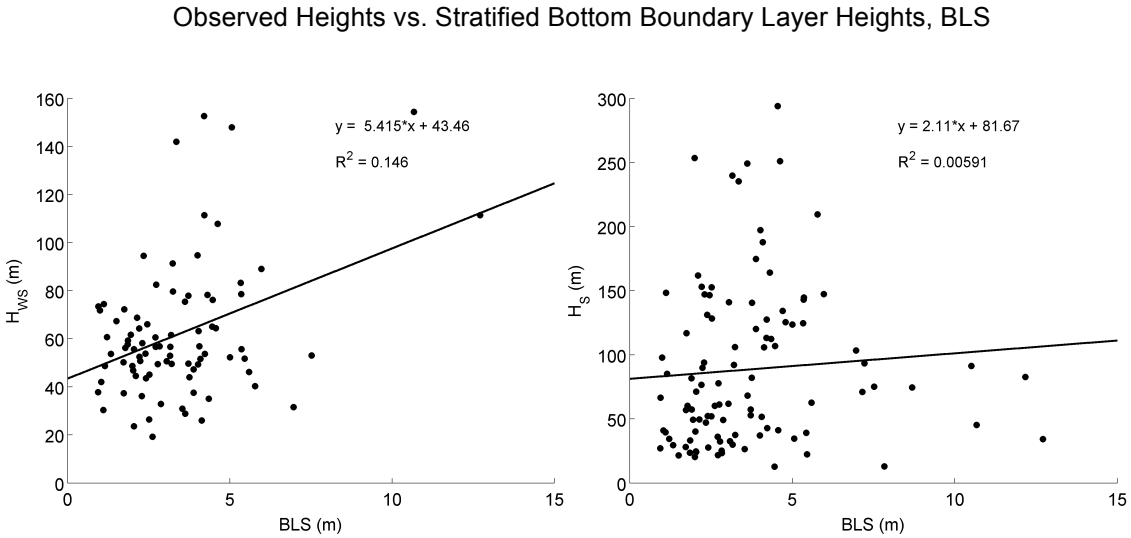

Figure 47. (*left*) Weakly stratified heights (m) from CTD time series versus stratified bottom boundary layer heights (m), BLS, calculated from CTD/LADCP data. (*right*) Shear layer thickness (m) from LADCP time series versus BLS (m).

Other studies that have looked at bottom boundary layers have made observations based on temperature or density and also made predictions using equations for a turbulent Ekman layer height, $h_E = 0.4\,u_*/f$. Observations made by Armi and Millard (1976), found turbulent Ekman layers, h_E, thinner than observed mixed layer heights. The turbulent Ekman layer height, ($h_E = 0.4\,u_*/f$), was usually ~13 m and was half the mean bottom mixed layer height. Since their investigation was of the Hatteras abyssal plain, velocities were weaker than in more energetic environments such as canyons. Their mean speed was 0.07 m s^{-1}, whereas mean near-bottom velocities in the Monterey Canyon in this study were 0.14 m s^{-1}.

The results reported for canyons substantially differ from the thick persistent bottom mixed layers that exist in the abyssal ocean (e.g. Armi 1978) that may measure up to 100 m thick. The presence of thick H_{FBBL} (up to 100 m), even thicker stratified turbulent boundary layers (200-300 m), and thin bottom mixed layers (<50 m) has been observed in other studies on seamounts (Toole et al. 1997) and continental slopes (e.g. Nash et al. 2004; McPhee-Shaw et al. 2004). These studies saw thin bottom mixed layers between 10 and 50 m that were thin even though there were strong internal tides and intense mixing. Carter and Gregg (2002) observed bottom mixed layers that were usually thinner than 15 m in the Monterey Submarine Canyon, despite strong turbulence and tidal velocities in the canyon (Petruncio et al. 1998; Kunze et al. 2002). In contrast, H_{FBBL} varied from 70-100 m during the neap tide and up to 200 m during the spring tide (Kunze et al. 2002).

e. Bottom Nepheloid Layer Characteristics

Over the duration of sampling, regions of increased suspended sediment extended 100-200 mab, despite thin or absent bottom mixed layers. While the bottom nepheloid layer (BNL) typically had high levels of suspended sediment and turbidity and was often associated with the bottom mixed layer, in some cases, the BNL could be significantly thicker, measuring several hundred meters (Eittreim et al. 1975). Intense mixing and turbulence, observed by the thick turbulent layers (Kunze et al., *submitted*) likely results in greater amounts of suspended sediment near the bottom and regions of thick BNLs.

In addition to prominent BNLs, intermediate nepheloid layers were observed in Soquel Canyon between 100 and 200 m depth. These layers likely resulted from an intermediate nepheloid layer detaching from the continental shelf near the canyon head (Carter et al. 2005). An intermediate nepheloid layer was present near the canyon mouth at stations 42 and 44. This turbid region between 800 and 1000 m (±100 m) was bound by clear water above and below (Figure 48). The region of clear water below was between 1000 and 1100 m (±100 m) and likely originated from convergence of offshore waters being driven shoreward along the canyon (Kunze et al., *submitted*). Plots of density and beam attenuation reveal an INL between the canyon mouth and the Monterey Bend, at stations 33, 42, and 44 between σ_θ=27.18 and 27.33 kg m^{-3}.

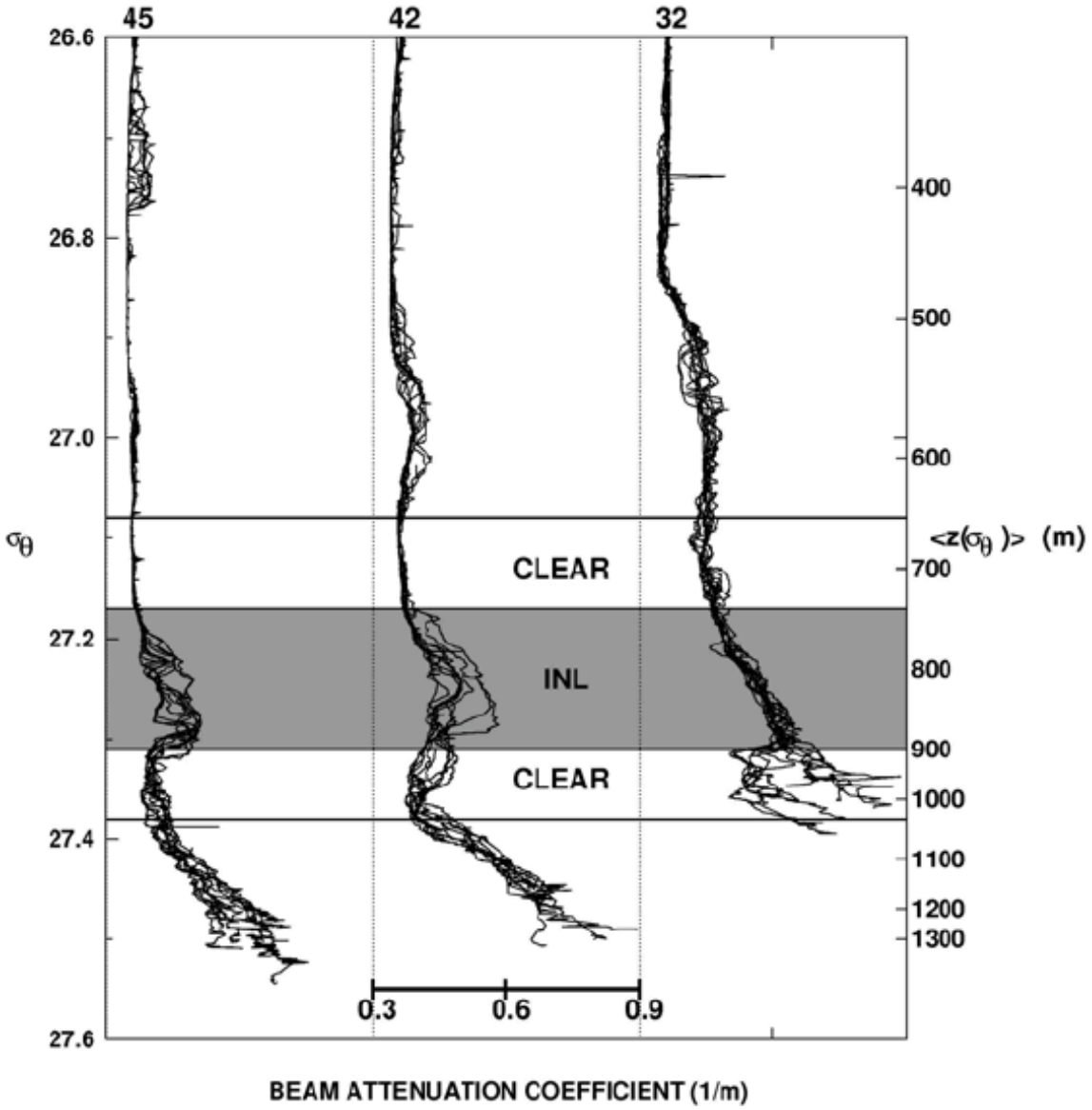

Figure 48. Beam attenuation coefficient profiles plotted as a function of density σ_θ. Station label 45 represents Station 44, and station label 32 represents Station 33. Reprinted with permission from Kunze et al., (*submitted)*.

Station 12 had very high beam attenuation values and among the shallower stations observed, it had thick observed BBL heights and greater temporal variation in BBL heights. The shear velocity also had great variability. The second occupation of

station 27 also showed increased levels of suspended sediment. While BNLs were observed at nearly every station, these two stations had beam attenuation coefficients greater than 1 m^{-1}. The region between these two stations (stations 22 and 16) did not have prominent BNLs. The upslope transport taken from Kunze et al. (*submitted*) identifies upslope flow divergence between stations 27 and 22 and convergence between stations 22 and 12 (Figure 49). These divergences and convergences might explain the increased amounts of suspended sediment observed at stations 12 and 27.

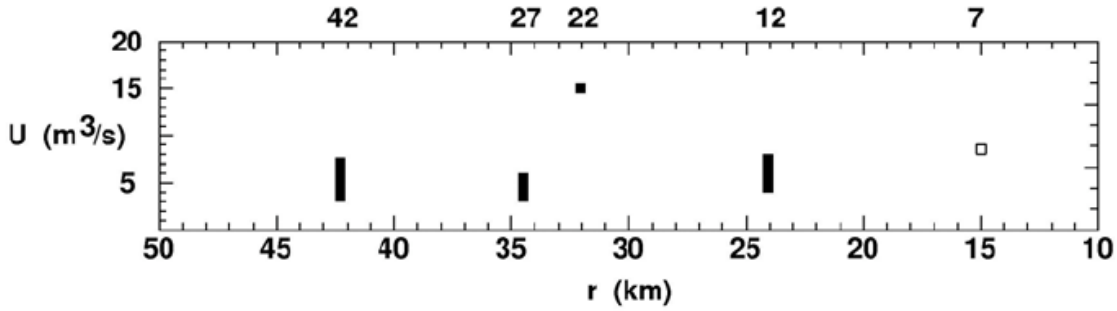

Figure 49. Upcanyon transports from integrals over 200 mab versus canyon distance. Station numbers are indicated at top. Reprinted with permission from Kunze et al. (*submitted*).

7. Conclusion

Most studies of oceanic bottom boundary layers have been conducted on continental shelves. Studies that have been conducted in the deep ocean have focused on the relatively flat abyssal ocean instead of over continental slopes or at sites with complex topography—such as canyons. This study provided insight about the spatial and temporal variations in bottom boundary layer features. Bottom mixed layers were thin or absent along the canyon axis and weakly stratified layers were up to 180 m thick. Shear layer thicknesses ranged from 50-300 m, and thick turbulent layers described by Kunze et al. (*submitted*) were 200-300 m. Although bottom boundary layer heights were greater farther offshore in deeper water, there were no major along-canyon variations. Likewise, while the bottom boundary layer heights varied significantly over the 12-hour sampling period, the temporal variations did not match up with the internal tide phase.

Thick turbulent layers and thin bottom mixed layers indicate that there is extensive mixing in the bottom boundary layer; however, the absence of well-mixed bottom boundary layers suggests that restratification is a dominant process in the canyon that maintains stratified conditions near the seafloor. The mixing contributes to increased levels of sediment near the bottom extending up to 200 m above the bottom. Although there is intense mixing in the bottom boundary layer, it is likely that a well-mixed layer is unable to develop due to tidal velocities that switch back and forth too frequently to allow for much growth of the bottom mixed layer.

Works Cited

Armi, L., 1978: Some evidence for boundary mixing in the deep ocean. *Journal of Geophysical Research*, **83**, 1971-1979.

Armi, L., and E. D'Asaro, 1980: Flow structures of the benthic ocean. *Journal of Geophysical Research*, **85**, C1, 469-484.

Armi, L., and R.C. Millard, 1976: The bottom boundary layer of the deep ocean. *Journal of Geophysical Research*, **81**: 4983-4990.

Batchelor, G.K., 1967: *An Introduction to Fluid Dynamics*. Cambridge University Press. 615 pp.

Carter, G.S., 2010: Barotropic and Baroclinic M_2 Tides in the Monterey Bay Region. *Journal of Physical Oceanography*, **40**, 1766-1783.

Carter, G.S., and M.C. Gregg, 2002: Intense, variable mixing near the head of Monterey Submarine Canyon. *Journal of Physical Oceanography*, **32**: 3145-3165.

Eittreim, S., P.E. Biscaye, and A.F. Amos, 1975: Benthic nepheloid layers and the Ekman thermal pump. *Journal of Geophysical Research*, **80**, 5061-5067.

Garrett, C.J.R., and D. Gilbert, 1988: Estimates of vertical mixing by internal waves reflected off a sloping bottom. *Small-Scale Turbulence and Mixing in the Ocean*. Nihoul, J.C.J., and B.M. Jamart, Ed., 405-424.

Hickey, B.M., 1979: The California Current System—hypotheses and facts. *Progress in Oceanography*, **8**, 191-279.

Hickey, B.M., 1995: Coastal submarine canyons. *Topographic Effects in the Ocean, 'Aha Huliko'a Hawaiian Winter Workshop*, Honolulu, HI, U of Hawaii at Manoa, 95-110.

Hotchkiss, F.S., and C. Wunsch, 1982: Internal waves in Hudson Canyon with possible geological implications. *Deep-Sea Research*, **29**, 415-442.

Hunter, C.N., 2006: Particulate Organic Carbon, Nitrogen and Total Suspended Matter Methodologies, Protocols and Analyses Used in the Development of Ocean Color Product Algorithms. *Moss Landing Marine Laboratories Technical Memorandum* 06-1, 13 pp.

Jachec, S.M., O.B. Fringer, M.G. Gerritsen and R.L. Street, 2006: Numerical simulation of internal tides and the resulting energetics within Monterey Bay and the surrounding area. *Geophysical Research Letters*, **33**, L12,605, doi: 1029/2006GL026314.

Kunze, E., E. Firing, J.M. Hummon, T.K. Chereskin, and A.M. Thurnherr, 2006: Global abyssal mixing inferred from lowered ADCP shear and CTD strain profiles. *Journal of Physical Oceanography*, **36**, 1553-1576.

Kunze, E., C. MacKay, E.E. McPhee-Shaw, K.J. Morrice, J. Girton, and S. Terker: On turbulent mixing and exchange with interior waters on sloping boundaries. *Journal of Physical Oceanography*, submitted.

Kunze, E., L.K. Rosenfeld, G.S. Carter, and M.C. Gregg, 2002: Internal Waves in Monterey Submarine Canyon. *Journal of Physical Oceanography,* **32**, 1890-1913.

Lentz, S.J., and J.H. Trowbridge, 1991: The bottom boundary layer over the northern California shelf. *Journal of Physical Oceanography*, **21**, 1186-1201.

Lueck, R.G., and T.R. Osborn, 1985: Turbulence measurements in a submarine canyon. *Continental Shelf Research*, **4**, 681-698.

Maas, L.R.M., and J.J.M. van Haren, 1987: Observations on the vertical structure of tidal and inertial currents in the central North Sea. *Journal of Marine Research*, **45**, 293-318.

McPhee-Shaw, E.E., and E. Kunze, 2002: Boundary-layer intrusions from a sloping bottom: A mechanism for generating intermediate nepheloid layers. *Journal of Geophysical Research*, **107**, DOI: 10.1029/2001JC000801.

McPhee-Shaw, E.E., R.W. Sternberg, B. Mullenbach, and A.S. Ogston, 2004: Observations of intermediate nepheloid layers on the northern California continental margin. *Continental Shelf Research*, **24**, 693-720.

Moum, J.N., A. Perlin, J.M. Klymak, M.D. Levine, T. Boyd, and P.M. Kosro, 2004: Convectively driven mixing in the bottom boundary layer. *Journal of Physical Oceanography*, **34**, 2189-2022.

Munk, W.H., 1966: Abyssal Recipes. *Deep-Sea Research*, **13**, 707-730.

Munk, W., and C. Wunsch, 1998: Abyssal recipes II: Energetics of tidal and wind mixing. *Deep-Sea Research I,* **45**, 1977-2010.

Nash, J.D., E. Kunze, J.M. Toole, and R.W. Schmitt, 2004: Internal tide reflection and turbulent mixing on the continental slope. *Journal of Physical Oceanography*, **34**, 1117-1134.

Osborn, T.R., 1980: Estimates of the local rate of vertical diffusion from dissipation measurements. *Journal of Physical Oceanography*, **10**, 83-89.

Perlin, A., J.N. Moum, J.M. Klymak, M.D. Levine, T. Boyd, and P.M. Kosro, 2007: Organization of stratification, turbulence, and veering in bottom Ekman layers. *Journal of Geophysical Research*, **112**, C05S90, DOI: 10.1029/2004JC002641.

Petruncio, E.T., L.K. Rosenfeld, and J.D. Paduan, 1998: Observations of the internal tide in Monterey Canyon. *Journal of Physical Oceanography*, **28**, 1873-1903.

Pollard, R.T., P.B. Rhines, and R.O.R.Y. Thompson, 1973: The deepening of the wind-mixed layer. *Geophysical Fluid Dynamics*, **3**, 381-404.

Polzin, K.L., J.M Toole, J.R. Ledwell, and R.W. Schmitt, 1997: Spatial variability of turbulent mixing in the abyssal ocean. *Science*, **276**, 93-96.

Prandle, D., 1982: The vertical structure of tidal currents and other oscillatory flows. *Continental Shelf Research*, **1**, 191-207.

Richards, K.J., 1990: Physical processes in the benthic boundary layer. *Philosophical Transactions of the Royal Society of London, Series A*, **331**, 3-13.

Rosenfeld, L.K., R.E. Schramm, J.B. Paduan, G.A. Hatcher, and T. Anderson, 1994: Hydrographic data collected in Monterey Bay during 1 September 1988 to 16 December 1992. Technical Report 94-15, Monterey Bay Research Aquarium, 549 pp.

Shepard, F.P., N.F. Marshall, P.A. McLoughlin, and G.G. Sullivan, 1979: *Currents in Submarine Canyons and Other Sea Valleys*. AAPG Studies in Geology, Vol. 8, American Association of Petroleum Geologists, 173 pp.

Souza, A., and C. Friedrichs, 2005: Near-bottom boundary layers. *Marine Turbulence: Theories, Observations, and Models. Results of the CARTUM Project*, H.Z. Baumert, J. Simpson, and J. Sündermann, Ed., Cambridge University Press.

Sternberg, R.W., 1968: Friction factors in tidal channels with differing bed roughness. *Marine Geology*, **6**, 243-260.

Taylor, J.R., and S. Sarkar, 2008: Stratification effects in a bottom Ekman layer. *Journal of Physical Oceanography*, **38**, 2535-2555.

Thorpe, S.A., 2005: *The Turbulent Ocean*. Cambridge University Press. 439 pp.

Thorpe, S.A., P. Hall, and M. White, 1990: The variability of mixing on a continental slope. *Proceedings of the Royal Society of London* A, **439**, 115-130.

Toole, J.M., R.W. Schmitt, K.L. Polzin, and E. Kunze, 1997: Near-boundary mixing above the flanks of a mid-latitude seamount. *Journal of Geophysical Research,* **102**, 947-959.

van Haren, H., M. Oakey, and C. Garrett, 1994: Measurements of internal wave band eddy fluxes above a sloping bottom. *Journal of Marine Research*, **52,** 909-946.

Weatherly, G.L., and P.P. Niiler, 1974: Bottom homogeneous layers in the Florida Current. *Geophysical Research Letters*, **1**, 316–319.

Wunsch, C, 1975: Internal tides in the ocean. *Reviews of Geophysics and Space Physics*, **35**, 131-144.

Xu, J.P., M.A. Noble, S.L. Eittreim, L.K. Rosenfeld, G.B. Schwing, and C.H. Pilskaln, 2002: Distribution and transport of suspected particulate matter in Monterey Canyon, California. *Marine Geology,* **181**, 215–234.

Xu, J.P., and M.A. Noble, 2009: Currents in Monterey Submarine Canyon. *Journal of Geophysical Research*, **114**, C03004, DOI: 10.1029/2008JC004992.